Analysis of Offset Pulse Position Modulation

Indrani Ray

University of Huddersfield

A dissertation submitted in part fulfillment for the degree of Doctor of Philosophy in Electronics and Communication Engineering

January 2015

To Sourav and my parents

for their

love and understanding

Contents

Abstract

This work presents the performance analysis of the offset pulse position modulation (PPM) scheme using graded-index plastic optical fibre with a Gaussian impulse response. The aim of this analysis is to predict how sensitivity, error, number of required photons, threshold voltage, and the effect of inter-symbol interference will change with the change in the number of data bits encoded at a rate of 1 Gbit/s. An information theory analysis is presented in detail and also the band-utilization efficiency is determined. Results are compared to equivalent digital PPM and multiple PPM schemes and it is also shown that offset PPM gives an advantage over on-off keying (OOK).

Bit error rate (BER) analysis has been presented numerically. The errors due to different coding techniques are compared. It has also been shown that offset pulse position modulation is more power efficient than multiple pulse position modulation.

The spectral analysis of offset pulse position modulation coding scheme has been carried out. For an offset PPM sequence the spectral characteristics is presented both theoretically and numerically. The results show strong frequency components at the frame rate and, if return-to-zero pulses are used, the slot rate. Slot synchronisation has been taken into consideration for the first time as offset PPM spectrum exhibits discrete slot rate component. The effect of pulse shaping and modulating index on the spectrum has been

shown. The dependency of slot component on the pulse shape is examined. The results show that the frame synchronisation is possible for offset PPM as this coding exhibits a strong frame rate component. A comparison of spectral characteristics has been presented considering digital, multiple and shortened PPM. For ease of implementation an offset PPM coder has been designed.

In this work an efficient clock recovery topology is presented for offset PPM data sequence at the receiver end. For clock recovery, a phase locked loop is designed. Data recovery has also been presented. It is shown that a frame clock can be extracted from the data sequence that yields the possibility of frame synchronization. A detailed noise analysis has been performed for random offset PPM input.

It has been shown that the proposed clock recovery system is also effective for extracting other data sequence. To elucidate, a multiple Pulse Position Modulation (MPPM) data sequence is considered. The MPPM data sequence has also been synchronised with the recovered clock. A noise analysis is carried out for multiple PPM.

Keywords: *Digital pulse position modulation, Information theory, Maximum likelihood detection, Optical communication, Offset pulse position modulation, Pulse detection errors, Bit error rate, Pulse modulation, Spectral analysis, Fourier transform, Synchronization, Phase Locked Loop, Noise analysis.*

Acknowledgements

The author wishes to express her sincere gratitude and respect to her supervisor, Dr. Martin J. N. Sibley, University of Huddersfield, for his valuable guidance and encouragement for the PhD studies and especially for his technical support, his teaching, editing reviews and constant mental support.

She would also like to thank head of the Department, Electronics and Communication Engineering for giving support and facilities for her studies. The author wishes to express her regard to Professor Bob Cryan for his valuable discussion.

She also would like to thank to her second supervisor Dr. Peter Mather for supporting throughout her studies. She would also like to thank all the faculty members and all the staff of her university.

Special thanks to Sourav, for his love, support, help and inspiration during this work.

Last but not the least, she is extremely grateful to her parents.

Declaration

No portion of the work referred to in this thesis has been submitted in support of an application for another degree or qualification of this or any other university or other institute of learning.

List of Papers

- I. Ray, M. J. N. Sibley and P. J. Mather, "Performance Analysis of Offset Pulse Position Modulation Over Optical Channel", *IEEE Journal of Lightwave Technology*, vol. 30, No. 3, pp. 325-330, February, 2012.

- I. Ray, M. J. N. Sibley and P. J. Mather, "Spectral Characterisation of Offset Pulse Position Modulation", *IET Optoelectronics*, In press.

- I. Ray, M. J. N. Sibley and P. J. Mather, "Bit Error Rate (BER) and Power Efficiency Analysis of Offset Pulse Position Modulation", submitted in *Photonics Letters*.

- I. Ray, M. J. N. Sibley and P. J. Mather, "An Efficient Timing Extraction System Design Using PLL for 1 GHz offset Pulse Position Modulation Data Sequence", submitted in *IET Optoelectronics*.

- I. Ray, M.J.N. Sibley and P. J. Mather, "Slot and Frame synchronization for 1 GHz multiple Pulse Position Modulation Data Sequence", to be submitted.

List of Figures

List of Tables

List of Abbreviations and Notations

PCM ..... Pulse Code Modulation

OOK ..... On-Off Keying

PPM ..... Pulse Position Modulation

DPPM ..... Digital Pulse Position Modulation

OPPM ..... Offset Pulse Position Modulation

MPPM ..... Multiple Pulse Position Modulation

RS code ..... Reed-Solomon Code

GI-POF ..... Graded-Index Plastic Optical Fibre

AWGN ..... Additive White Gaussian Noise

BER ..... Bit Error Rate

PSD ..... Power Spectral Density

DFT ..... Discrete Fourier Transform

ISI ..... Inter-Symbol Interference

IFI ..... Inter-Frame Interference

dBm ..... decibel referenced to $1mW$

$Mbit/s$ ..... Mega bits per second

$erfc$ ..... Complementary error function

cps ..... Cycle per second

rms ..... Root mean square

$\binom{n}{k}$ ..... ${}^nC_k$

T_s ..... Slot time

T_f ..... Frame time

α ..... Positive integer

P_s ..... Probability of wrong slot error

P_r ..... Probability of erasure error

P_f ..... Probability of false alarm error

$\langle n_0^2 \rangle$ ..... Noise on the detected signal

slope (t_d) ..... Slope of the received pulse at the threshold crossing instant

t_d ..... Threshold crossing instant

$v_0(t_d)$ ..... The signal voltage in the slot considered

v_d ..... Decision or threshold level voltage

T_s/τ_R ..... Number of uncorrelated samples per time slot

τ_R ..... Autocorrelation time

v_d ..... Threshold crossing voltage

v_{pk} ..... Peak voltage of the pulse

v_{ISI} ..... Pulse voltage at a particular time slot

Q_s ..... Fraction defined as $\frac{T_s}{2} \times \frac{slope(t_d)}{\sqrt{\langle {n_0}^2 \rangle}}$

Q_r ..... Fraction defined as $\frac{v_{pk}-v_d}{\sqrt{\langle {n_0}^2 \rangle}}$

Q_f ..... Fraction defined as $\frac{v_d-v_{ISI}}{\sqrt{\langle {n_0}^2 \rangle}}$

b ..... Number of photons per pulse

$h_p(t)$ ..... Received Gaussian pulse shape

f_n ..... Channel bandwidth

η ..... Quantum efficiency

q ..... Electronic charge

R_T ..... Mid-band transimpedance of the receiver

S_0 ..... Double-sided noise current spectral density

ξ ..... Transmission efficiency

R/B ..... Band-utilization efficiency

p_{av} ..... Average number of pulse in a codeword of offset PPM

$p(t)$ ..... Square pulse shape

$\mathbb{E}\{\cdot\}$ ..... Expected value

$\langle\cdot\rangle$ ..... Time average

$\mathcal{F}_{\mathcal{T}}\{\cdot\}$ ..... Fourier transform

$S_m^c(f)$ ..... Continuous power spectral density

$S_m^d(f)$ ..... Discrete power spectral density

k_d ..... Phase detector gain

k_v ..... VCO gain

I_{cp} ..... Charge pump current

$A(s)$ ..... Open loop transfer function of PLL

$G(s)$ ..... Closed loop transfer function of PLL

e_{ss} ..... Steady state error

Chapter 1

Introduction

An optical communication system consists of a transmitter which encodes a message into an optical signal, a channel which carries a signal to its destination, and a receiver which reproduces the message from the received optical signal. The information is transmitted in two forms – analog and digital. In analog communication, three key parameters of a carrier signal, namely amplitude, phase and frequency, are modified (modulated) according to the message signal to obtain the modulated signal. Variation of these key parameters produces three modulation schemes – amplitude modulation (AM), phase modulation (PM) and frequency modulation (FM), and the aim is to transmit a signal from transmitter to receiver with as little distortion as possible. In digital transmission the information is converted into binary symbols (bits). The optical carrier is modulated by the information which is detected and decoded by the receiver into the original format. The digital

information is transmitted over the optical link on a bit-by-bit basis (binary encoding) or on a data word basis (block encoding). Two fundamental types of coding generally are used to improve system performance: source coding, channel coding. Source coding is used to reduce the redundancy of the source. Channel coding is used to improve the reliability of the system performance when the information is passed through a noisy or dispersive medium. While the line coding is introduced to overcome the impairment of information due to a noisy channel. In a broader view, the line coding is used to achieve a specific form of information from the incoming data which is more reliable to transmit. The source data is generated in a random manner and thus statistical analysis is required. Two types of source generation are possible: memoryless and with memory. In the literature (in the next section), various coding techniques have been proposed to encode data in the transmitter side so that the receiver can decode data with least error or distortion by utilizing the channel bandwidth properly. Analog signal is converted into digital format by using pulse code modulation (PCM).

In optical communication, the positions of the pulses can be changed according to the incoming digital data. This general form of coding is called pulse position modulation (in Chapter 2). Figure 1.1 shows an optical receiver system, where an optical signal, received by a photodiode, is amplified by an amplifier to a level that helps it to receive data with least distortion due to noisy channel. A filter is used to pass the signal with a specific bandwidth which in turn reduces high frequency noise. The receiver predicts position

of the pulse by using a threshold crossing detection system. A decoder is used to regenerate the signal into its original form. Timing synchronization system is used at the receiver side to synchronize the clock of the incoming data with the received data, so that errors in the received signal can be made as small as possible. Various types of coding techniques have been proposed, analyzed and developed by many authors as discussed in Section 1.1. Also, some form of coding techniques have been discussed in detail in Chapter 2.

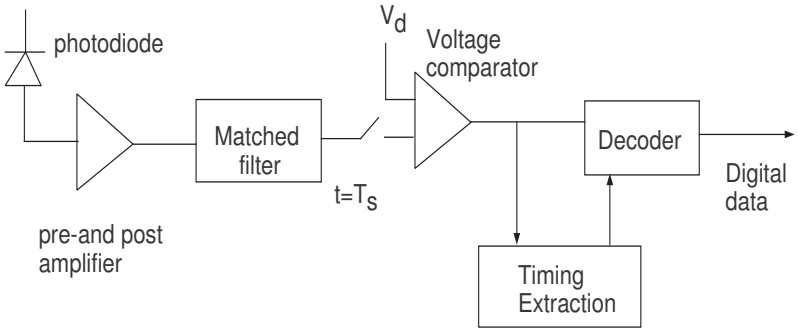

Figure 1.1: Schematic of an optical receiver system

1.1 Literature Review

Pulse Code Modulation (PCM) is a general scheme for transmitting analog data in a binary form independent of the complexity of analog waveform. In [1], Shannon introduced a detailed analysis on the characteristics of digital data at the time of transmission, where the total information was represented by logarithmic function. If the source has to encode N bits of binary data, the total amount of information is equal to $\log_2 2^N = N$. Considering a dis-

crete noiseless channel, it was also shown in [1] that the channel capacity is directly proportional to the amount of information for a time duration. This was mathematically represented as $C = \lim_{T\to\infty} \frac{\log N(T)}{T}$, where $N(T)$ is the amount of information for the time duration T. Also in [1], a framework for statistical analysis of information sources (probability of occurrence, uncertainty, etc.) and characteristics of different types of sources were presented. If a binary memoryless source is considered where the probability of occurrence for symbol 1 is p and for symbol 0 is $q = (1-p)$, then the entropy of the source is calculated as $H = -(p \log p + q \log q)$. All the above characteristics considering the noisy channel were also derived. These results are key to communication theory and afterwards, the analysis of coding theory begins by invoking Shannon's concept of information theory.

Optical communication is a method where photons are used to form an optical pulse and some optical pulse coding techniques have been introduced by changing the temporal position of the pulses. In [3], McEliece described photon counting technology in optical communications. He showed that channel capacity can be increased infinitely considering a noiseless channel and also the signalling efficiency can be 10 *nats/photon* by sacrificing a considerable amount of bandwidth. To overcome this problem, pulse position modulation coding with Reed-Solomon coding was proposed leading to a balanced photon counting channel operated at the efficiency of 3 *nats/photon*. Based on McEliece's idea, Massey [4] analyzed the various factors of the channel such as capacity, cut-off rate, etc. It was shown that the convolutional code system

with Viterbi decoders performed much better compared to the code proposed by McEliece. Marsh and Kahn [5] experimented with indoor data transmission using on-off keying at a data rate of 50 $Mbit/s$. Kobayashi [6] covered different types of coding techniques to overcome random noise with reduced inter-symbol interference (ISI). To overcome synchronization problems, the inclusion of self clocking was introduced. In [7] and [8], the authors investigated the transmission characteristics using low dispersion and dispersionless single mode fibre.

To overcome the difficulties of PCM, many authors proposed different types of pulse modulation techniques. Garret introduced digital PPM ([9], [10]) in its original form to increase the receiver sensitivity with respect to PCM but at the cost of higher line rate or bandwidth expansion. In his work the effect on errors due to the use of direct and heterodyne receiver over a slightly dispersive channel was considered. Timing extraction at the receiver was discussed. Many authors ([11]- [15]) have sought to improve on this scheme. In [11] theoretical analysis of optical digital PPM at the data rate of 50 $Mbit/s$ was implemented considering a PIN-BJT receiver and also assuming a Gaussian pulse. The authors concluded that digital PPM outperforms that of the same PCM system while sacrificing bandwidth. Massarella and Sibley [12] presented an error detection and correction method to reduce the effects of inter-frame interference (IFI). They proposed an error correction method using Reed-Solomon (RS) code applied with digital PPM. Calvert, Sibley and Unwin [13] also examined theoretical modeling of digital

PPM and concluded that digital PPM system can offer better sensitivity (4.2 dB) than an equivalent binary PCM system. Sibley [14] also designed high speed digital PPM and analyzed the system performance.

To consider the line rate reduction, differential PPM, a simple modification of PPM, was introduced. Zwillinger established in [16] that differential PPM has a higher throughput of data than an equivalent digital PPM system. Shiu and Kahn [17] have described differential PPM considering several detection systems in the presence of Additive White Gaussian Noise (AWGN). They derived the expressions of error probability and power spectral density for differential PPM. They showed that differential PPM is more power efficient and has a reduced hardware complexity. In overlapping PPM, described by Bar-David and Kaplan [18], adjacent pulse positions are allowed to overlap that results in line rate reduction. In that paper, they emphasized the merits of overlapping PPM in terms of capacity, cut-off rate, throughput in comparison with OOK and PPM. Patarasen and Georghiades [19] considered the synchronization issues of overlapping PPM as the frame lengths vary in this case. They studied the performance of overlapping PPM using computer simulation considering optimal frame synchronization rules as well as suboptimal approximations. Results were compared with PPM. In [20], authors improved the drawbacks of optical overlapping PPM allowing multiple pulses to overlap without increasing bandwidth. The proposed technique offers better capacity and cut-off rate compared to OOK, PPM and MPPM (Multiple Pulse Position Modulation). Another application of overlapping

PPM with RS codes was also studied in [20]. Synchronization issues were investigated by Calderbank and Georghiades in [21]. They designed a finite state machine and proposed an algorithm for proper synchronization. Shalaby [23] restricted the upper and lower bounds for the overlapping index such that overlapping PPM outperforms digital PPM. It was also addressed by Shalaby in [22] that throughput can be increased by 0.2 $nats/slot$ allowing two pulse positions per pulsewidth to overlap and, as a result, energy requirement is reduced. The achieved maximum throughput is 0.5 $nats/slot$ considering some constraints.

Another coding method called Digital Pulse Interval Modulation (D-PIM), a variation of digital PPM suppressing empty slots preceding a pulse, results in line rate reduction. Using threshold detection scheme, the probability of error for pulse-interval modulation was found by Lee and Schroeder [24] and in support of this scheme, both analytical and numerical results were presented. The performance of this coding technique was investigated in [25] using direct-detection receiver design. Ghassemlooy and Hayes [26] discussed D-PIM for optical wireless communication. Expressions for transmission capacity, power spectrum and error probability were also presented by them. Spectral characterization of D-PIM was evaluated by Cariolaro, Erseghe, and Vangelista [27]. A similar scheme, Dual Header Pulse Interval Modulation (DH-PIM) which uses dual header, was introduced by Aldibbiat et al. ([28]-[32]). This coding scheme offers similar transmission capacity and more bandwidth efficiency compared to PPM and PIM. Also it has self synchronization

capacity. The authors also studied the power efficiency scheme of DH-PIM. The working principle of DH-PIM in the indoor optical wireless environment was demonstrated and subsequently a mathematical derivation for the bit error rate was presented. Spectral properties and closed form expressions for spectral characteristics have been derived by Aldibbiat et al. [32]. In [33], Yan and Minthis analyzed the performance of some modulation schemes such as OOK, PPM, DPPM, DPIM and DH-PIM in terms of bandwidth efficiency, transmission capacity, power efficiency and slot error rate by taking into consideration the optical wireless channel. They concluded from theoretical and numerical results that DPPM, DPIM and DH-PIM are useful for optical wireless communication.

Sibley proposed a combination of a tertiary code (Dicode) and digital PPM to give dicode PPM. In Dicode PPM [34] only data transitions are coded into one of two data slots. It results in a bandwidth expansion of 2 if no guard interval is used, and the sensitivity is comparable with digital PPM. But it gives a sensitivity improvement of 5–11 dB in comparison with PCM. In [35], it was shown that effective three types of errors (wrong slot, false alarm and erasure) can be reduced by using a Maximum Likelihood Sequence Detector (MLSD) algorithm at the receiver side and theoretical results for errors were presented when 1 $Gbit/s$ PCM data was transmitted over a dispersive medium. In [36] the performance of dicode PPM in the presence of a third-order Butterworth filter with a zero-guard interval was examined considering Gaussian pulses. Using this filter the receiver sensitiv-

ity becomes -37.48 dBm for $f_n = 100$ and -32.24 dBm for $f_n = 1.2$ where f_n is the normalised bandwidth. It was also studied that if a PIN-FET receiver is used [37], dicode PPM offers sensitivity of -53.33 dBm at a bandwidth of 1.5 times the PCM bit rate. Cryan in [38] derived expressions for dicode PPM spectrum and the theoretical results were presented in comparison with numerically predicted data. Shortened PPM was introduced for underwater wireless communication. In [39], Cryan derived continuous and discrete spectral equations and theoretical results were compared with numerical results. It was concluded that as SPPM gives both slot and frame rate components, both slot and frame synchronization could be possible.

Multiple PPM is the most bandwidth efficient coding theory among the above mentioned coding techniques. Sugiyama and Nosu in [40] gave a detailed analysis of MPPM on the basis of bandwidth expansion, bit error rate analysis and the amount of information transmitted. Sibley [41] analysed MPPM operating over graded-index plastic optical fibre that offers a sensitivity of -35.51 dBm for a $\binom{12}{2}$ system (12 slot 2 pulse system) with low dispersion. Nikolaidis and Sibley [42] investigated MPPM for eight different numbers of slots over a highly dispersive channel. The analysis showed that small MPPM families are more efficient than the higher families. But middle order families are better for use when bandwidth is considered. They also investigated [43] Gray coding the most effective among linear increment, linear decrement, and random mapping as it minimises the Hamming distance between adjacent multiple PPM words. In [44], they have shown that $\binom{12}{2}$

and $\binom{12}{3}$ MPPM systems offer optimum mapping on the basis of error rate. Although MPPM is the most bandwidth efficient code and its response is satisfactory for ideal channels, the system performance is degraded on multipath channels due to multipath dispersion. This was investigated by Park and Barry [45] in the presence of ISI, and the upper and lower bounds for this system were found. They also proposed a Trellis coded MPPM to combat ISI [46] and the performance of that scheme was examined over a multipath channel. This proposed partial-response precoding is suitable for a wireless infrared channel. The performance of MPPM was also examined by Simon and Vilnrotter [47]. Although MPPM is the most bandwidth efficient code, the implementation of this system is complex. Partial-response was investigated by many authors ([48]- [49]).

Keeping in mind the advantages and disadvantages of all above mentioned coding techniques, Sibley [50] proposed a new coding theory, offset pulse position modulation which is the subject of research in this thesis. An analysis of the different types of errors occurring due to ISI and IFI using graded-index plastic optical fibre (GI-POF) was given by Sibley.

Spectral characterization of different types of coding and how to find closed-form expressions ([58]- [76]) have been research topics for many years. In [58], Cryan presented both the analytical and the numerical power spectral density of n^k PPM. Most of the analytical spectral equations were derived by using the Wiener-Khintchine theorem; Power Spectral Density (PSD) is the Fourier transform of the autocorrelation function considering cyclostationary

properties of the modulation format. However, a discrete time signal is said to be cyclostationary, or to be wide-sense stationary, if the statistical properties are repeated periodically. Gardner ([66]- [69]) did thorough research on cyclostationary and correlation properties, and analysed the effect of those properties on random data sequence and on the spectrum characteristics. In [71], Win derived spectral equations considering different types of data source such as uncorrelated data pulse stream, independent identically distributed binary antipodal data pulse stream, zero-mean Markov source data stream and interleaving independent first-order Markov sources. The analytical results were compared with those numerically obtained values. Win also derived spectral equations considering different types of timing jitter. Elmirghani ([73]- [75]) considered both slot rate and frame rate spectral components for digital PPM and showed that both slot and frame synchronization could be possible. Investigations show that digital PPM exhibits a slot rate component at the slot repetition frequency when return-to-zero pulse is used, but does not provide a frame rate component as the frame has a uniform distribution of pulses. To get the frame rate component at the frame repetition frequency, a guard interval is used consisting of a number of empty slots at the end of the frame.

In order to regenerate binary data at the receiving end of the digital transmission system with the fewest bit errors, the received data must be sampled at optimum instants of time. Since it is usually impractical to transmit the required sampling clock signal separately from the data, timing

information is generally derived from the incoming data itself. The extraction of the clock signal from incoming data is called clock recovery. Timing synchronization in the receiver side has been a strong research problem for decades. Saltzberg [77] introduced timing recovery procedure for binary data transmission. It is shown that by adjusting the sampling time of a random incoming data, frequency offset, jitter, additive noise can be easily calculated and adjusted. Later, many clock recovery processes have been introduced. A reliable approach for clock recovery is the use of a Phase Locked Loop (PLL). Razavi ([78]- [79]) presented clock recovery using monlithic Phase Locked Loop (PLL). The working principle of each individual building block of a PLL was presented and the problem of clock recovery processes was discussed. Many authors ([80]- [93]) proposed different timing extraction procedures with their advantages and disadvantages. Kalita [94] described modeling and simulation of an analytical phase noise model of PLL frequency synthesizer. A detailed noise analysis on all elements of PLL topology has been shown. Mehrotra [95] addressed the problem of noise analysis of a PLL which was formulated using stochastic differential equation solved in the presence of circuit white noise sources. Perrott [96] gave a detailed analysis of different type of PLL design procedures.

1.2 Organization of the Thesis

This thesis consists of eight chapters. The remainder of this thesis is organized as follows:

Chapter 2: Preliminaries

In this chapter, background material is presented which lays the foundation of this thesis. At first, some of the coding techniques are described along with their application areas, advantages and disadvantages. Then, the Fourier transform, the sampling theorem and discrete Fourier transform are briefly reviewed. Next, the Discrete Fourier Transform (DFT) of some signals has been presented. Finally, errors due to discrete Fourier transform are discussed.

Chapter 3: Offset Pulse Position Modulation

This chapter presents the offset pulse position modulation coding scheme. How the requirement of photons per pulse, threshold voltage, sensitivity, and errors change with the variations in coding level in an offset PPM system are presented. Then, a detailed analysis of offset PPM is given. Next, comparisons are made to digital PPM, multiple PPM, and for reference on-off keying (OOK). In this chapter, graded-index plastic optical fiber (GI-POF) is chosen as optical channel and a Gaussian-shaped impulse response is taken into consideration. At last, information theory analysis is given for the first time for offset pulse position modulation.

Chapter 4: Bit Error Rate and Power Efficiency

Bit error rate analysis has been performed in this chapter considering offset pulse position modulation data sequence. The effect of signal-to-noise ratio (SNR) on the signal, when AWGN channel is used, has been shown. Also the power requirement on the basis of photon per pulse is presented.

Chapter 5: Spectrum Analysis

This chapter contains the spectral analysis of offset pulse position modulation, where both the theoretical and numerical results are presented. Slot synchronisation has been discussed as the offset PPM spectrum exhibits a discrete slot rate component. The effect of pulse shaping and modulating index on the spectrum is also presented. Then, frame synchronisation has been taken up as offset PPM exhibits a strong frame rate component. Next, the change of frame rate component with the modulating index is examined. A comparative study on spectral characteristics of digital, multiple and shortened PPM on the basis of dc value, frame rate component and slot rate component is presented. A flow chart for designing offset PPM coder is also given in this chapter.

Chapter 6: Timing Extraction

In this chapter, a Phase Locked Loop (PLL) for clock recovery has been designed. Using the designed PLL, steady state error analysis has been presented. Then, clock recovery technique is presented considering the input data sequence as offset PPM. Next, a data recovery circuit has been used to

recover input OPPM data sequence. In this chapter, it has been shown that frame synchronization is possible using PLL. Finally, a detailed noise analysis has been presented for random OPPM input to elucidate the effectiveness of the designed scheme.

Chapter 7: Timing Synchronization of Multiple PPM

In this chapter, a discussion on slot and frame synchronization is presented on the basis of spectrum. Timing extraction technique presented in Chapter 6 is extended in this chapter using multiple pulse position modulation random data sequence. Using PLL topology, slot clock extraction from MPPM data sequence at the receiver end is presented. Next, noise analysis has been carried out for multiple PPM data sequence.

Chapter 8: Conclusions and Future Works

This chapter concludes the thesis with a summary of the main contributions and an outline of several suggestions for future research in this area.

1.3 Contribution of the Thesis

The main contributions of this thesis are summarised below.

- A detailed analysis of offset PPM coding scheme has been presented. The variation of different parameters such as photons per pulse, threshold voltage, sensitivity, and errors has been measured by changing the coding level in an offset PPM. Comparisons are given considering digital

PPM, multiple PPM, and for reference on-off keying (OOK). Information theory analysis has also been presented for offset pulse position modulation.

- Bit error rate analysis has been carried out considering the offset PPM data sequence, and a comparison with digital PPM and multiple PPM has been presented. The effects of AWGN on offset PPM data sequence is examined. The power efficiency on the basis of photon per pulse has been analysed.

- The spectral analysis of offset pulse position modulation has been presented, where both theoretical and numerical results are given. The slot and frame synchronization have been studied as the offset PPM spectrum exhibits strong slot rate and frame rate component as well. The dependency of spectrum on pulse shape, data distribution on a frame and modulation index is examined. A comparative study on the spectral characteristics considering digital, multiple and shortened PPM is presented. An offset PPM coder has also been designed.

- For clock recovery, an efficient Phase Locked Loop (PLL) has been designed. Using the PLL, it has been shown that the slot clock can be extracted from the data frame with zero steady state error. Data synchronisation can also be made possible with the recovered clock by using data recovery circuit. It is also shown that the frame clock can be recovered and subsequently that frame synchronization is also

possible. These applications have been shown for offset Pulse Position Modulation (OPPM). Furthermore, a detailed noise analysis has been presented for the designed PLL scheme.

- A timing extraction topology is explored in further detail considering different parameters using Multiple Pulse Position Modulation (MPPM) random data sequence. Extraction of a slot clock from the MPPM data sequence at receiver is presented. A noise analysis for the designed scheme is carried out. Results show that the received data can be synchronized with the extracted clock. Based on the spectral characteristics a discussion has also been presented for slot and frame synchronization.

Chapter 2

Preliminaries

In this chapter some background materials are presented which will be required to establish the main results of this thesis. Coding theory is described in brief in Section 2.1. The Fourier transform is revisited in Section 2.2. Section 2.3 presents the sampling theorem. Discrete Fourier Transform (DFT) and the errors due to DFT are described in Section 2.4 and 2.5 respectively. The Wiener-Khintchine theorem is described in Section 2.6.

2.1 Brief Description of Coding Schemes

Some of the coding schemes are discussed here with their advantages and disadvantages.

2.1.1 Pulse Code Modulation (PCM)

Materials presented in this subsection are taken from [105]. Pulse Code Modulation (PCM) is a modulation format to represent any kind of analog signals into digital format. In this modulation format, the amplitude of the analog signal is sampled regularly at uniform intervals, and each sample is quantized to the nearest value within a range of digital steps. The fidelity of a PCM data stream can be categorized using two properties: sampling rate and bit depth. Figure 2.1 shows an analog sine wave sampled at regular intervals. The quantized values at the sampling time instants are 7, 9, 11, 12, 13, 14, 15,

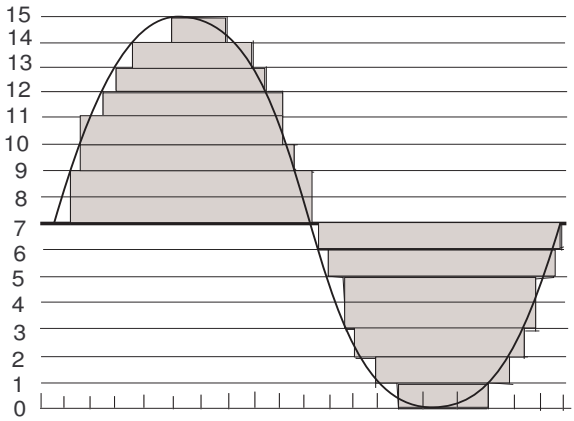

Figure 2.1: Pulse Code Modulation

15, 14, etc. These values will then be encoded into a binary representation to form a set of binary nibbles such as: 0111, 1001, 1011, 1100, 1101, 1110, 1111, 1111, 1110, etc. These digital values could then be further processed or analyzed by a digital signal processor and transmitted as a multiple stream using Time-Division-Multiplexing (TDM) over a single physical layer. This

coding scheme is widely used in digital audio in computers, Compact Discs, modern public telephone system and other digital audio applications. In the receiver side, data is recovered using an Digital-to-Analog Converter (DAC).

2.1.2 On-Off Keying (OOK)

On-off keying is the simplest form of modulation which can represent the digital data independent of the presence of carrier wave. It has low power consumption and low implementation cost. OOK is also used in optical communication systems, RF carrier waves, remote control system.

2.1.3 Digital Pulse Position Modulation (DPPM)

Digital PPM has been proposed ([9]- [15]) for the proper utilization of bandwidth available in optical fibre links. It codes M bits of data into a single pulse that occupies one of 2^M time slots in a block. The coding system is shown in Table 2.1. Sometimes a guard interval consisting of a number of empty time slots is used at the end of the frame to reduce the effects of Inter-Symbol Interference (ISI) and Inter-Frame Interference (IFI) caused by channel dispersion. This coding technique exhibits better sensitivity with respect to on-off keying, but the line rate and bandwidth are increased. The data rate is counted, for example, 10.7 times that of the OOK when encoding 6 bits of data into 64 slots with no guard bits. Although DPPM has great demand in processing electronics, the bandwidth expansion, a disadvantage

of DPPM, restricts its use in other applications; however, it is still a simple and less expensive coding scheme.

2.1.4 Multiple Pulse Position Modulation (MPPM)

This coding scheme ([40]- [47]) uses a number of pulses in a frame where data is being transmitted by $\binom{n}{k}$ number of possible coding combinations (n = number of slots, k = number of pulses in one frame). If $k = 1$, MPPM becomes simple digital PPM. Table 2.1 shows $\binom{5}{2}$ multiple PPM in which a 5-slot frame uses two data pulses to code 3 bits of OOK. Ideally, $k = 2$ is used in $\binom{n}{k}$ for ease of implementation. The Pascal's triangle concept is generally used to choose the values of n and k for a particular OOK bit. Multiple PPM also offers better sensitivity than the digital PPM with reduced line rate. Multiple PPM is the most bandwidth efficient code. Due to the use of different values of pulses in a codeword multiple PPM can run at a lower speed than digital PPM. It is a more complex code and so is costly to implement.

2.1.5 Differential Pulse Position Modulation

Differential Pulse Position Modulation ([17], [16]) is a variation of PPM coding. In differential PPM, data is encoded by removing the zeroes following a pulse. Like digital PIM, in this coding technique the receiver measures the relative distance between successive signals.

2.1.6 Digital Pulse Interval Modulation (DPIM)

Digital Pulse Interval Modulation ([25], [26]) is an asynchronous Pulse Time Modulation (PTM) technique. In this modulation technique data is coded as a number of discrete time intervals or slots, and the information depends on the relative distance between successive pulses but not on the position of the pulses in a frame. It uses a variable frame length. If a symbol encodes M bits of data, the minimum and maximum symbol lengths are $2T_s$ and $(L+1)T_s$, respectively, where T_s is the slot duration and $L = 2^M$. Table 2.1 shows the DPIM coding technique when it encodes 3 bits of data. In order to avoid symbols in which the time between adjacent pulses is zero, an additional guard slot can be added to each symbol immediately after the pulse. The difficulty of this technique is mainly due to the variable word length structure for spectral evaluation. But this variable word length property plays a key role when considering synchronization, since the DPIM does not require symbol synchronization as each signal is initiated with a pulse. Compared to digital PPM, DPIM offers better performance in terms of transmission efficiency and bandwidth requirement.

2.1.7 Shortened Pulse Position Modulation (SPPM)

Shortened Pulse Position Modulation [39] is a coding scheme which was proposed for underwater wireless optical communication. M bits of OOK data are encoded into n bits of the SPPM coding scheme where $n = 1 + 2^{M-1}$.

From Table 2.1 it is apparent that the first bit of OOK is carried on to the first position of the SPPM codeword and the remaining $(M-1)$ OOK bits are conveyed by changing the position of a single pulse in one of the remaining 2^{M-1} time slots. SPPM is more bandwidth efficient than digital PPM as SPPM has bandwidth expansion of $(1+2^{M-1})/M$ whereas digital PPM has $2^M/M$ over OOK.

Table 2.1: Generation of different types of coding from equivalent 3 bits of data

OOK	Digital PPM	Differential PPM	Digital PIM	DH-PIM	Offset PPM	SPPM	MPPM
000	0000 0001	0000 0001	1	100	0000	0 0001	11000
001	0000 0010	0000 001	10	1000	0001	0 0010	10100
010	0000 0100	0000 01	100	1000 0	0010	0 0100	10010
011	0000 1000	0000 1	1000	1000 00	0100	0 1000	10001
100	0001 0000	0001	1 0000	1100 00	1000	1 0001	01100
101	0010 0000	001	10 0000	1100 0	1001	1 0010	01010
110	0100 0000	01	100 0000	1100	1010	1 0100	01001
111	1000 0000	1	1000 0000	110	1100	1 1000	00110

2.1.8 Dual Header Pulse Interval Modulation (DH-PIM)

Dual Header Pulse Interval Modulation ([28]- [32]) is comparatively more complex modulation scheme which offers shorter frame length. It also offers improved frame synchronisation by initiating each frame with one of the two

different types of header pulses. For M bits of OOK signal word, maximum number of slots is $n = 2^M$. Now if OOK frame maps to DH-PIM frame, it starts with a header representing the weight of the input word and then the remaining dT_s (where T_s is the slot duration and $d \in \{0, 1, ..., (2^{M-1}))\}$ represent the information of the input frame. There are possibly two types of header which initiate the word. Depending on the pulse width each header starts with a pulse followed by guard slots consisting of empty slots to avoid multipath dispersion. Figure 2.2 shows the header one (H1) and header two (H2) having pulse duration $\alpha T_s/2$ and αT_s respectively, where α ia a positive integer. It has higher bit rate and requires less transmission bandwidth compared to digital PPM.

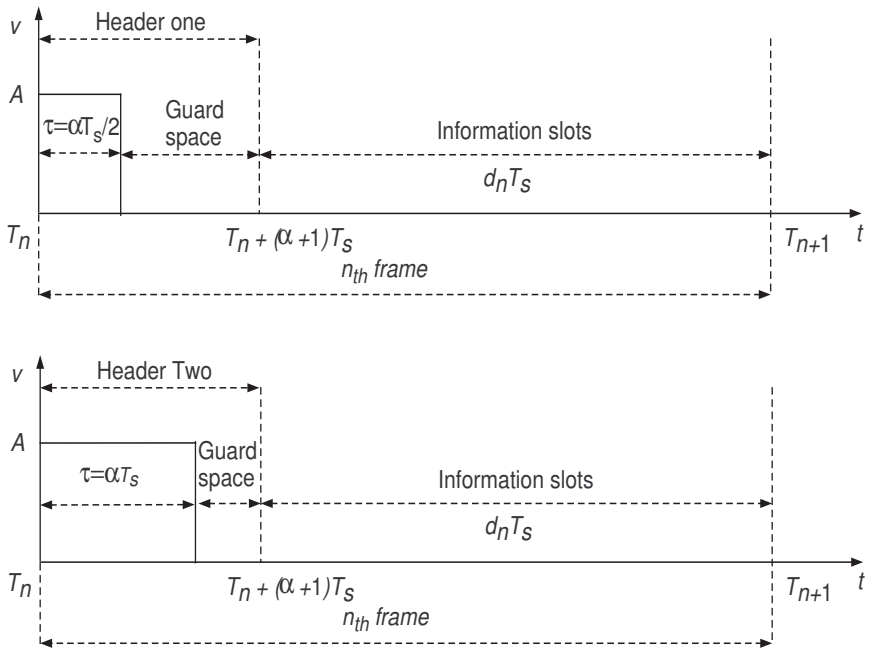

Figure 2.2: DH-PIM word with Header one (up) and Header two (down)

2.1.9 Dicode Pulse Position Modulation

In the dicode technique ([34]- [38]), digital signals are coded according to the data transitions occurring in OOK. So, no signal is transmitted when OOK data is constant. When OOK data transitions occur from logic zero to logic one, the dicode is coded as $+V$ and when data transitions change from logic one to logic zero, the dicode is coded as $-V$, shown in Figure 2.3. From this figure it is seen that no signal is transmitted when there is no change in the logic level. $+V$ pulses are generally regarded as pulse SET (setting data to logic one) and $-V$ pulses are regarded as pulse RESET (resetting the data to logic zero). These two signals are converted into two pulse positions in a data frame. Sometimes two guard slots can be used in dicode PPM to reduce the effects of inter-symbol interference (ISI).

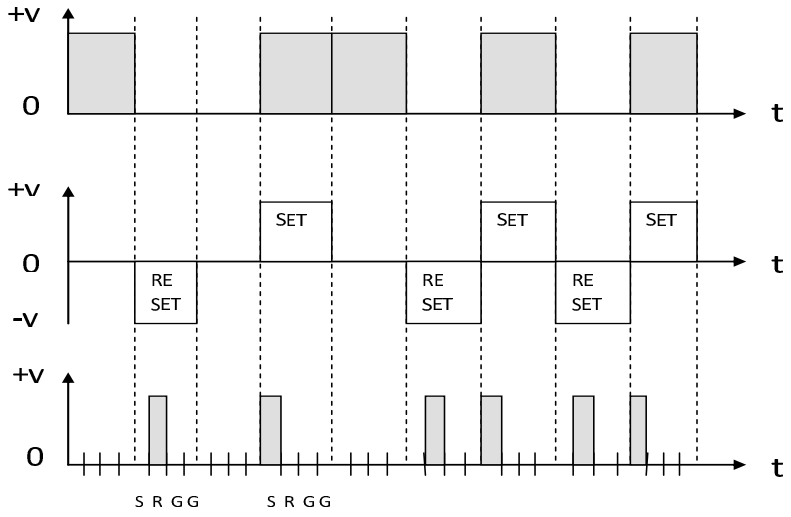

Figure 2.3: Dicode Pulse Position Modulation

2.1.10 Overlapping Pulse Position Modulation

In overlapping Pulse Position Modulation ([23]- [21]) adjacent pulse positions are allowed to overlap. It is a modification of digital PPM. As the pulse positions are overlapped, the line rate is reduced compared to digital PPM but it exhibits higher transmission rate. Also it suffers from the loss of orthogonality due to overlapping. It places more restriction on the synchronization procedure as the frame length is variable. This coding technique also has advantages such as low cycle, ease of decoding and much better throughput efficiency compared to digital PPM which makes it attractive.

2.2 Fourier Transform

The Fourier transform is applied to a signal which is not a periodic signal ([98], [105]). Fourier transform of a continuous signal is defined as

$$X(\omega) = \int_{-\infty}^{\infty} x(t)e^{-j\omega t}dt \tag{2.1}$$

where $x(t)$ and $X(\omega)$ represent the time domain and the frequency domain signals respectively. A signal is fourier transformable if it satisfies the Dirichlet condition. If the signal is continuous in the time domain, it will become aperiodic in the frequency domain and if it is aperiodic in the time domain, it will become continuous signal in the frequency domain.

2.3 Sampling Theorem

The sampling theorem (also known "Shannon's Sampling Theorem" [1]) states that if a function $x(t)$ contains no frequencies higher than B cps, it is completely determined by giving its ordinates at a series of points spaced $1/(2B)$ seconds apart.

A sufficient sample-rate is therefore $2B$ samples/second, or anything larger. Conversely, for a given sample rate f_s the band limit for perfect reconstruction is $B \leq f_s/2$. When the band limit is very high (or there is no band limit), the reconstruction exhibits imperfections, known as aliasing. To sample a continuous time signal, the signal needs to be multiplied by an impulse train and the resultant sampled version leads to periodicity in the frequency domain. To avoid overlapping (i.e., aliasing) in the frequency domain, generally a guard band is used at the end of the signal.

2.4 Discrete Fourier Transform (DFT)

A real, N-periodic, discrete-time signal $x[n]$ can be represented [99] by a linear combination of the complex exponential signals

$$X(k) = \sum_{n=0}^{(N-1)} x[n] e^{-j(2\pi kn/N)} \tag{2.2}$$

where $k = 0, 1, 2, ..., (N-1)$. Here $x[n]$ is a periodic function of period N. To make a non-periodic signal into a periodic one at a certain interval, first, the signal has to be sampled. If the signal is discrete in the time domain, it

becomes periodic in the frequency domain and also, if the signal is aperiodic in the time domain, it will become continuous in the frequency domain by the discrete Fourier transform. Equation (2.2) is concerned with the frequency domain sampling of a finite energy sequence $x[n]$.

Here are some different sampled signals and their DFTs by using Matlab. All the left hand side figures are sampled signals with unit amplitude and the right hand side figures represent their corresponding DFT.

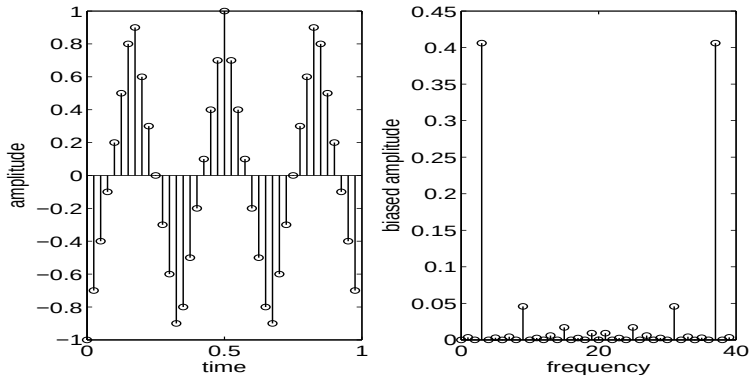

Figure 2.4: Sawtooth wave (left) and discrete Fourier transform (right)

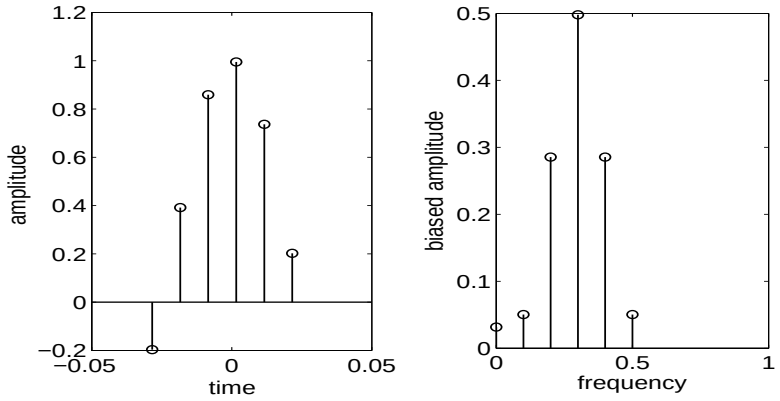

Figure 2.5: Gaussian pulse (left) and discrete Fourier transform (right)

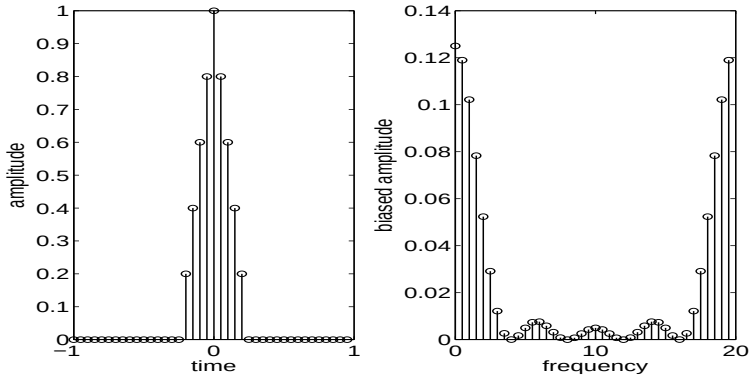

Figure 2.6: Triangular pulse (left) and discrete Fourier transform (right)

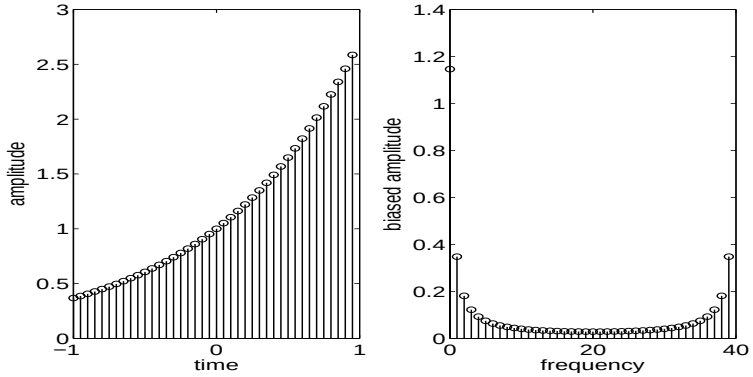

Figure 2.7: Exponential pulse (left) and discrete Fourier transform (right)

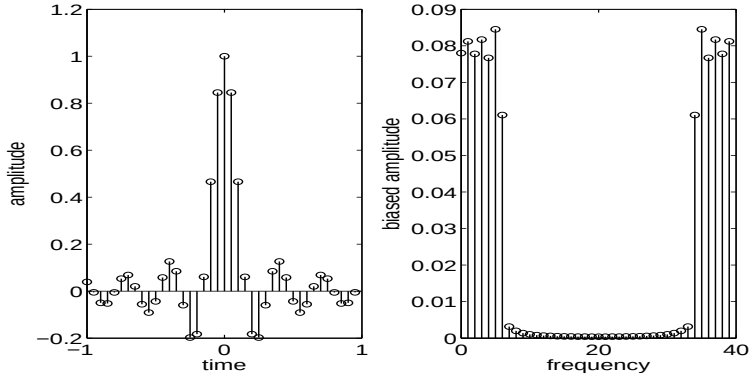

Figure 2.8: Sinc pulse (left) and discrete Fourier transform (right)

2.5 Errors of DFT

There are two types of error that occur in a signal due to the application of DFT: aliasing and leakage.

2.5.1 Aliasing

If signal samples, which represent the high frequency components of the underlying function, are not spaced sufficiently close to DFT values, then those values are corrupted by aliasing. In order to minimize this error, a continuous signal needs to be sampled faster than the Nyquist sample rate of the signal bandwidth, or to be pre-filtered in minimizing its high frequency spectral contents. When the DFT is applied at a sampling frequency exactly equal to twice the frequency of the signal, the spectrum is visible. Figure 2.9 shows the case when continuous time cosine wave with frequency 3 Hz is sampled at 3 Hz, the spectrum is visible but cannot be identified. If a DFT is applied at a sampling frequency which is greater than twice the frequency of the signal, all spectrum is visible and can be identified clearly. Figure 2.10 shows that, if continuous time cosine signal of frequency 3 Hz is sampled at 18 Hz, the spectrum is identified clearly. It can be seen from Figures 2.9 and 2.10 that if the sampling frequency is greater than twice of the signal frequency, then only the spectrum can be identified separately. If the sampling frequency is below the signal frequency, then the spectrum cannot be identified separately and also complete spectrum is not visible.

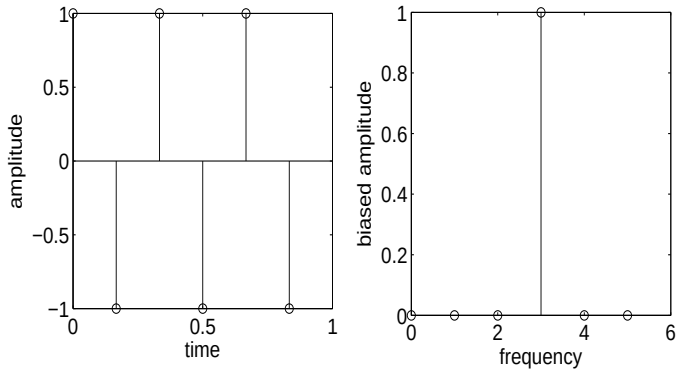

Figure 2.9: Aliasing error (sampling frequency = signal frequency)

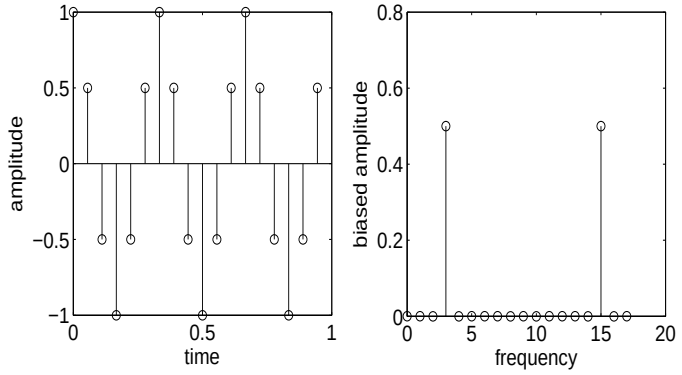

Figure 2.10: Aliasing error (sampling frequency = 18 Hz, signal frequency = 3 Hz)

2.5.2 Leakage

The Fourier transform (equation (2.2)) of a periodic waveform requires summation to be performed over the interval $-\infty$ to $+\infty$ or over an integer number of cycles of the waveform. If it is attempted to complete the DFT over a non-integer number of cycles of the input signal, then the transform must be corrupted in some way. This is indeed the case, as will now be

shown. Consider 3 cycles of a sine wave and the DFT of the signal is shown in Figure 2.11, which is the normal expected spectrum. Now, if there are 3.5 cycles of a sine wave, then the DFT becomes as shown in Figure 2.12. The spectrum for the case of 3.5 cycles is corrupted near the peak. From the above example it is clear that if there is an integer number of cycles of a periodic waveform in the time domain, then a proper spectrum is obtained. If, however, there is not an integer number of cycles (3.5 cycles for example) then there is a discontinuity which is due to leakage. Leakage can be reduced by using a window. Even an increase in DFT length results in a reduction of leakage. Figure 2.13 (left) shows the DFT for 3.5 cycles of a sine wave by appending some number of zeros to increase the window length. Also this leakage can be minimized by increasing the DFT length which is shown in Figure 2.13 (right). Here the DFT length is increased by $N = 128$.

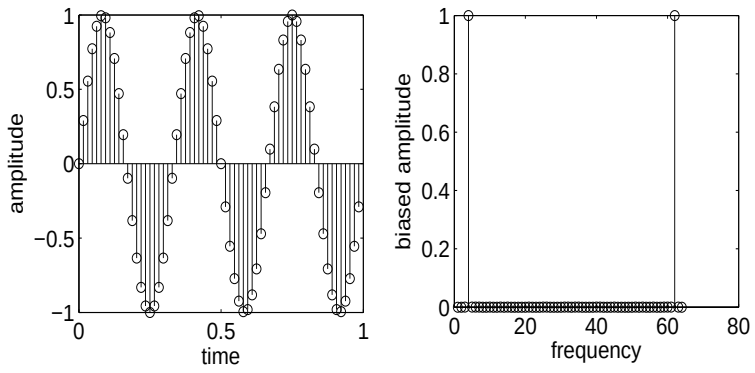

Figure 2.11: Leakage error (DFT of a sine wave for 3 cycles)

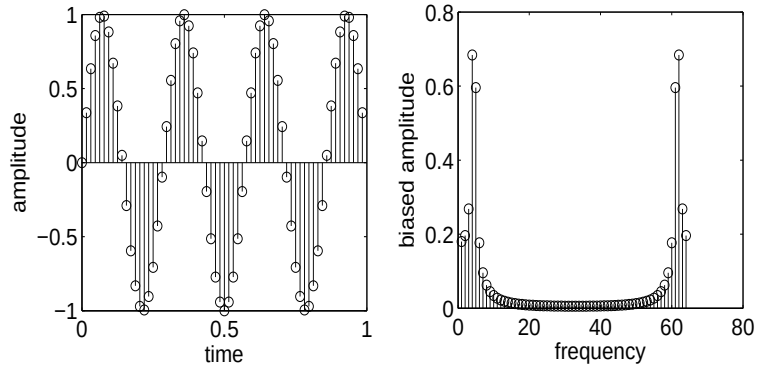

Figure 2.12: Leakage error (DFT of a sine wave for 3.5 cycles)

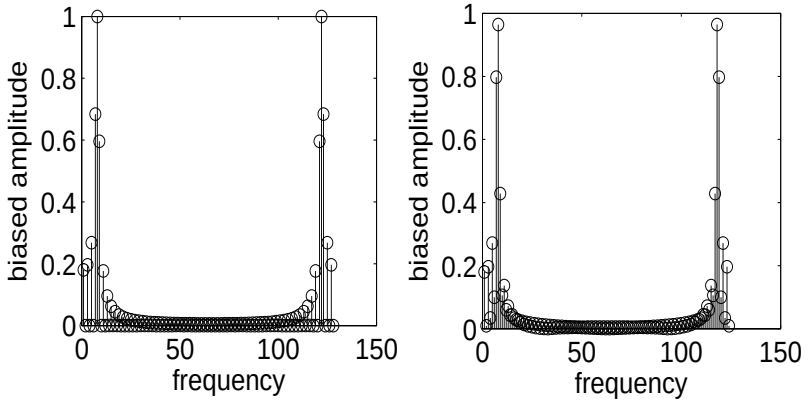

Figure 2.13: DFT of sine wave for 3.5 cycles; increasing window length by appending 60 zeros (left), increasing DFT length by 128 (right)

2.6 Wiener-Khintchine Theorem

The Wiener-Khintchine theorem states that the autocorrelation function of a wide-sense stationary random process has a spectral decomposition given by the power spectrum of that process [105]. In a simple way, the power spectral density is the Fourier transform of the autocorrelation function of a

signal and also autocorrelation function is the inverse Fourier transform of the power spectral density function. This implies that autocorrelation and power spectral density are a Fourier transform pair. A signal to be sampled may be periodic signal or continuous signal. Let $x(t)$ be a real wide-sense stationary process with autocorrelation function $R_{xx}(\tau)$, then,

$$R_{xx}(\tau) = E[x(t)x(t+\tau)] \tag{2.3}$$

where $E[\cdot]$ is the expected value of the signal $x(t)$ and τ is the time difference. Now the power spectral density, $S_{xx}(f)$ becomes according to the Wiener-Khintchine theorem

$$S_{xx}(f) = \int_{-\infty}^{\infty} R_{xx}(\tau)e^{-j2\pi f\tau}d\tau \tag{2.4}$$

and also,

$$R_{xx}(\tau) = \int_{-\infty}^{\infty} S_{xx}(f)e^{j2\pi f\tau}df \ . \tag{2.5}$$

2.7 Stationarity

A random process is said to be stationary process if all the statistical properties, such as mean and autocorrelation, do not change with time [105]. Suppose a random process $X(t)$ has PDF $P_X(x;t_1)$ at time instant t_1, and $P_X(x;t_2)$ at time instant t_2. For a real stationary process,

$$P_X(x;t_1) = P_X(x;t_2). \tag{2.6}$$

For a stationary process the autocorrelation function depends on the time origin through time difference.

$$R_X(t_1, t_2) = R_X(t_1 - t_2) \tag{2.7}$$

Here $R_X(t_1, t_2)$ depends on t_1 and t_2. This could only be possible if the process is time independent. So, all practical processes which are changing with time are not stationary processes. If the autocorrelation function of a process depends only on the time difference $(t_1 - t_2)$ is called a Wide Sense Stationary (WSS) process, i.e.,

$$R_X(t_1, t_2) = R_X(\tau) \tag{2.8}$$

which implies that, for WSS process, it does not matter from where it starts and where it stops but only depends on τ. A wide-sense cyclostationary (WSCS) process is characterized by an autocorrelation function which is periodic in time. That implies,

$$R_X(\tau) = R_X(\tau + T) \tag{2.9}$$

where T is the period and also $R_X(\tau)$ is periodic in τ with period T. Virtually all communication signals exhibit cyclostationarity with cycle frequencies related to hidden periodicities underlying the signal. Often these signals are appropriately modeled by random processes that are cyclostationary (CS), i.e., processes with statistical parameters, such as mean and autocorrelation, that fluctuate periodically with time. These cyclostationary (CS) random processes occur in a wide variety of systems including biological, social, economic, and mechanical as well as electrical systems.

Chapter 3

Sensitivity and Information Theory Analysis

A new coding method, offset Pulse Position Modulation, was proposed in [50] to improve error rate and sensitivity, and to reduce the line rate. This chapter presents a detailed study on the efficiency of this coding approach.

3.1 Coding Scheme

In digital PPM, information is sent by changing the position of the pulse within $N = 2^M$ slots where M is the number of bits to be coded. In offset PPM the concept of a sign bit is used and the number of slots used in one frame is half that of (2^{M-1}) of the equivalent digital PPM scheme. Table 2.1, given in previous chapter, shows the coding scheme when 3 bits of data

are encoded. This scheme is similar to digital PPM except for the use of the sign bit (most significant bit). The introduction of the sign bit reduces the line rate by deciding whether the offset is taken from 0000 or from 1000. No pulse is sent for the 0000 case whereas with digital PPM one pulse is always sent. In this chapter, a performance comparison is carried out with multiple PPM as there are similarities between offset and multiple PPM as shown in Table 2.1.

3.2 Errors

Like other PPM systems, offset PPM suffers from wrong slot, erasure and false alarm errors, and these errors are much affected by Inter-Symbol-Interference (ISI) and Inter-Frame-Interference (IFI) when operating over a highly dispersive channel. The probability of errors is calculated assuming the receiver output noise voltage is a Gaussian random variable. In order to consider the effects of ISI/IFI, particular sequences are considered, such as, ***0*** and ***1*** as isolated pulses and other sequences such as ***0***1, 1***0***, ***1***0, 0***1***, ***1***1, 1***1***, 1***0***1 and 1***1***0. Here the symbol in italics style indicates the position of the error. The derivation of the three possible errors is given by the following [9], [10] and [50].

3.2.1 Wrong Slot Errors

Wrong slot errors are caused by the noise on the leading edge of a pulse producing a threshold crossing preceding or following the current time slot. This error can be minimized if the pulse is detected in the middle of the slot. The error probability is given by

$$P_s = 0.5\ erfc\left(\frac{Q_s}{\sqrt{2}}\right) \tag{3.1}$$

where

$$Q_s = \frac{T_s}{2} \times \frac{slope(t_d)}{\sqrt{\langle {n_0}^2 \rangle}} \tag{3.2}$$

of which T_s is the slot time, slope (t_d) is the slope of the pulse when the pulse is received at the receiver at decision time t_d and $\langle {n_0}^2 \rangle$ is the mean squared noise.

3.2.2 Erasure Errors

This type of error occurs if the receiver fails to detect a pulse within the time frame. Due to noise corruption the pulse amplitude drops down below the decision voltage level (t_d). The error probability is represented as

$$P_r = 0.5\ erfc\left(\frac{Q_r}{\sqrt{2}}\right) \tag{3.3}$$

where

$$Q_r = \frac{v_{pk} - v_d}{\sqrt{\langle {n_0}^2 \rangle}} \tag{3.4}$$

of which v_{pk} represents the peak signal voltage of a particular time slot and v_d represents the decision voltage.

3.2.3 False Alarm Errors

False alarm errors occur if any pulse is detected in the empty slot due to noise. This error can be minimized if the threshold voltage is increased and the corresponding error probability is given by

$$P_f = \left(\frac{T_s}{\tau_R}\right) 0.5\ erfc\left(\frac{Q_t}{\sqrt{2}}\right) \tag{3.5}$$

where the ratio $\frac{T_s}{\tau_R}$ represents the number of uncorrelated noise samples per time slot and τ_R is the time at which the autocorrelation function gives the minimum value.

$$Q_t = \frac{v_d - v_{ISI}}{\sqrt{\langle {n_0}^2 \rangle}} \tag{3.6}$$

where v_{ISI} represents the signal voltage level at a particular time slot and depends upon the error sequences. Figure 3.1 shows the generation of different types of errors from Gaussian type pulse shape.

3.3 Maximum Likelihood Sequence Detection (MLSD)

MLSD is used in the receiver side to minimize the error rate. For example, if an erasure error occurs in any block, the receiver will receive the block containing all zeros or with single pulse in a codeword. Suppose an offset PPM codeword of 1010 (corresponding OOK is 110) is affected by erasure in its first time slot and produces the codeword 0010 corresponding to 010

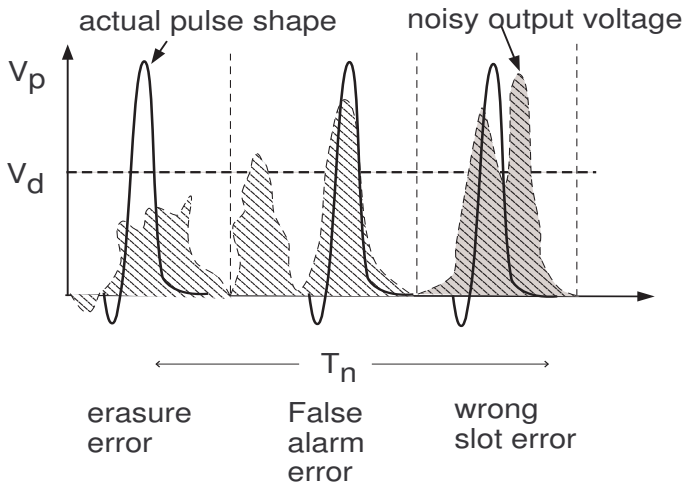

Figure 3.1: Generation of different types of error considering Gaussian type pulse shape

– an error of 1 bit. Erasure of the second pulse gives a valid word of 1000 corresponding to an OOK word of 100 which is also in error by one bit. Thus the average error for this codeword is one bit in three OOK bits.

In the case of a false alarm error, suppose the transmitter transmits the previous codeword and the receiver receives the code as 1110 or 1011. The MLSD here produces four possible valid codewords and the output is in error by an average of 0.75 bits for the three bit OOK word, giving a OOK error of 0.25 ($M = 3$). Other codewords are dealt with in an identical manner and the average is computed. Wrong slot errors are dealt with in a similar way to false alarm errors.

ISI/IFI terms are dealt with by considering particular sequences such as the 1***1*** sequence in which the second pulse suffers with ISI/IFI due to the

first. This sequence is generated when the preceding word has a pulse in the last slot (i.e. 0001 or 1001) and the following word has a pulse in the first slot (i.e. 1XXX where X is the "don't care" condition). The MLSD produces all possible sequences and the error probabilities are calculated as with false alarms. If an MLSD is not used, the receiver will generate random errors. Figure 3.2 represents how the MLSD creates possible codewords to minimise error.

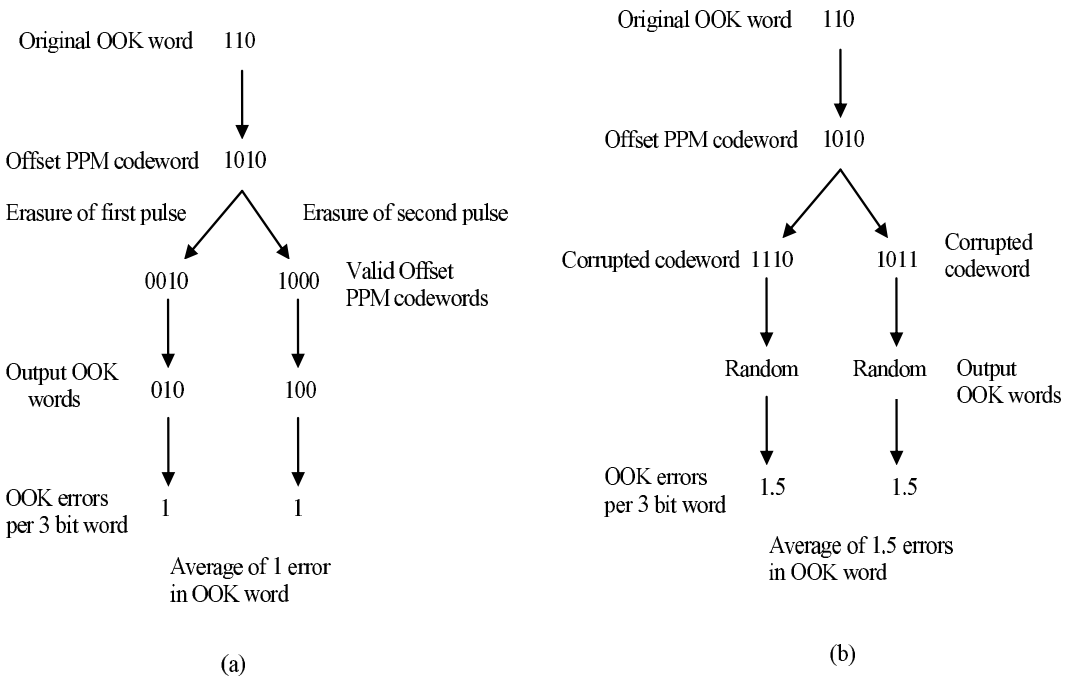

Figure 3.2: Shown how (a) erasures and (b) false alarms affect the decoding of offset PPM

3.4 System Modeling

To analyse the system performance, a 1.2 GHz bandwidth PIN-BJT receiver having a noise current spectral density of $16 \times 10^{-24}\ A^2/Hz$ (double sided) was used. The optical channel used in the simulation had a Gaussian impulse response, as obtained from the graded-index plastic optical fibre (GI-POF) [2]. An operating wavelength of 650 nm was taken, corresponding to the first transmission window in POF, and the photo-diode quantum efficiency was considered to be 100%. An algorithm was used to calculate the number of photons per pulse (b) needed to give an error rate of 1 error in 10^9 pulses of the uncoded data.

Let the received pulse shape, $h_p(t)$, has the following property:

$$\int_{-\infty}^{\infty} h_p(t) = 1. \tag{3.7}$$

The impulse response of the channel (GI-POF) can be approximated to a Gaussian and thus

$$h_p(t) = \frac{1}{\sqrt{2\pi\alpha^2}} \exp\left(-\frac{t^2}{2\alpha^2}\right) \tag{3.8}$$

with a Fourier transform of

$$H_p(\omega) = \exp\left(-\frac{\alpha^2\omega^2}{2}\right). \tag{3.9}$$

The pulse variance, α, is linked to the fibre bandwidth by

$$\alpha = \frac{\sqrt{2\ln 2}\ T_b}{2\pi f_n} \tag{3.10}$$

where T_b is the bit time and f_n is the channel bandwidth normalised to the uncoded data rate, denoted by DR, given by

$$f_n = \frac{f}{DR}. \tag{3.11}$$

Here f is the 3 dB bandwidth of the fibre. As a classical matched filter is being used, the pulse shape presented to the threshold detector is

$$v_o(t) = \frac{b\eta q}{2\pi} \int_{-\infty}^{\infty} H_p(\omega)^2 Z_T(\omega) \exp(j\omega t)\, d\omega \tag{3.12}$$

where b is the number of photons per pulse, η is the quantum efficiency of the detector (taken to be unity), q is the electronic charge and $Z_T(\omega)$ is the frequency dependent transimpedance of the receiver (assumed to be single pole). The solution to equation (3.12) is

$$v_o(t) = b\eta q R_T \frac{\omega_c}{2} \exp\left(\alpha^2\omega^2\right) \exp(-\omega_c t)\, erfc\left(\alpha\omega_c - \frac{t}{2\alpha}\right) \tag{3.13}$$

where R_T is the mid-band transimpedance of the receiver and ω_c is the -3 dB bandwidth of the receiver. The noise on this signal is given by

$$\left\langle n_o^2 \right\rangle = \frac{S_o}{2\pi} \int_{-\infty}^{\infty} |Z_T(\omega) H_p(\omega)|^2 d\omega \tag{3.14}$$

$$= S_o \frac{\omega_c}{2} R_T^2 \exp\left(\alpha^2\omega_c^2\right) erfc(\alpha\omega_c) \tag{3.15}$$

where S_o is the double-sided, equivalent input noise current spectral density of the receiver. A PIN photodiode has been used and hence its shot noise can be ignored.

The total equivalent data error probability is obtained by adding all individual probabilities. These probabilities are found by using the probability

equations [50] and multiplying by the weightings from the MLSD analysis. The OOK error probability has been taken 1 error in 10^9 bits. The pulse shapes, derivatives, noise and the number of photons per pulse were calculated using system parameters. False alarm and erasure errors depend on the threshold voltage v_{th} which has been defined as

$$v_{th} = \frac{v_d}{v_{pk}} \tag{3.16}$$

where v_{pk} is the peak voltage of the signal. To find the sensitivity of the system, the photons (b) required per pulse is calculated using an algorithm, and the sensitivity (S_{DPPM}) is defined for digital PPM as

$$S_{\text{DPPM}} = 10\log_{10}\left(1 \times b \times \text{energy} \times \frac{DR}{M} \times \frac{1}{10^{-3}}\right)\ dBm \tag{3.17}$$

where DR is the uncoded data rate. Similarly, with offset PPM the sensitivity (S_{offset}) is defined as

$$S_{\text{offset}} = 10\log_{10}\left(p_{av} \times b \times \text{energy} \times \frac{DR}{M} \times \frac{1}{10^{-3}}\right)\ dBm\ . \tag{3.18}$$

As there is uneven distribution of the pulse in the offset PPM code, the average number of pulse, p_{av}, in a offset codeword is used. For a 2 pulse multiple PPM system the sensitivity is defined as

$$S_{\text{MPPM}} = 10\log_{10}\left(2 \times b \times \text{energy} \times \frac{DR}{M} \times \frac{1}{10^{-3}}\right)\ dBm\ . \tag{3.19}$$

The energy/photon is defined as

$$\text{energy} = \frac{hc}{\lambda}\ \ J \tag{3.20}$$

where h is the Planck's constant; c is the speed of light in vacuum; λ is the wavelength of the transmitted light.

3.5 Theoretical Result Analysis

Figure 3.3 depicts the variation in photons per pulse versus the channel bandwidth f_n, normalised to the uncoded data rate, for different coding levels. From this figure it can be seen that as the number of data bits is

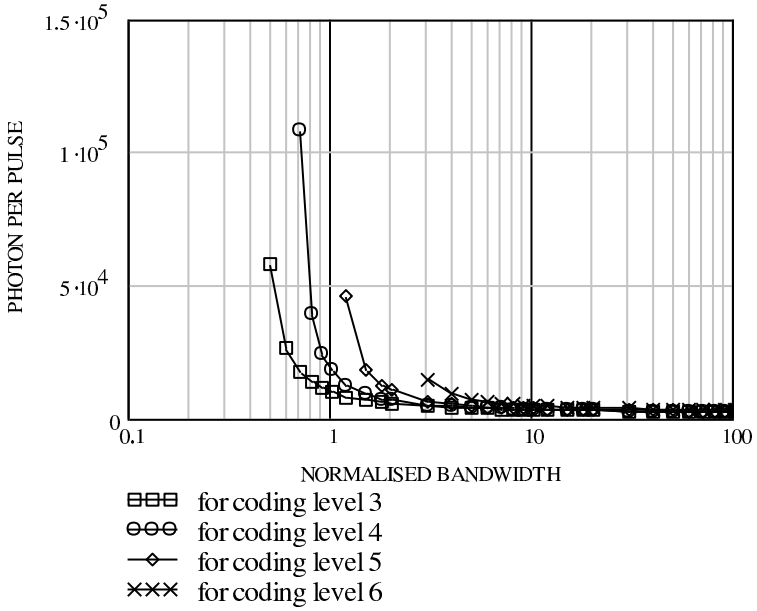

Figure 3.3: Required photon vs. bandwidth Plot

increased, the number of photons required per pulse will also increase for a particular bandwidth. As a result the sensitivity decreases with an increase in the coding level and this sensitivity variation is shown in Figure 3.4. In the lower bandwidth the photon requirement increases as the effects of ISI is increased. The effect of ISI and threshold level has a great impact on the errors and depends on the coding level as well as bandwidth. When the bandwidth $f_n = 1.2$ (Figure 3.5), the threshold voltage is just below the

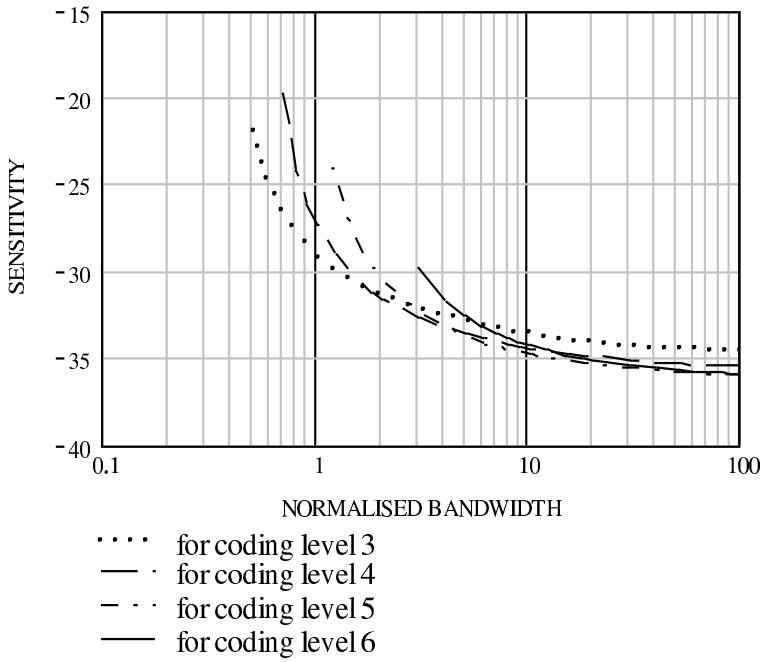

Figure 3.4: Sensitivity plot

minimum voltage for offset PPM when the equivalent data codeword is 110. It implies the probability of erasure error is increased, but the probability of false alarm error is reduced. With the increase in the coding level the threshold level also increases resulting in a decrease in the false alarm errors (Figure 3.6). How the errors will change with the change in bandwidth and with the coding level is clearly shown in Table 3.1.

Figure 3.7 compares offset PPM with digital PPM, multiple PPM and on-off keying for coding level 6 bits on the basis of sensitivity change. In this figure at $f_n = 10$, the sensitivity for offset PPM, digital PPM, multiple PPM and on-off keying are respectively -34.25 dBm, -33.06 dBm, -34.49 dBm and

Table 3.1: Error table for offset PPM

Number of OOK bits	Bandwidth f_n	False Alarm				Erasure	Wrong Slot
		P_f	P_{f01}	P_{f10}	P_{f101}	P_{e01}	P_s
4	100	1.433×10^{-10}	3.124×10^{-11}	2.824×10^{-10}	3.68×10^{-11}	5.064×10^{-10}	0
	10	7.707×10^{-11}	1.68×10^{-11}	3.425×10^{-10}	4.463×10^{-11}	5.191×10^{-10}	0
	3	5.122×10^{-13}	1.117×10^{-13}	4.183×10^{-10}	5.452×10^{-11}	5.27×10^{-10}	0
5	100	1.444×10^{-13}	2.01×10^{-14}	4.182×10^{-10}	5.437×10^{-11}	5.273×10^{-10}	0
	10	1.915×10^{-15}	0	4.249×10^{-10}	5.523×10^{-11}	5.208×10^{-10}	0
	3	0	0	3.769×10^{-10}	4.945×10^{-11}	5.753×10^{-10}	0
6	100	0	0	2.904×10^{-10}	1.629×10^{-10}	5.477×10^{-10}	0
	10	0	0	2.955×10^{-10}	1.657×10^{-10}	5.385×10^{-10}	0
	3	0	0	1.147×10^{-14}	3.457×10^{-10}	6.546×10^{-10}	0

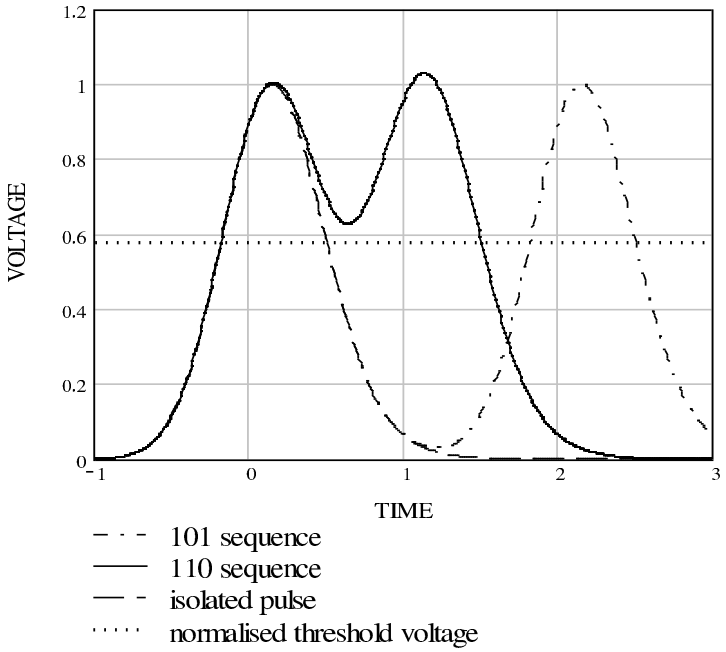

Figure 3.5: Effect of ISI for 3 bits of coding at $f_n = 1.2$

-26.05 dBm. With the increase in bandwidth the sensitivity for offset PPM has been increased and at $f_n = 30$ and onwards, offset PPM gives better sensitivity in comparison with the other coding. At the lower bandwidth $f_n = 3$, offset PPM gives 3.7 dB advantage over on-off keying and 3.2 dB advantage over digital PPM. With the increase in coding level the threshold voltage also increases as shown in Figure 3.8 and the comparison with digital PPM for coding level 6 is shown in Figure 3.9. An increase in the threshold voltage means a decrease in the false alarm error.

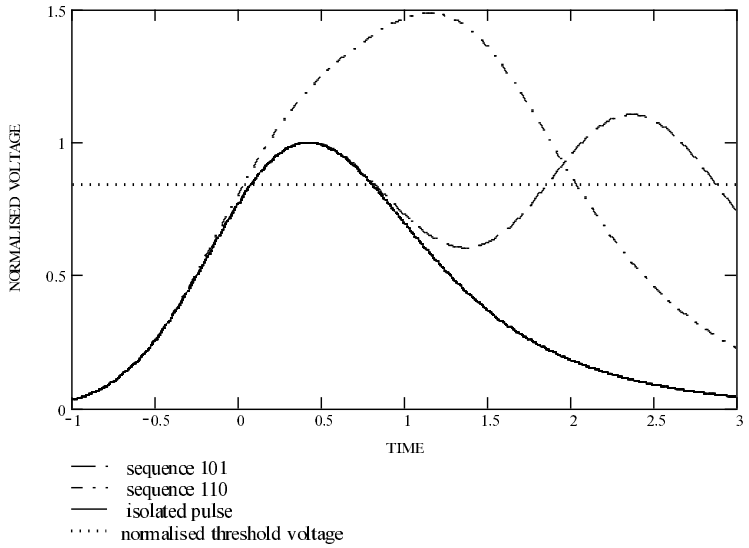

Figure 3.6: Effect of ISI for 6 bits of coding at bandwidth $f_n = 3$

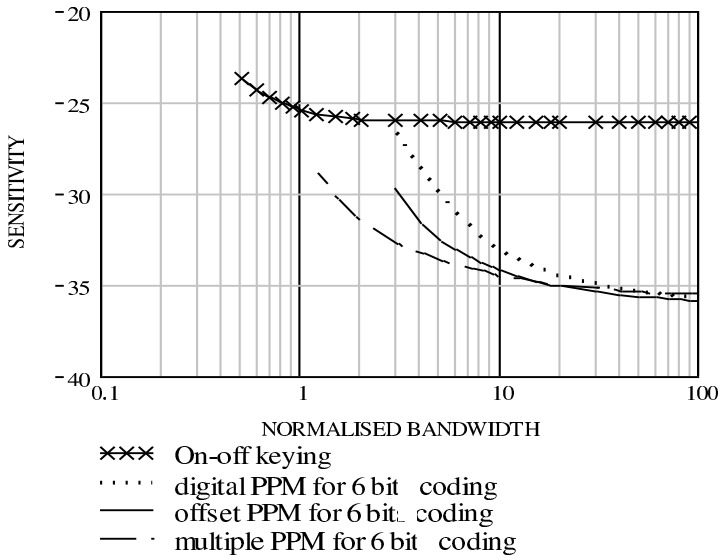

Figure 3.7: Comparison of the sensitivity for offset PPM, digital PPM, multiple PPM and on-off keying

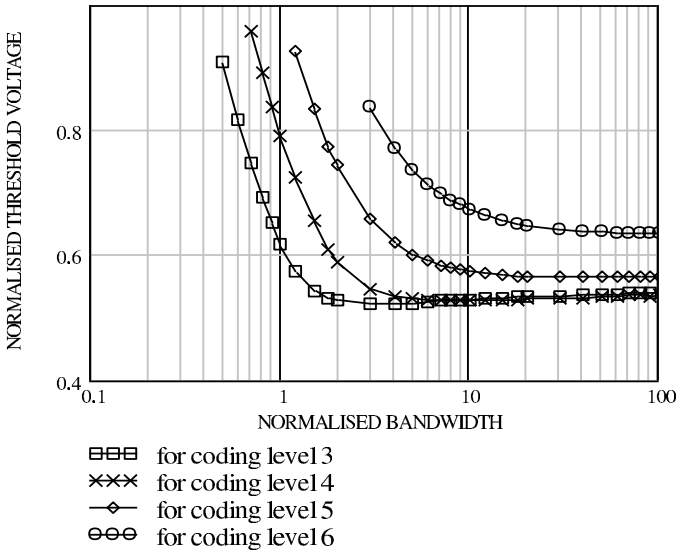

Figure 3.8: Threshold parameter vs. normalized frequency plot

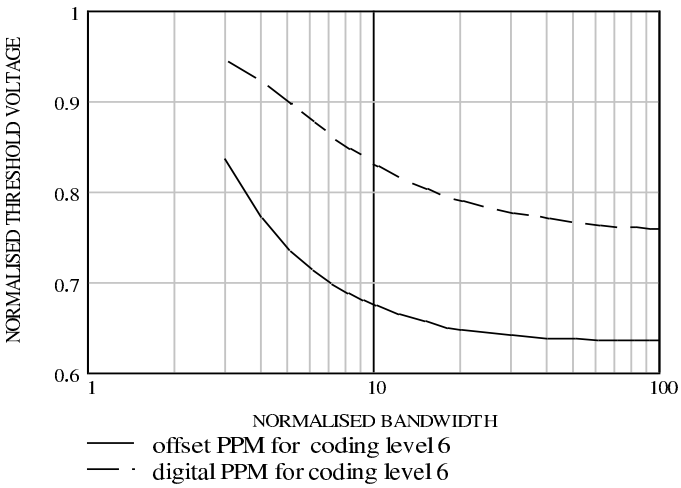

Figure 3.9: Comparison of threshold parameter between offset PPM and digital PPM for 6 bits of coding

3.6 Information Theory Analysis

In digital PPM each signal block is divided into N equal time slots. One optical pulse is transmitted in any one of the time slots for each frame. So information is sent by the position of the pulses in the frame. Therefore the amount of information sent during each signal block is $\log_2 N$ bits. In the receiver, a threshold detector detects the position of the pulses within the N slots. The amount of information (bits) transmitted per photon, defined as transmission efficiency, depends upon the intensity of the optical pulses which is set at such a level that the receiver can detect them.

One optical pulse carries $\log_2 N$ bits of information. Therefore the transmission efficiency (ξ) can be expressed as [40]

$$\xi = \frac{(\log_2 N)}{b} \tag{3.21}$$

where b is the number of photons per pulse. According to this expression the transmission efficiency can be increased theoretically infinitely. In practical terms this is not possible because the value of b cannot be reduced beyond a certain level as the error rate is increased. If N is increased, the pulse width is reduced and the bandwidth requirement will expand, and, in turn increase the noise.

The time required to transmit one frame of N slots is represented by T. Thus a bandwidth term can be expressed as

$$B = \frac{N}{T} \quad (Hz) \ . \tag{3.22}$$

From equation (3.22) it can be seen that B is directly proportional to N. The information rate can be derived as

$$R = \frac{(\log_2 N)}{T} \ (bits/s) \ . \tag{3.23}$$

If the value of N is increased, R varies logarithmically with N and, as a result, the band-utilization efficiency (R/B) degrades rapidly as shown by

$$\frac{R}{B} = \frac{(\log_2 N)}{N}. \tag{3.24}$$

For example if $N = 32$, (R/B) will become 0.156 which means a band-utilization efficiency of approximately 16%.

In the case of offset PPM, there is a nonuniform distribution of pulses (for 000 = no pulse, 001 = p, 110 = $2p$). So, the average number of pulse per codeword must be taken. Thus

$$p_{av} = \frac{2(2^{(M-1)} - 1) + 2^{(M-1)}}{2^M} \ . \tag{3.25}$$

So, the amount of information per pulse (shown in Figure 3.10) becomes $(\log_2 N)/p_{av}$ and information rate can be written as

$$R = \frac{(\log_2 N)}{p_{av} T} \ (bits/s) \tag{3.26}$$

and the band-utilization efficiency (R/B) becomes

$$\frac{R}{B} = \frac{(\log_2 N)}{p_{av} N'} = \frac{2(\log_2 N)}{p_{av} N}. \tag{3.27}$$

Here N' is the number of slots in offset PPM and always $N' = N/2$. Taking $N = 32$, R/B will become 0.217 which means, offset PPM has a band-utilization efficiency of 22%.

How the band-utilization efficiency changes with the change in the coding levels is shown in Figure 3.11. The digital PPM curve is shown for comparison. Figure 3.12 gives a clear picture of the change of transmission efficiency with the change in the bandwidth.

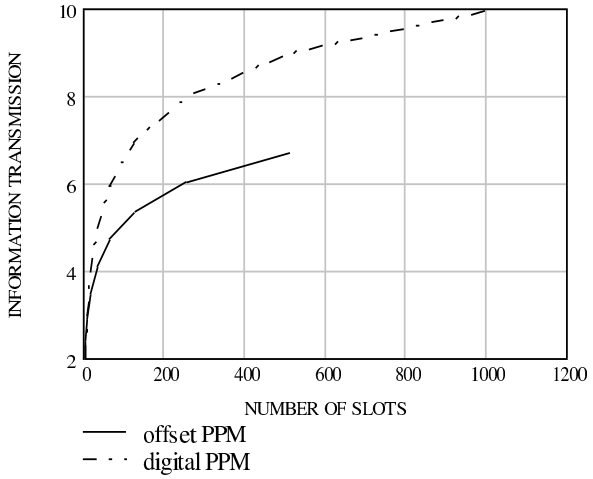

Figure 3.10: Information transmission rate vs. number of slots plot

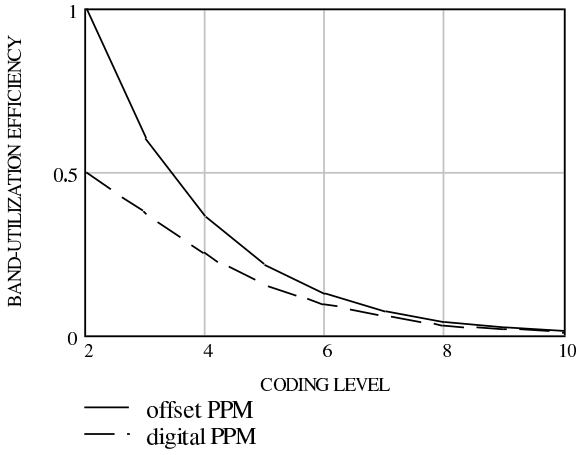

Figure 3.11: Band-utilization efficiency vs. number of coded bits

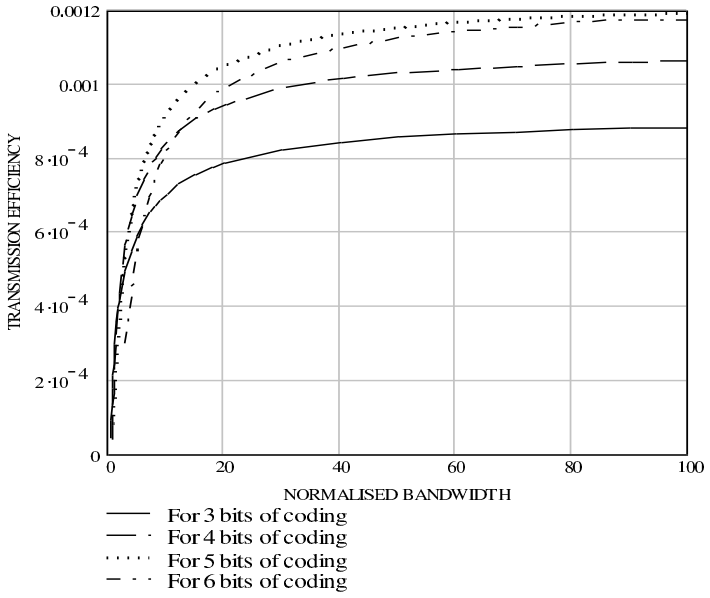

Figure 3.12: Transmission efficiency vs. normalised bandwidth plot for different coding level in offset PPM

In multiple PPM, optical pulses are transmitted in multiple slots in one signal block. If the number of the optical pulses transmitted during one signal block is K, then $\binom{N}{K}$ pulse patterns can be formed by combining the position of the pulses. This means that multiple PPM transmits $\log_2\binom{N}{K}$ bits of information per signal block. Transmission efficiency becomes for multiple PPM scheme

$$\xi = \frac{\log_2\binom{N}{K}}{b} \ . \tag{3.28}$$

Here b is the number of photons required. Now the information transmission rate will become

$$R = \frac{\log_2\binom{N}{K}}{T} \ (bits/s) \ . \tag{3.29}$$

Band-utilization efficiency (R/B) is derived as

$$\frac{R}{B} = \frac{\log_2(\binom{N}{K})}{N} \ . \tag{3.30}$$

Figure 3.13 shows the change of band-utilisation efficiency with the change in the number of slots keeping $K = 2$. Table 3.2 gives the comparison among offset PPM, digital PPM and multiple PPM. As can be clearly seen, this analysis shows that digital PPM has the poorest band-utilisation (BU) efficiency. This is important when considering low bandwidth channels.

Figure 3.14 shows how information transmission rate will change for different values of K in case of MPPM scheme. Figure 3.15 shows the comparison of the transmission efficiency between OPPM and MPPM for 6 bits of coding.

Figure 3.13: Band-utilization efficiency vs. number of slots plot for multiple PPM

Table 3.2: Comparison of offset PPM, digital PPM and multiple PPM

	Offset PPM				Digital PPM				Multiple PPM			
Coding level	3	4	5	6	3	4	5	6	3	4	5	6
Information (bit)	2.4	2.9	3.5	4.1	3	4	5	6	3.3	4.4	5.2	11
BU efficiency	60%	36%	22%	13%	36%	25%	16%	10%	66%	63%	56%	50%

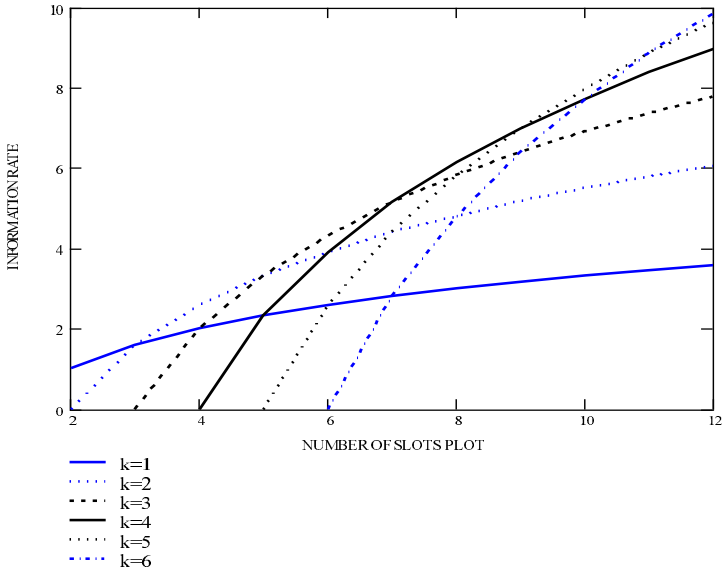

Figure 3.14: Information rate vs. number of slots plot for different value of k for MPPM

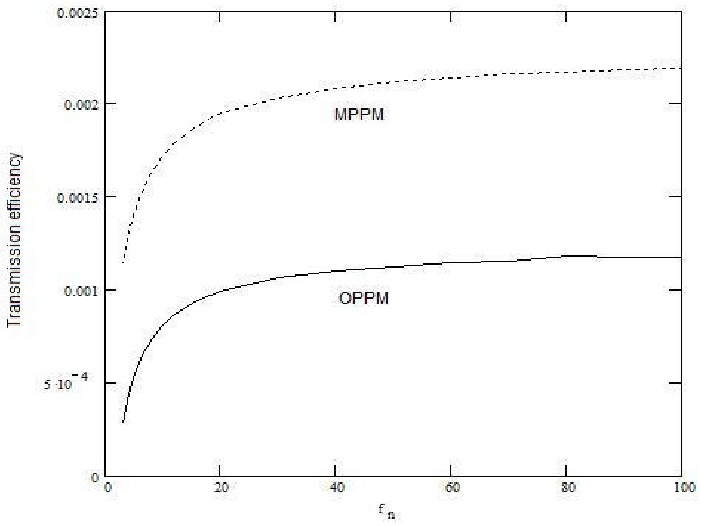

Figure 3.15: Comparison of transmission-efficiency for OPPM and MPPM

3.7 Conclusion

The performance of offset PPM in terms of varying coding level and channel bandwidth has been analysed in this chapter. In order to implement the system a Gaussian impulse response is considered and the performance of the offset PPM has been compared to that of OOK, digital PPM and multiple PPM using MathCad toolbox.

The theoretical model, presented in this chapter, shows that offset PPM offers a sensitivity 3.27 dB greater than digital PPM when both are operating at a normalised bandwidth of 3 with a coding level of 6. At the higher channel bandwidth, where minimal inter-symbol interference occurs, offset PPM offers a significant sensitivity advantage over the On-Off Keying of nearly 10 dB. It has been shown that the effect of ISI will increase when there is an increase in the bandwidth as well as in the coding level. Offset PPM also has a better sensitivity than that of multiple PPM at higher bandwidth channels.

In this chapter, Information theory analysis has also been considered when there is an uneven distribution of pulses. Results show that offset PPM has better band-utilization efficiency as well as transmission efficiency than digital PPM.

Chapter 4

Bit Error Rate and Power Efficiency

This chapter presents the performance of offset PPM on the basis of Bit Error Rate (BER) and power requirement. The main objective of any communication system is to receive the transmitted data with the minimum number of errors possible; the BER depends on the selection of a suitable modulation technique.

4.1 Bit Error Rate

In digital transmission the number of bit errors is the number of received bits of a data stream over a communication channel which are altered due to noise, interference, distortion or bit synchronization errors. Numerically

the bit error rate (BER) is the number of bits in error divided by the total number of transferred bits during a particular time interval and is given by [105]

$$\text{Bit Error Rate} = \frac{\text{Number of bits in error}}{\text{Total number of transmitted bits}}.$$

In essence, BER is the probability of receiving a single bit in error. The probability of receiving a bit in error is equivalent to the BER of a communication link when an infinite number of bits are sent and received. If the propagation medium is extremely good and the signal to noise ratio is also very high, then BER becomes negligible in the overall system. To evaluate a system, BER assessment is the best way as it gives full system performance including transmitter, receiver and also the medium.

In order to accurately analyse BER, the contribution from each signal level must be accounted for by weighting the BER of a particular signal level with the probability of the signal being at that level. The BER is very sensitive to SNR. Accordingly, a small increase in the signal level results in a small improvement in SNR which, in turn, provides significant improvement in BER. In addition to voltage signal-related effects, timing uncertainty or jitter can often lead to degradation of link BER. In brief, the primary point of concern related to timing is the relative relationship in time between the data and clock. Under ideal conditions, the receiver samples the incoming data stream at the point in eye diagram where the signal margin is the largest. By doing so, the BER will be optimized. The factors which affect BER the most are SNR ratio, bandwidth selection of the channel, channel model and

modulation schemes. For a fibre optic system, the BER is mainly introduced because of signal dispersion, attenuation and imperfection of the components used in the data link. Reduction of bandwidth limits the data throughput which could be controlled by increasing the power level.

The BER is different for each modulation method. The energy per bit can be increased and the BER can be reduced by using higher power transmission. However, this may not always be possible. Hence, optimizing the signal to noise ratio E_b/N_o is a trade-off among these factors, where E_b is the energy in one bit and N_o is the noise power spectral density.

The offset Pulse Position Modulation technique has been described in the previous chapter. The introduction of a sign bit has reduced the line rate as well as bandwidth in comparison to digital PPM (Table 2.1, Chapter 2). The performance of an offset PPM based modulation system is measured by calculating its probability of error with an assumption that systems are operating with additive white Gaussian noise (AWGN). The probability of error (where the probability of a zero occuring = probability of a one occuring = 1/2) is given by [105]

$$P_b = Q\left(\sqrt{\frac{E_b}{N_0}}\right) \tag{4.1}$$

where $Q = \frac{1}{2}erfc(\frac{x}{\sqrt{2}})$. Equation (4.1) is the mathematical expression for BER and the numerical evaluation is done by Matlab. For the numerical analysis, the input data sequence is considered to be an offset PPM data sequence (256 frames are taken randomly). Each bit of that sequence is sampled with a sampling frequency more than the carrier frequency. The

sampled sequence is then modulated using the pulse position modulation method ('ppm' in Matlab). To add Gaussian noise, the modulated signal is passed through an AWGN channel. How the channel noise affects the signal with change in the SNR ratio is shown in Figure 4.1. The channel output signal is received at the receiver which demodulates the signal using pulse position demodulation method. The transmitted offset PPM data sequence and the demodulated data sequence are then compared to calculate bit error. The result is shown in Figure 4.2. It is clear from the figure that, with the increase in SNR, BER will be reduced. Here a comparative study is presented considering digital PPM and multiple PPM. This figure depicts that multiple PPM produces a greater number of errors than other codes for the same SNR.

4.2 Power Requirement

The average power required to transmit one frame is calculated as

$$\text{Required Power (P)} = \frac{\text{number of pulses present}}{\text{number of slots in that frame}} \ . \tag{4.2}$$

Here the term 'power' represents the amount of photons per slot, or in other words, the amount of energy required to transmit a single frame. How the number of photons varies with the change in bandwidth is shown in Figure 3.3 (in the previous chapter). If the number of pulses is changed, the photon requirement also changes; and if the number of slots in a frame is changed, the bandwidth changes. It implies that all three terms (photon requirement,

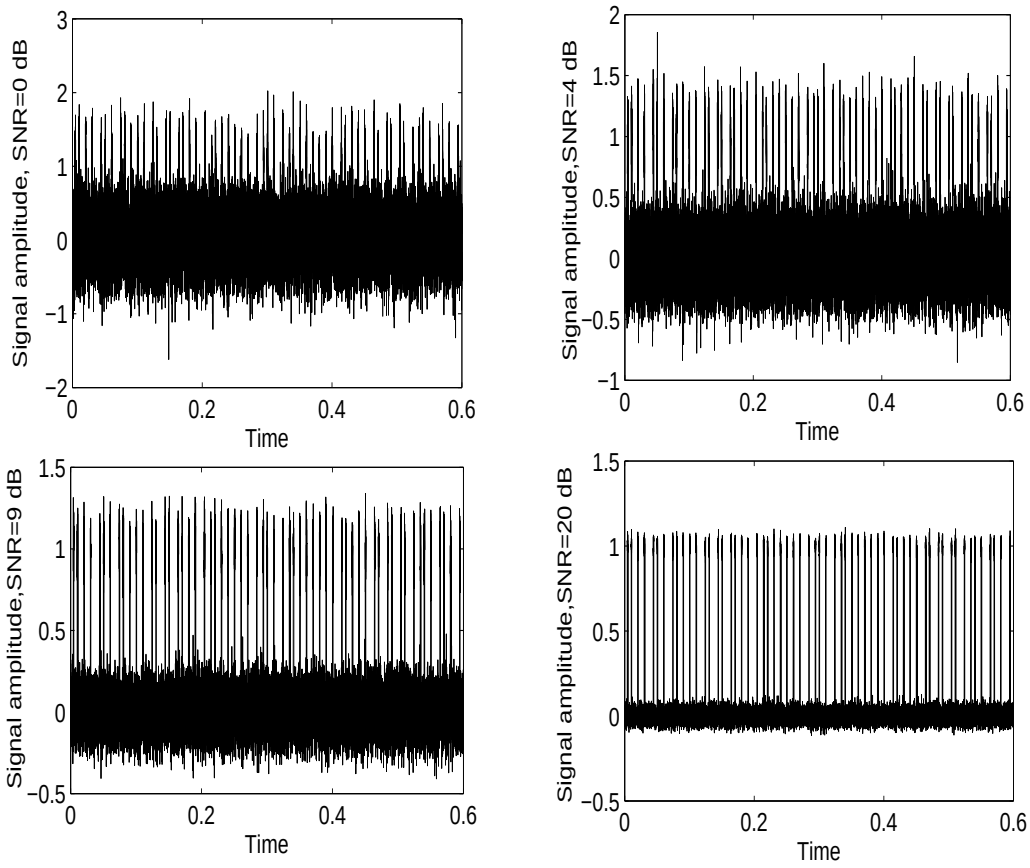

Figure 4.1: OPPM signal after passing through AWGN channel at different SNR (dB)

number of slots and number of pulses) are related. Here an analysis has been done measuring the power requirement. For MPPM, one frame always uses fixed number of pulses; for example, if $k = 2$, the required power is

$$P_{MPPM} = \frac{2}{\text{number of slots}}. \tag{4.3}$$

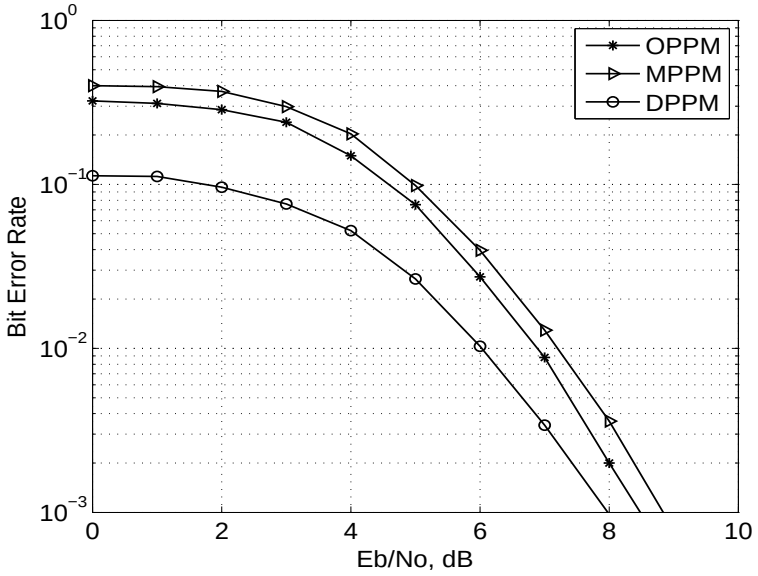

Figure 4.2: BER for 3 bits of coding using AWGN noise

But as OPPM has uneven distribution of pulses, the average value of pulses is taken and the required power for OPPM becomes

$$P_{OPPM} = \left(\frac{2(2^{(M-1)}-1)+2^{(M-1)}}{2^M}\right) \Big/ (\text{number of slots})\,. \tag{4.4}$$

Figure 4.3 shows how the power requirement changes with the change in the number of slots for MPPM. In Table 4.1, it has been shown clearly how power requirement will change with the change in the number of OOK bits for OPPM (Figure 4.4). It can be seen from both Table 4.1 and Figure 4.4 that, the average number of pulses has become constant (1.5) for the higher bits of coding. If Figures 4.3 and 4.4 are compared for the equivalent code, then it can be inferred that OPPM is more power efficient than MPPM.

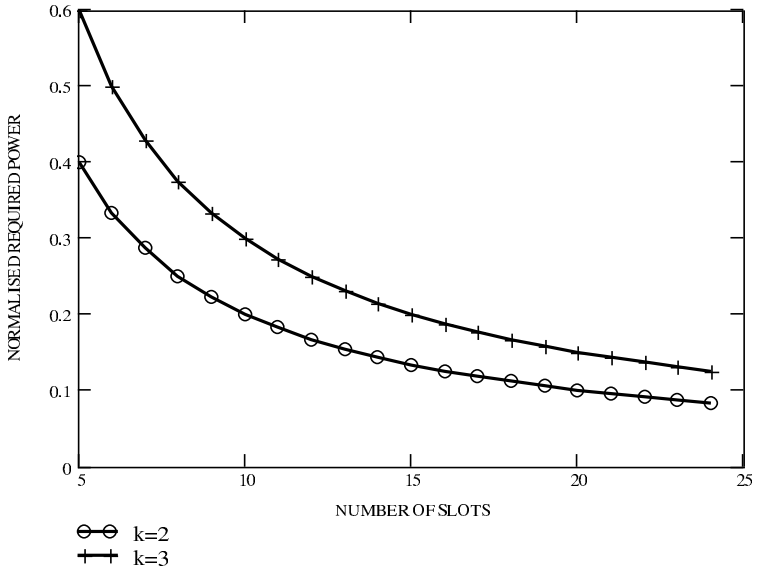

Figure 4.3: Normalised power requirement for MPPM

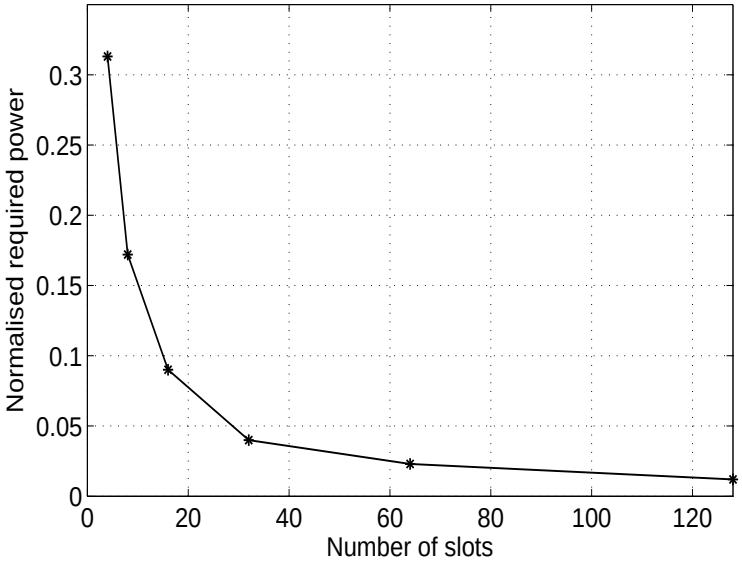

Figure 4.4: Normalised power requirement for offset PPM

Table 4.1: Power requirement with respect to the number of OOK bits

Number of OOK bits	Average number of pulse present in OPPM	Required power for OPPM
3	1.25	0.313
4	1.375	0.172
5	1.438	0.09
6	1.469	0.04
7	1.484	0.023
8	1.492	0.012
9	1.496	0.005
10	1.498	0.002
11	1.499	0.001
12	1.5	0.0007
13	1.5	0.0003
14	1.5	0.0001

4.3 Conclusion

In this chapter, BER has been calculated numerically in the MATLAB environment considering the channel noise as AWGN. Results show that a small improvement in SNR will have significant improvement in BER. Since offset PPM gives the lowest number of errors in comparison with multiple PPM, the former will produce more error-free data at the receiver. It has also been shown that with the increase in the number of slots, bandwidth will increase. Also, with the increase in the number of pulses, photon requirement will increase and hence the required power level is increased. So, a trade-off between bandwidth and power requirement is evident.

Chapter 5

Spectrum Analysis

In statistical signal processing and physics, the spectral density, power spectral density (PSD), or energy spectral density (ESD), is a positive real function of a frequency variable associated with a stationary stochastic process, or a deterministic function of time, which has dimensions of power per Hertz (Hz), or energy per Hertz. It is often called the spectrum of the signal. Intuitively, the spectral density measures the frequency content of a stochastic process and helps to identify its periodicity. The spectral density function, or power spectrum, of a random sequence of signals is defined as the distribution of the average power with respect to frequency. Spectral analysis is important to the design of any system because it indicates one of the most important characteristics of a signal (i.e. bandwidth) and also the amount of total average power of that signal in any frequency band. The Fourier transform of the autocorrelation function of a signal gives the spectral density

in the frequency domain. For spectral analysis, Fourier transform, discrete Fourier transform, autocorrelation and sampling theorem are essential and are presented in Chapter 2.

The discrete Fourier transform is performed in this work using the fast Fourier transform (FFT) algorithm. If power spectral density (PSD) is computed using the DFT, good results are not obtained when the signal is corrupted by noise. There are many approaches available [97] for calculating PSD that include Periodogram method, Welch method, Multitaper method, Yule-Walker AR method, etc. The Wiener-Khintchine theorem (WKT) gives better estimate of PSD compared to DFT in case of noisy signals. As in this work a random data sequence is considered, the use of the Wiener-Khintchine theorem is appropriate to evaluate PSD of a random offset PPM data sequence. Two types of pulse shape have been considered – return-to-zero (RZ) and non-return-to-zero (NRZ). RZ format requires larger bandwidth than NRZ format. However RZ format is used to produce slot rate powers when slot synchronization is required. Difficulty appears for frame synchronisation in the case of some modulation schemes (Differential PPM, Digital PIM, Dual Header PIM) as the frame length is variable and buffers are required in coder and decoder.

5.1 Spectral Analysis for Offset Pulse Position Modulation

An offset PPM sequence can be represented as

$$m(t) = \sum_{n=-\infty}^{\infty} a_n p(t - nT) \tag{5.1}$$

where $\{a_n\}$ is the offset pulse sequence and $p(t)$ is the pulse shape. To implement the probability distribution, 4-slot offset PPM was considered and 64 frames were taken randomly to form a offset data sequence. This data sequence was used to find out the probability distribution of zeros and ones using Matlab which is shown in Figure 5.1. The sequence can be made to have a zero mean, $M(t)$, as

$$M(t) = m(t) - \overline{m(t)}. \tag{5.2}$$

Here $\overline{m(t)}$ is the mean of $m(t)$ and is defined as

$$\overline{m(t)} \triangleq \mathbb{E}\{m(t)\} = \sum_{n=-\infty}^{\infty} \mathbb{E}\{a_n\}\mathbb{E}\{p(t - nT)\}. \tag{5.3}$$

$\mathbb{E}\{\cdot\}$ represents the expected value. According to Wiener-Khintchine theorem, the Power Spectral Density is the Fourier transform of the autocorrelation function of a data sequence. So, to find the PSD, autocorrelation function needs to be derived.

Now, by definition the autocorrelation function of the zero mean process $M(t)$ is given by ([60], [71], [103])

$$R_M(t;\tau) = \mathbb{E}\{M(t)M^*(t+\tau)\} \tag{5.4}$$

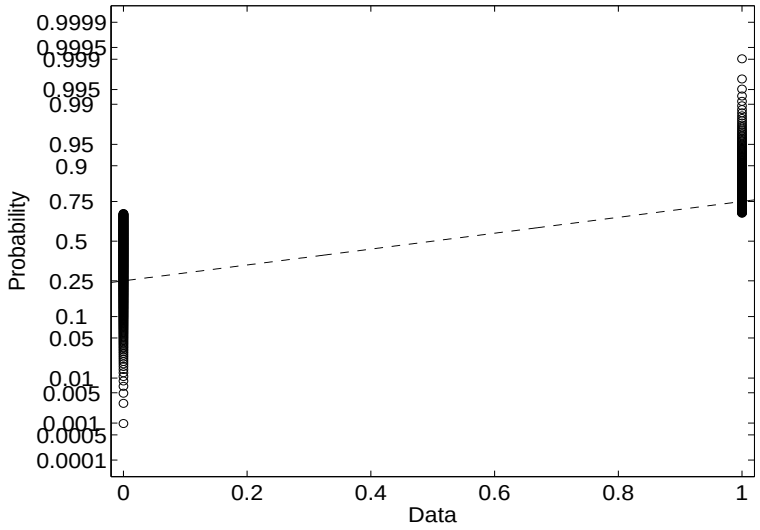

Figure 5.1: Probability distribution for 4-slot offset PPM

Expanding the above equation with the value of $M(t)$ and $M^*(t+\tau)$ auto-correlation becomes

$$R_M(t;\tau) = \mathbb{E}\{ \sum_{n=-\infty}^{\infty} [a_n p(t-nT) - \mathbb{E}\{a_n\}\mathbb{E}\{p(t-nT)\}] \tag{5.5}$$

$$\times \sum_{m=-\infty}^{\infty} [a_m p(t+\tau-mT) - \mathbb{E}\{a_m\}\mathbb{E}\{p(t+\tau-mT)\}]^*\}. \tag{5.6}$$

This can be rewritten as

$$R_M(t;\tau) = \sum_{n=-\infty}^{\infty}\sum_{m=-\infty}^{\infty} \mathbb{E}\{a_n a_m^* p(t-nT)p^*(t+\tau-mT)\}$$
$$-\mathbb{E}\{a_n\}\mathbb{E}\{a_m^*\} \times \mathbb{E}\{p(t-nT)\}\mathbb{E}\{p^*(t+\tau-mT)\} \tag{5.7}$$

using the property $\mathbb{E}\{(X-\bar{X})(Y-\bar{Y})\} = \mathbb{E}\{XY\} - \mathbb{E}\{X\}\mathbb{E}\{Y\}$. Since,

$$p(t) = \int_{-\infty}^{\infty} P(f)e^{+j2\pi ft}df \tag{5.8}$$

$$p^*(t) = \int_{-\infty}^{\infty} P^*(f)e^{-j2\pi ft}df \tag{5.9}$$

$$p(t-nT) = \int_{-\infty}^{\infty} P(f)e^{+j2\pi ft}e^{-j2\pi nT}df \tag{5.10}$$

where $P(f)$ is the Fourier transform of $p(t)$. Substituting (5.8),(5.9) and (5.10) into (5.7) gives

$$\begin{aligned}
R_M(t;\tau) &= \sum_{n=-\infty}^{\infty}\sum_{m=-\infty}^{\infty}\int_y\int_z [\mathbb{E}\{a_n a_n^*\} - \mathbb{E}\{a_n\}\mathbb{E}\{a_m^*\}] \\
&\times P(y)P^*(z)e^{-j2\pi ynT}e^{+j2\pi yt}e^{-j2\pi z(\tau-mT)}e^{-j2\pi zt}dydz \\
R_M(t;\tau) &= \sum_{n=-\infty}^{\infty}\sum_{m=-\infty}^{\infty}\int_y\int_z [\mathbb{E}\{a_n a_n^*\} - \mathbb{E}\{a_n\}\mathbb{E}\{a_m^*\}] \\
&\times P(y)P^*(z)e^{-j2\pi ynT}e^{+j2\pi yt}e^{-j2\pi z\tau}e^{+j2\pi zmT}e^{-j2\pi zt}dydz \\
R_M(t;\tau) &= \sum_{n=-\infty}^{\infty}\sum_{m=-\infty}^{\infty}\int_y\int_z [\mathbb{E}\{a_n a_n^*\} - \mathbb{E}\{a_n\}\mathbb{E}\{a_m^*\}] \\
&\times P(y)P^*(z)e^{-j2\pi ynT}e^{+j2\pi zmT}e^{+j2\pi(y-z)t}e^{-j2\pi z\tau}dydz.
\end{aligned} \tag{5.11}$$

Now, the Kernel is defined as

$$K_a(n;m-n,-y,-z) \triangleq \mathbb{E}\{a_n a_m^*\} - \mathbb{E}\{a_n\}\mathbb{E}\{a_m^*\} \tag{5.12}$$

where $-y = -z = f$. Using the definition of Kernel, the autocorrelation function becomes

$$\begin{aligned}
R_M(t;\tau) &= \sum_{n=-\infty}^{\infty}\sum_{m=-\infty}^{\infty}\int_y\int_z K_a(n;m-n,-y,-z) \\
&\times P(y)P^*(z)e^{-j2\pi ynT}e^{+j2\pi zmT}e^{+j2\pi(y-z)t}e^{-j2\pi z\tau}dydz.
\end{aligned} \tag{5.13}$$

The autocorrelation function considering the data sequence as a random 4-bit offset PPM is shown in Figure 5.2. In general the Power Spectral Density (PSD) of a digital pulse stream consists of both continuous and discrete components irrespective of the properties of the pulse stream $\{a_n\}$. The

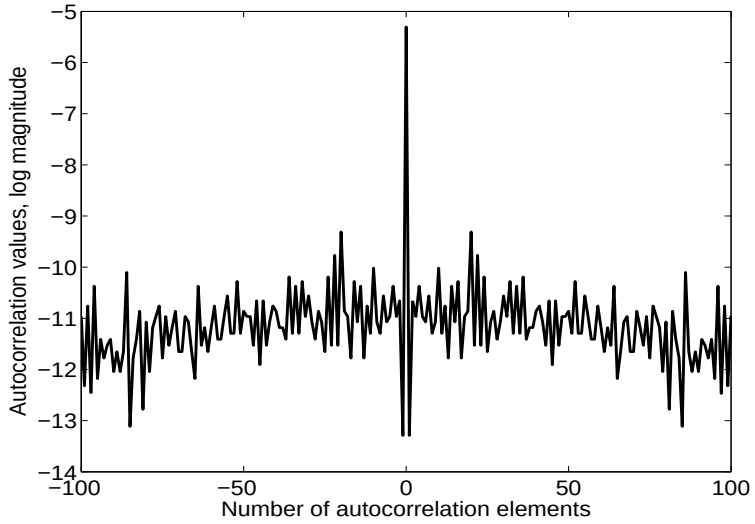

Figure 5.2: Autocorrelation function of offset PPM data sequence

continuous spectrum of the offset PPM data sequence can be represented by using Wiener-Khintchine theorem. Thus the continuous PSD of $m(t)$ is given by

$$S_m^c(f) = \mathcal{F}_{\mathcal{T}}\{\langle R_M(t:\tau)\rangle_\tau\}$$

where $\langle\cdot\rangle$ denotes time average for time duration t. Using the values of autocorrelation from equation (5.13) into the above equation continuous PSD becomes,

$$S_m^c(f) = \sum_{n=-\infty}^{\infty}\sum_{m=-\infty}^{\infty}\int_y\int_z K_a(n;m-n,-y,-z)P(y)P^*(z)$$

$$\times e^{-j2\pi ynT}e^{+j2\pi zmT}\langle e^{+j2\pi(y-z)t}\rangle \underbrace{\mathcal{F}\{e^{-j2\pi z\tau}\}}_{\delta(f+z)}\,dydz. \tag{5.14}$$

Now integrating over z, the term which is under-brace becomes,

$$\mathcal{F}\{e^{-j2\pi z\tau}\} = \delta(f+z).$$

The continuous PSD becomes

$$S_m^c(f) = \int_y \sum_{n=-\infty}^{\infty} \sum_{m=-\infty}^{\infty} K_a(n; m-n, -y, f) P(y) P^*(-f)$$

$$\times e^{-j2\pi ynT} e^{-j2\pi fmT} \langle e^{+j2\pi(y+f)t} \rangle dy$$

$$= \int_y \sum_{n=-\infty}^{\infty} \sum_{m=-\infty}^{\infty} K_a(n; m-n, -y, f) P(y) P^*(-f)$$

$$\times e^{-j2\pi ynT} e^{-j2\pi nfT} e^{j2\pi nfT} e^{-j2\pi fmT} \langle e^{+j2\pi(y+f)t} \rangle dy$$

$$= \int_y \sum_{n=-\infty}^{\infty} \sum_{m=-\infty}^{\infty} K_a(n; m-n, -y, f) P(y) P^*(-f)$$

$$\times e^{-j2\pi f(m-n)T} e^{-j2\pi(y+f)nT} \langle e^{+j2\pi(y+f)t} \rangle dy. \quad (5.15)$$

Letting $l = (m-n)$, $K_a(n; l, -y, f)$ is periodic in n with period N for a WSCS sequence, it can be easily shown that

$$\sum_{n=-\infty}^{\infty} K_a(n; l, -y, f) e^{-j2\pi(y+f)nT} =$$

$$\sum_{n=1}^{N} K_a(n; l, -y, f) e^{-j2\pi(y+f)nT} \sum_{k=-\infty}^{\infty} e^{-j2\pi(y+f)kNT}.$$

Using the Poisson sum formula

$$\sum_{n=-\infty}^{\infty} e^{-j2\pi xnT} = \frac{1}{T} \sum_{k=-\infty}^{\infty} \delta(x - \frac{k}{T}) \quad (5.16)$$

the above equation becomes

$$\sum_{n=-\infty}^{\infty} K_a(n; l, -y, f) e^{-j2\pi(y+f)nT} =$$

$$= \left[\sum_{n=1}^{N} K_a(n; l, -y, f) e^{-j2\pi(y+f)nT} \right] \times \left[\frac{1}{NT} \sum_{k=-\infty}^{\infty} \delta(y + f - \frac{k}{NT}) \right]. \quad (5.17)$$

Using equation (5.17) and integrating over y, equation (5.15) becomes

$$S_m^c(f) = \sum_{k=-\infty}^{\infty} \sum_{l=-\infty}^{\infty} \frac{1}{NT} \sum_{n=1}^{N} K_a(n; l, f - \frac{k}{NT}, f)$$

$$\times P(-f + \frac{k}{NT}) P^*(-f) e^{-j2\pi n \frac{k}{N}} e^{-j2\pi flT} \langle e^{j2\pi \frac{k}{NT} t} \rangle. \tag{5.18}$$

For a real pulse shape $p(t)$, $|P(f)| = |P(-f)|$ and also,

$$\langle e^{j2\pi \frac{k}{NT} t} \rangle = \frac{1}{NT} \int_{-\frac{NT}{2}}^{\frac{NT}{2}} e^{j2\pi \frac{k}{NT} t} dt = \begin{cases} 1, & \text{k=0} \\ 0, & \text{k}\neq 0. \end{cases} \tag{5.19}$$

Therefore equation for the continuous spectrum becomes

$$S_m^c(f) = \frac{1}{T} |P(f)|^2 \sum_{l=-\infty}^{\infty} \left[\frac{1}{N} \sum_{n=1}^{N} K_a(n; l) \right] e^{-j2\pi flT} = S_p(f) S_a(f). \tag{5.20}$$

The term $|P(f)|^2$, in equation (5.20), represents the Fourier transform of the pulse shape $p(t)$. Assume the pulse is a rectangular pulse of height A, pulse width t_p and offset PPM frame time T_f, $S_p(f)$ is the part of spectral component due to square pulse and $S_a(f)$ is the part of spectral component due to data sequence $\{a_n\}$. Now, $S_p(f)$ can be calculated as follows.

$$S_p(f) = \frac{1}{T} |P(f)|^2 = A t_p sinc \left(\frac{f t_p}{T_f} \right) \tag{5.21}$$

Using the values of equation (5.21) in equation (5.20), the final equation of the continuous spectrum can be written as

$$S_m^c(f) = A t_p sinc \left(\frac{f t_p}{T_f} \right) \sum_{l=-\infty}^{\infty} \left[\frac{1}{N} \sum_{n=1}^{N} K_a(n : l) \right] e^{-j2\pi flT}. \tag{5.22}$$

The discrete PSD of m(t) is given by ([71], [103])

$$S_m^d(f) = \mathcal{F}_{\mathcal{T}} \{ \langle \sum_{n=-\infty}^{\infty} \sum_{m=-\infty}^{\infty} \mathbb{E}\{a_n\} \mathbb{E}\{p(t - nT)\} \times \mathbb{E}\{a_m^*\} \mathbb{E}\{p^*(t + \tau - mT)\} \rangle \}$$

$$= \mathcal{F}_{\mathcal{T}}\{ \sum_{n=-\infty}^{\infty} \sum_{m=-\infty}^{\infty} \mathbb{E}\{a_n\}\mathbb{E}\{a_m^*\} \times \langle \mathbb{E}\{ \int_y P(y) e^{-j2\pi ynT} e^{+j2\pi yt} dy\}$$

$$\times \mathbb{E}\{ \int_z P^*(z) e^{-j2\pi z\tau} e^{+j2\pi zmT} e^{-j2\pi zt} dz\}\rangle\}$$

$$= \int_y \int_z \sum_{n=-\infty}^{\infty} \sum_{m=-\infty}^{\infty} \mathbb{E}\{a_n\}\mathbb{E}\{a_m^*\} \times P(y)P^*(z) \times e^{-j2\pi ynT} e^{+j2\pi zmT}$$

$$\times \langle e^{+j2\pi(y-z)t}\rangle \underbrace{\mathcal{F}_{\mathcal{T}}\{e^{-j2\pi z\tau}\}}_{\delta(f+z)} dydz. \tag{5.23}$$

Integrating over z and rearranging terms gives

$$S_m^d(f) = \int_y \sum_{n=-\infty}^{\infty} \mathbb{E}\{a_n\} e^{-j2\pi ynT} \sum_{m=-\infty}^{\infty} \mathbb{E}\{a_m^*\} e^{-j2\pi fmT}$$

$$\times P(y)P^*(-f)\langle e^{+j2\pi(y+f)t}\rangle dy. \tag{5.24}$$

$\mathbb{E}\{a_n\}$ is periodic in n with period N, so,

$$\sum_{n=-\infty}^{\infty} \mathbb{E}\{a_n\} e^{-j2\pi ynT} = \sum_{n=1}^{N} \mathbb{E}\{a_n\} e^{-j2\pi ynT} \times \sum_{k=-\infty}^{\infty} e^{-j2\pi ykNT}. \tag{5.25}$$

Using the Poisson sum formula given in equation (5.16) the above equation becomes,

$$\sum_{n=-\infty}^{\infty} \mathbb{E}\{a_n\} e^{-j2\pi ynT} = \left[\sum_{n=1}^{N} \mathbb{E}\{a_n\} e^{-j2\pi ynT}\right] \times \left[\frac{1}{NT} \sum_{k=-\infty}^{\infty} \delta\left(y - \frac{k}{NT}\right)\right] \tag{5.26}$$

and also,

$$\sum_{m=-\infty}^{\infty} \mathbb{E}\{a_m\} e^{-j2\pi fmT} = \left[\sum_{m=1}^{N} \mathbb{E}\{a_m\} e^{-j2\pi fmT}\right] \times \left[\frac{1}{NT} \sum_{l=-\infty}^{\infty} \delta\left(f - \frac{l}{NT}\right)\right]. \tag{5.27}$$

Using equations (5.26) and (5.27) in equation (5.24) and integrating over y the equation (5.24) expression becomes

$$S_m^d(f) = \frac{1}{NT} \sum_{k=-\infty}^{\infty} \sum_{n=1}^{N} \mathbb{E}\{a_n\} e^{-j2\pi \frac{kn}{N}} \times$$

$$\frac{1}{NT}\sum_{l=-\infty}^{\infty}\sum_{m=1}^{N}\mathbb{E}\{a_m^*\}e^{-j2\pi\frac{lm}{N}}\delta(f-\frac{l}{NT})P(\frac{k}{NT})\times P^*(-\frac{l}{NT})\langle e^{+j2\pi(\frac{k+l}{NT})t}\rangle. \tag{5.28}$$

Using equation (5.19) the above expression reduces to

$$S_m^d(f)=\frac{1}{(NT)^2}\sum_{l=-\infty}^{\infty}\left|P(\frac{l}{NT})\right|^2\times\left|\sum_{n=1}^{N}\mathbb{E}\{a_n\}e^{+j2\pi\frac{ln}{N}}\right|^2\delta(f-\frac{l}{NT}) \tag{5.29}$$

$$=\frac{1}{T_f^2}\sum_{l=-\infty}^{\infty}\left|P(\frac{l}{T_f})\right|^2\times\left|\sum_{n=1}^{N}\mathbb{E}\{a_n\}e^{+j(\frac{2\pi}{N}ln)}\right|^2\delta\left(f-\frac{l}{T_f}\right). \tag{5.30}$$

The term $\sum_{n=1}^{N}\mathbb{E}\{a_n\}e^{+j(\frac{2\pi}{N}ln)}$ represents the characteristic function of the data distribution of the offset PPM sequence and $T_f=(NT)$ is the total frame time.

5.2 Offset PPM Coder Design

The offset PPM coding scheme has been described in Chapter 3 and illustrated in Table 2.1. To determine the spectral characteristic of offset PPM, an offset PPM coder was designed using Matlab. For a number, M, pulses to be coded, the length of a codeword is $n=2^{M-1}$ where $N=2^M$ is the number of possible codewords in an offset PPM sequence. Table 2.1 shows how the codewords are generated in an offset PPM sequence. In offset PPM, all n positions of a codeword are initially reset to zero corresponding to the first codeword in the sequence. The second codeword in the sequence is obtained by setting the Least Significant Bit (LSB) to one. Subsequent codewords in

the sequence are produced by shifting the LSB to left until the Most Significant Bit (MSB) is reached. With reference to Figure 5.3, the MSB is kept at one and the next codeword in the sequence is formed by setting the LSB to one. This is done by using OR operation between the generated sequence and the output of the first loop to keep the MSB set. Subsequent codewords are formed by left shifting the LSB up to $(n-1)$ positions. A buffer is used to store all the codewords produced sequentially in each step. The output gives all the possible offset PPM codewords.

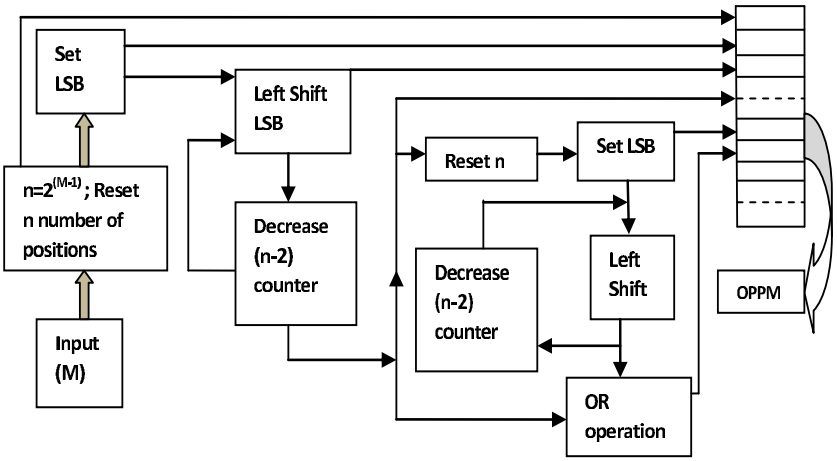

Figure 5.3: Schematic diagram of the offset PPM coder

5.3 Result and Discussion

The PSD of offset PPM was evaluated both theoretically, using the results of Section 5.1, and numerically using the coder schematic and the fast Fourier transform. Eight samples per offset PPM slot were considered, 256 frames

were taken randomly and 50 FFT's were averaged in order to decrease the noise due to randomness of the data sequence and due to averaging, the variance was reduced from 0.15 to 0.12. The X-axis has been normalised to the frame rate by dividing the total number of slots and no data windowing was considered.

Figure 5.4 shows the theoretically and numerically obtained PSD of offset PPM data sequence for coding 3 bits of data ($2^{3-1} = 4$ offset PPM data slots) using non-return-to-zero (NRZ) pulses. As can be seen, there is excellent agreement between theoretical and numerical results. There are 3 distinct spectral components corresponding to the frame rate and its associated harmonics. There should be 4 spectral lines but, as is normal with NRZ signalling, there is a null in the spectrum corresponding to the frequency equal to the inverse of the pulse width and this coincides with the frequency of the missing line. To confirm this, Figure 5.5 has been evaluated for 4 bits of data and in the similar way 7 distinct spectral components corresponding to the frame rate and 8-th one is missing. The same implementation has been performed in Figure 5.6 and shows the spectrum obtained using 50% return-to-zero (RZ) pulses for 3 bits of coding. As can be seen, the bandwidth is effectively doubled but there is a line at the slot frequency. Figure 5.7 represents the spectral characterization for 4 bits of coding with 50% duration of pulses. Figure 5.8 and Figure 5.9 represent the spectrum of offset PPM for 5 and 6 bits of coding respectively using RZ pulses and Figure 5.10 is for 7 bits of coding using full pulse width. Figures 5.11, 5.12 and 5.13

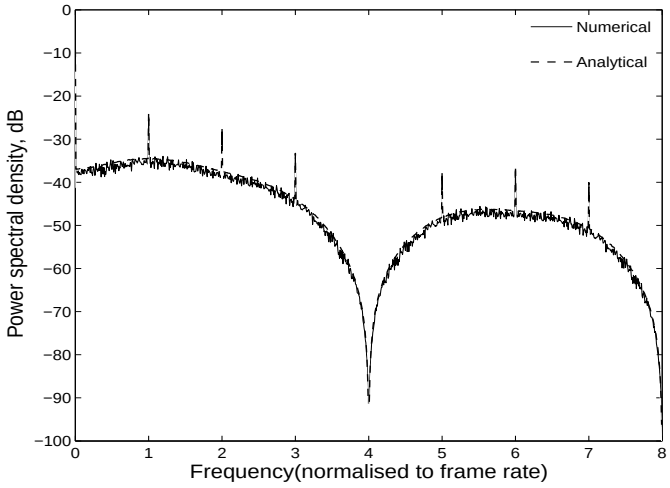

Figure 5.4: Comparison of theoretical and numerically obtained power spectral density of offset PPM for coding 3 bits of data using NRZ pulse

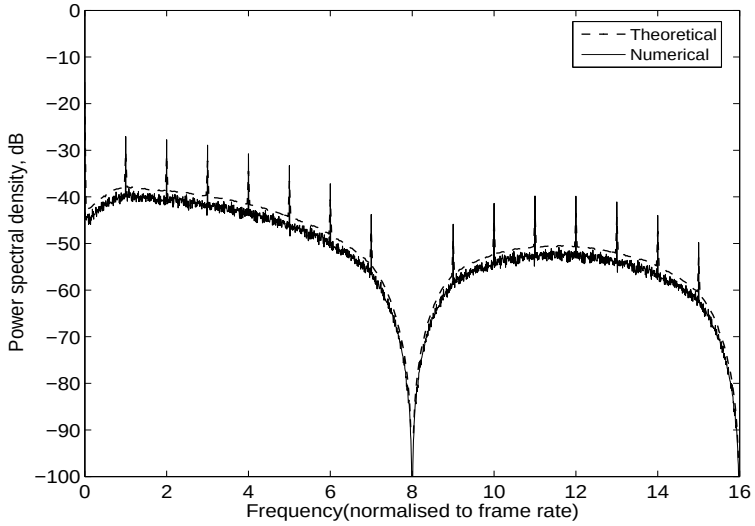

Figure 5.5: Comparison of theoretical and numerically obtained power spectral density of offset PPM for coding 4 bits of data using NRZ pulse

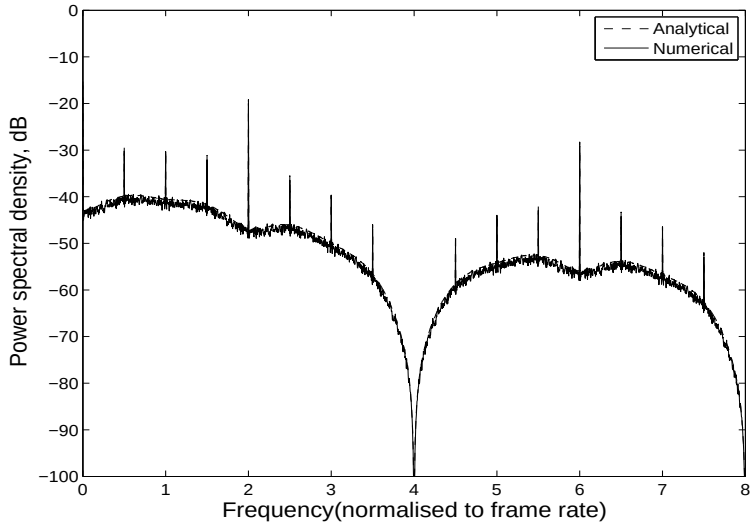

Figure 5.6: Comparison of theoretical and numerically obtained power spectral density of offset PPM for coding 3 bits of data using RZ pulse

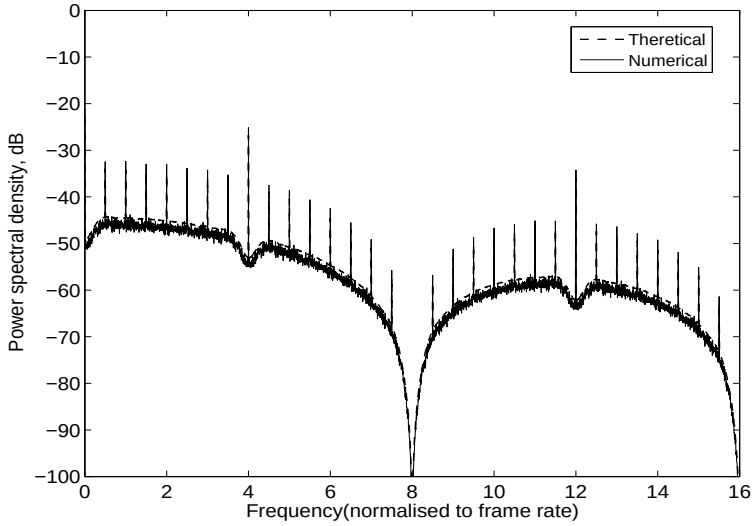

Figure 5.7: Comparison of theoretical and numerically obtained power spectral density of offset PPM for coding 4 bits of data using RZ pulse

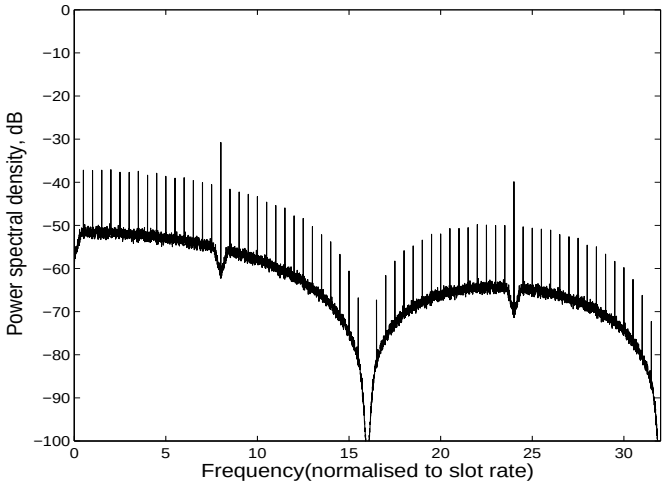

Figure 5.8: Numerical PSD of offset PPM for coding 5 bits of data using RZ pulse

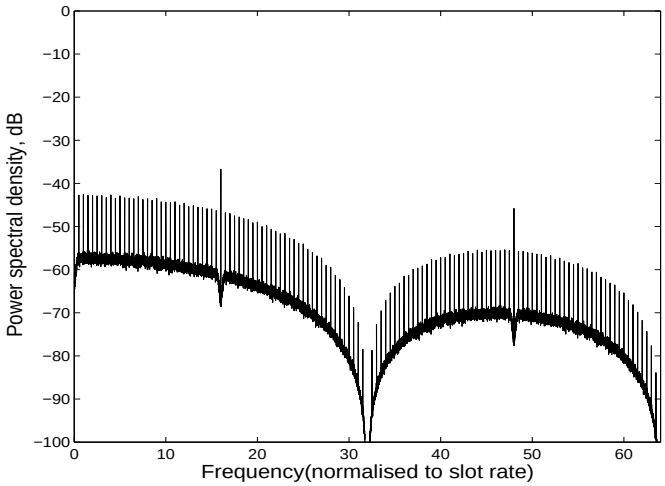

Figure 5.9: Numerical PSD of offset PPM for coding 6 bits of data using RZ pulse

show the numerically predicted PSD for digital, multiple and shortened PPM when coding 4 bits of data. As can be seen from Figure 5.11 for digital

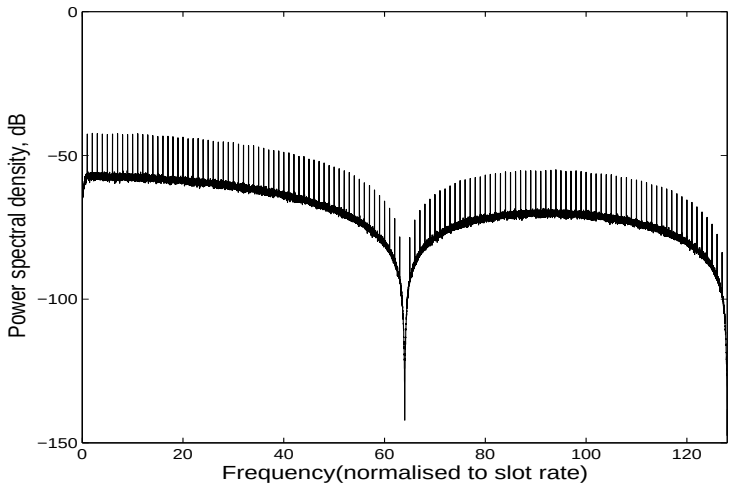

Figure 5.10: Numerical PSD of offset PPM for coding 7 bits of data using NRZ pulse

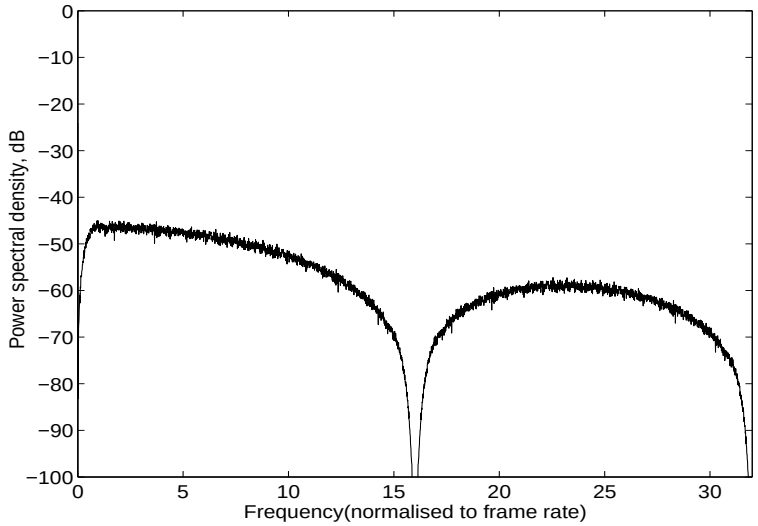

Figure 5.11: Numerical PSD of digital PPM for coding 4 bits of data

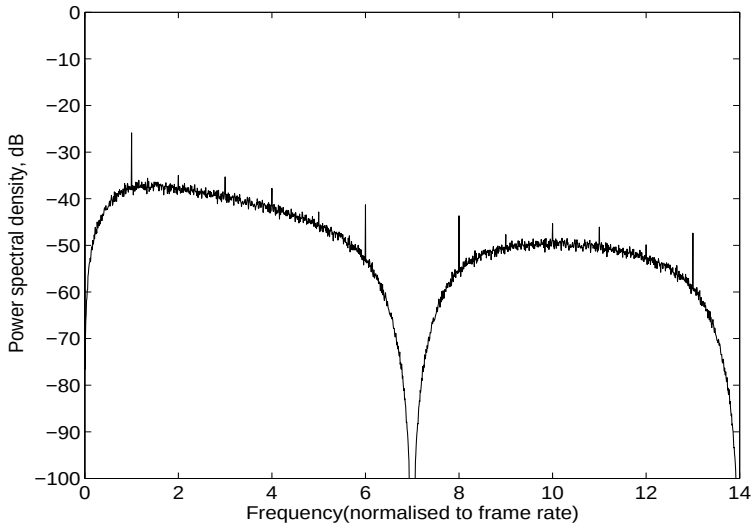

Figure 5.12: Numerical PSD of multiple PPM for coding 4 bits of data

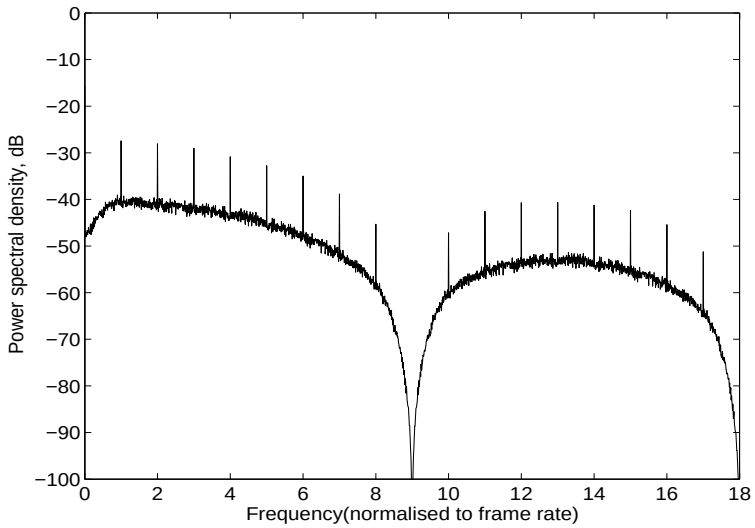

Figure 5.13: Numerical PSD of shortened PPM for coding 4 bits of data

PPM, there is no line at the frame rate (due to even distribution of bits in the codewords) and no line at the slot frequency, as expected. A frequency component at the frame frequency can be generated if the digital PPM frame

contains unmodulated guard slots at the end of the frame (see Section 5.4 later). Both multiple and shortened PPM (Figures 5.12 and 5.13) show discrete lines at the frame frequency but no line at the slot frequency due to the use of NRZ pulses. Comparing all the results that are represented for 4 bit coding, results can easily be compared in terms of line rate and bandwidth. Digital PPM gives maximum line rate among these 4 coding techniques as it uses 16 slots to transfer 4 bits of data and as a result it uses maximum bandwidth. Multiple PPM is the most bandwidth efficient code and it uses 7 slots to transfer 4 bits of data and likewise shortened PPM uses 9 slots and offset PPM uses 8 slots.

5.4 Frame Synchronization

Frame components are mostly affected by data distribution on a frame and modulating index. Table 5.1 compares the amplitude of the frame components for digital, multiple, shortened and offset PPM using NRZ pulses. Frame rate component is measured by the power at the first spike using non-return-to-zero pulse and the dc value is measured as the power at zero frequency. As previously discussed, the frame component in digital PPM is not present unless an empty guard interval is used. In order to obtain the frame component, a modulation index of 0.8 was used. The modulation index (Figure 5.14) is defined by the ratio of the effective band to the total

Table 5.1: Comparison of offset PPM, digital PPM and multiple PPM

Coding	Number of bits coded-coding level	dc Value	Slot rate power	Frame rate power
Offset PPM	3	-10.1 dB	-19.16 dB	-24.12 dB
	4	-15.23 dB	-25.16 dB	-26.82 dB
Digital PPM	3	-18.1 dB	-27.95 dB	-32.45 dB (m=0.8)
	4	-24.08 dB	-33.97 dB	-38.04 dB (m=0.8)
Multiple PPM	3	-7.96 dB	-17.85 dB	-25.82 dB
	4	-10.88 dB	-20.77 dB	-25.91 dB
Shortened PPM	3	-10.48 dB	-21.37 dB	-26.25 dB
	4	-15.51 dB	-25.41 dB	-27.88 dB

frame length and is given by

$$m = (nt_p)/T_f. \tag{5.31}$$

As can be seen from Table 5.1, offset PPM has the frame component with the highest amplitude. It is also worth noting that offset PPM has the lowest bandwidth expansion and this eases implementation.

Figures 5.15 and 5.16 show the change in frame rate power with a change in the modulating index; $m = 0.5$ when $n = 4$ for Figure 5.15 and $m = 0.5$ when $n = 8$ for Figure 5.16. In Figure 5.17, it is shown how the frame rate power changes with the variation in the modulating index. From this figure it can be said that the frame rate power is a maximum at a modulating index of $m = 0.5$.

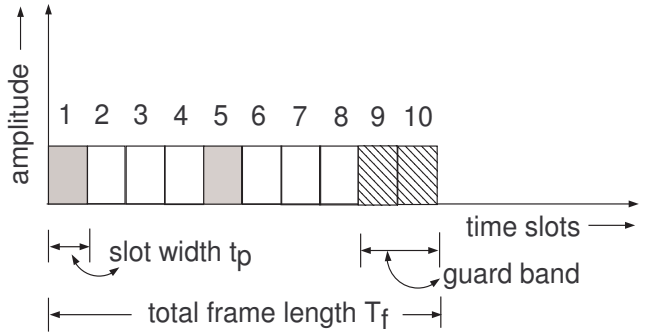

Figure 5.14: Consideration of frames for modulation index 0.8

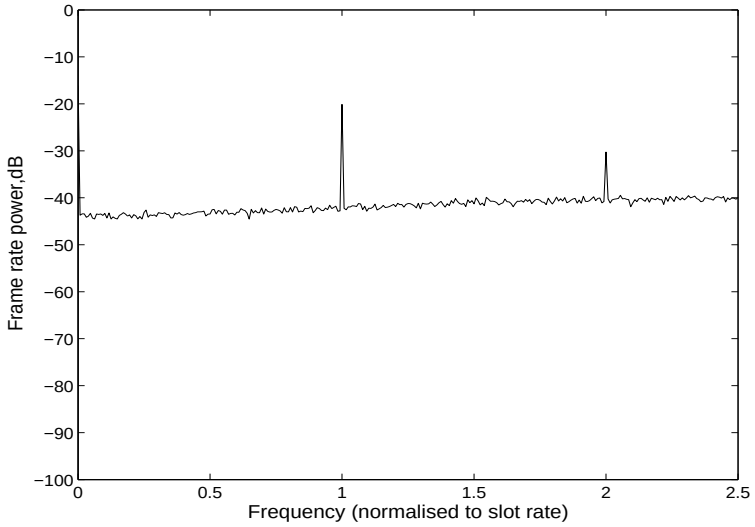

Figure 5.15: PSD of offset PPM for frame synchronization at modulating index = 0.5 and n = 4

5.5 Slot Synchronization

The strength of the slot clock is highly affected by the pulse shape (as already seen) and the modulation index. There are two ways to extract a slot clock from a PPM data stream: direct extraction of the slot clock; generation of the

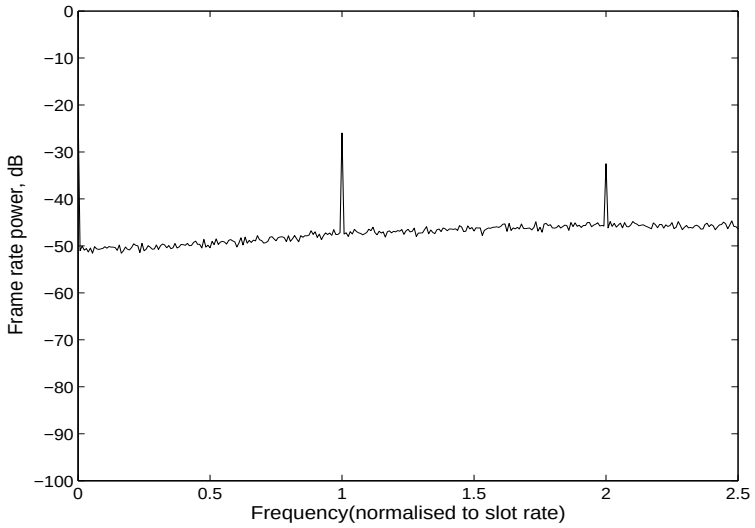

Figure 5.16: PSD of offset PPM for frame synchronization at modulating index = 0.5 and n = 8

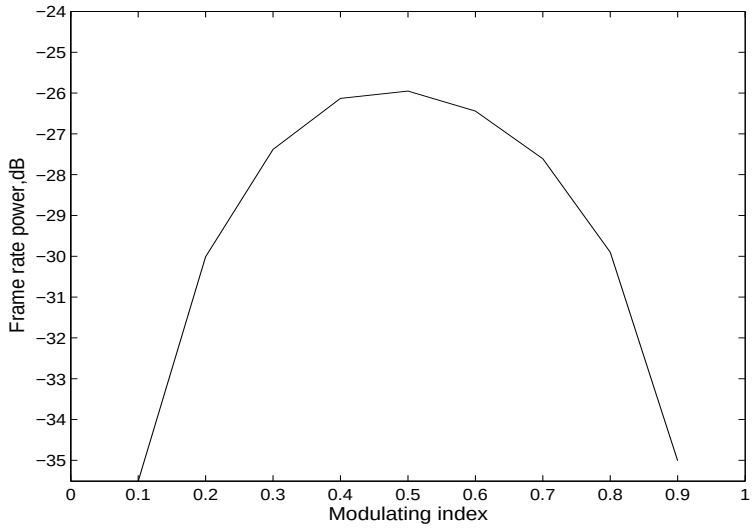

Figure 5.17: Offset PPM frame rate power with respect to modulating index when n = 8

slot clock using a Phase Lock Loop (PLL) locked to the frame frequency. As discussed previously, the spectra of the PPM systems show a null at the slot

frequency due to NRZ pulses being used. In order to extract the slot clock, the pulse width must be reduced to move this null to a higher frequency so that the slot clock can be extracted. Table 5.1 shows the amplitude of the slot component for all four codes using RZ pulses.

Some form of phase synchronization is needed with these codes when the data is to be demodulated rather than just regenerated. In this case the slot clock would have to be produced and phase locked to the frame component. This area of work is subject to another investigation and has been reported in the next chapter.

Table 5.2 shows how the dc, slot component and frame component strengths vary with coding level (number of bits coded) for offset PPM. As can be seen, the power in all components reduces as more bits of data are encoded. This is to be expected as the interval between pulses increases. Using the value of t_p from equation (5.31) in equation (5.22) the expression for continuous spectrum in terms of modulating index can be written as,

$$S_m^c(f) = \sum_{l=-\infty}^{\infty} Al \left| \frac{mT_f}{n} sinc\left(\frac{\frac{mT_f}{n}}{T_f} \right) \right|^2 \left[\frac{1}{N} \sum_{n=1}^{N} K_a(n:l) \right] e^{-j2\pi flT} \ . \quad (5.32)$$

From equation (5.32) it can be seen that the effect of modulating index on spectrum is directly proportional to modulating index and frame length. If the length of the guard interval is increased, while keeping the total frame length fixed, the modulation index will be reduced and the pulse width will also be reduced. This will affect the spectrum. A practical 4 slot offset PPM was evaluated considering 50% duration of the pulse and modulating index

Table 5.2: Dc value, slot rate power and frame rate power change with respect to coding level for offset PPM

Coding level of Offset PPM	dc value (dB) NRZ pulse	Slot rate power (dB) RZ pulse	Frame rate power (dB) NRZ pulse
3	-10.1	-19.16	-24.12
4	-15.23	-25.16	-26.82
5	-20.97	-30.76	-31.43
6	-26.75	-36.7	-36.69
7	-32.7	-42.62	-42.57
8	-38.7	-48.55	-48.18
9	-44.7	-54.57	-53.13
10	-50.72	-60.76	-60.09

$m = 0.3$. The numerically predicted result is shown in Figure 5.18. Figure 5.19 was implemented taking the same consideration as above when $m = 0.8$. The spectrum shows the presence of discrete slot rate components. The pulse shaping effect and the continuum due to the data randomness are also clear in Figure 5.20.

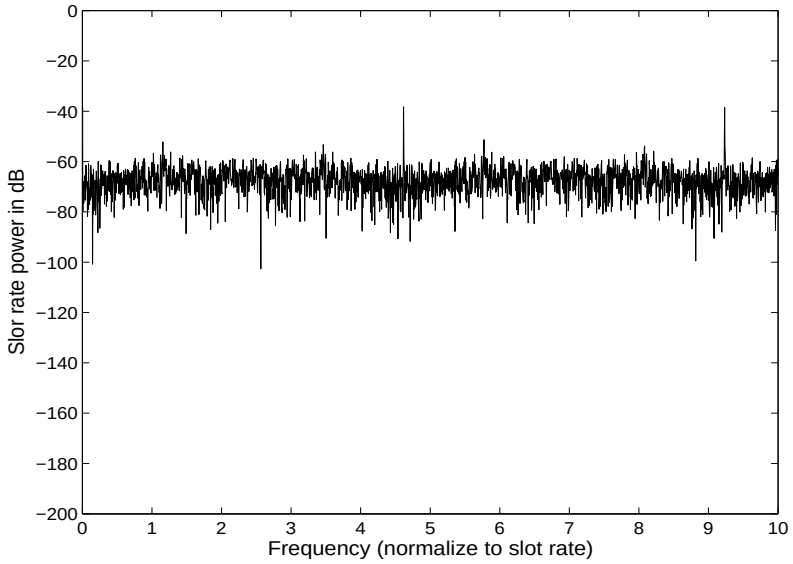

Figure 5.18: Slot rate component when n = 4, m = 0.3

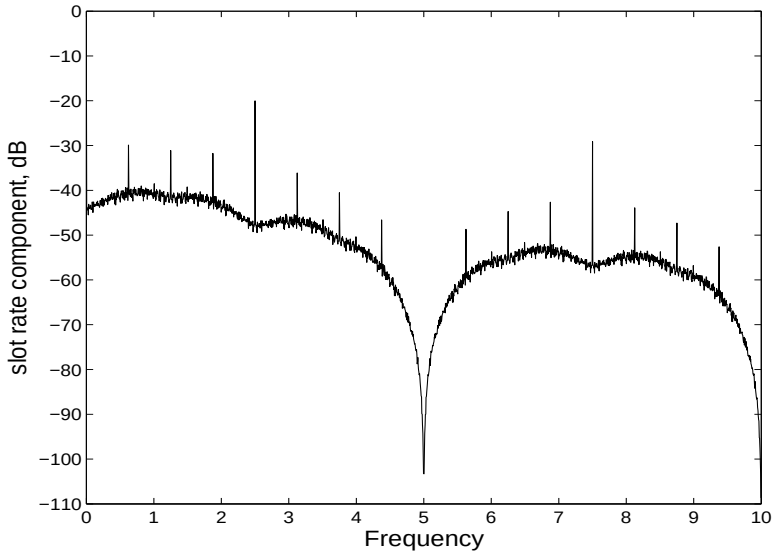

Figure 5.19: Slot rate component when n = 4, m = 0.8

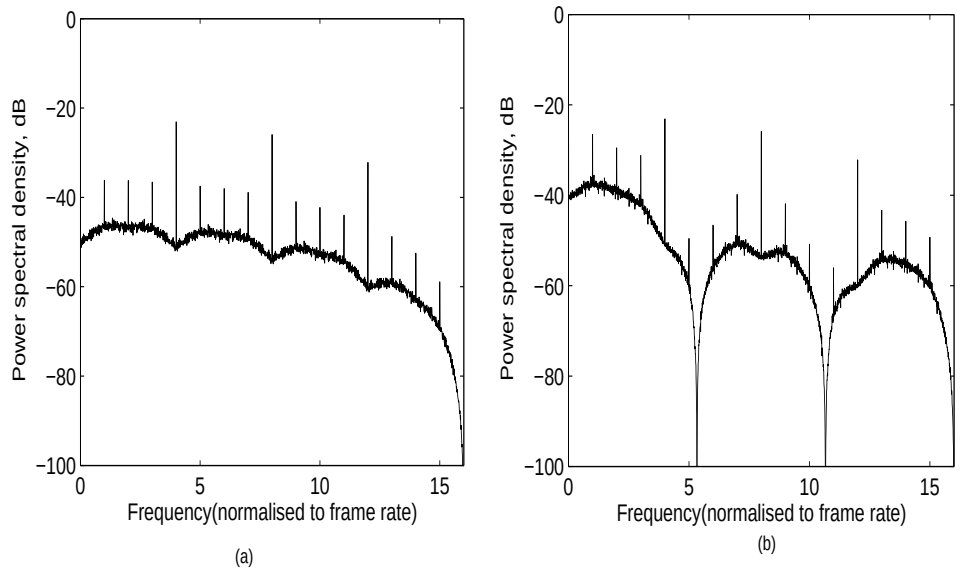

Figure 5.20: Effect of pulse shape on spectrum when (a) pulse width = 25 %, (b) pulse width = 75 %

5.6 Conclusion

This chapter presents the power spectral density of offset PPM using MATLAB simulation. Results obtained both theoretically and numerically are in excellent agreement. The results are compared with digital, multiple and shortened PPM. It has been shown that offset PPM has the strongest frame component. Furthermore, the modulation index has a strong impact on the frame rate component and at $m = 0.5$, offset PPM exhibits the highest frame rate component. In two ways modulating index can affect the frame

rate power. Firstly, as the modulation index is reduced the allowed band duration is shortened and the PPM frame periodicity is improved leading to an improved frame rate component. Secondly, reduction in the modulation index (while the frame duration is kept constant to preserve the bit rate) results in narrower PPM slots. However, due to the enhanced periodicity at low modulation index, the ratio of the discrete component to the continuum is equal and that is why $m = 0.3$ and $m = 0.7$ give the same frame rate power. For timing extraction purposes, a low modulation index ($m = 0.3$) is more suitable.

With an increase in the number of coding levels, all the powers (dc value, frame rate power, slot rate power) will increase. PSD shows that digital PPM does not give a discrete line at the frame repetition frequency, whereas offset, multiple and shortened PPM do. Offset PPM exhibits strong slot rate components when RZ pulses are used. So, slot synchronization could be possible by extracting slot rate component at the receiver end.

Chapter 6

Timing Extraction

Timing synchronization at receiver end has been a challenging research problem for decades. In order to decode a received signal properly, the received signal needs to be synchronized with an extracted received clock. Many synchronization procedures are available, among them the Phase Locked Loop (PLL) is a widely used technique as it is easy to implement and economic. Phase Locked Loop (PLL) has a wide area of application, primarily used in communication applications such as AM radio receivers, frequency demodulators, multipliers, dividers, frequency synthesizers, etc. Previously an analog PLL was used. In analog systems, the signal needs to be sampled continuously which is a drawback of this system. Whereas in digital communication systems, information is conveyed by a bit sequence of 1's and 0's, where 1 and 0 respectively represent the presence and the absence of a pulse. To process data correctly, the receiver usually synchronizes the frequency and

phase of the data with a clock and this process is called clock recovery [104].

This chapter gives a brief introduction to the basic of Phase Locked Loop (PLL) design for timing synchronization. Section 6.1 discusses various components and system properties of PLL. The study of loop characteristics and loop parameters is the subject of this section [101]. Clock and data recovery are presented in Section 6.2 considering the input data sequence as offset PPM. Frame synchronization has been shown in Section 6.3. The performance analysis of PLL in the presence of noise is presented in Section 6.4.

6.1 Phase Locked Loop Design

The basic block diagram of a PLL for clock and data recovery topology is shown in Figure 6.1. PLL comprises of a phase detector, a charge pump with loop-filter and a voltage controlled oscillator (VCO). The loop is considered as "locked" if the rate of change of phase of the output signal is constant with time, as a result, the frequency of the input and output signals becomes equal.

The phase detector (PD) compares the phase of the output signal to the phase of the reference signal. If there is a phase difference between these two signals (phase error), it generates a voltage proportional to the phase error. Due to this self correcting technique (feedback mechanism), the output signal becomes in phase with the reference signal. When both signals are synchronized, the PLL is said to be in locked condition. The phase error

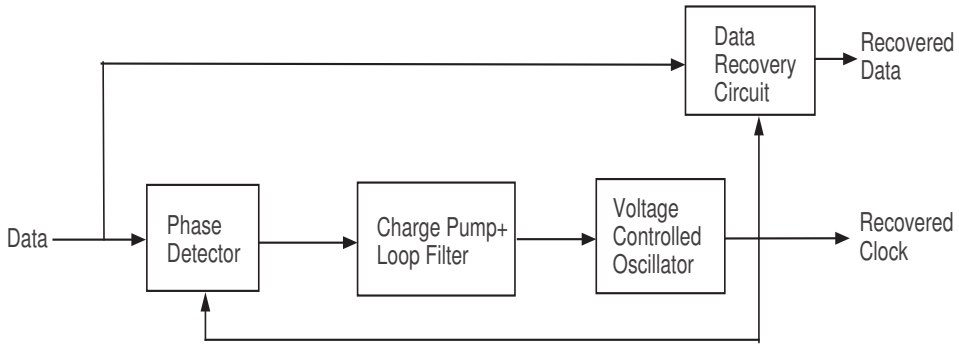

Figure 6.1: Basic block diagram for clock and data recovery

between the two signals is zero or almost zero in locked condition. The schematic diagram of a PLL is shown in Figure 6.2. The PD provides an error signal, $v_d(t)$, which is the difference between the frequency of the input data $\phi_i(t)$ and the output of VCO $\phi_0(t)$, multiplied by the detector gain k_d, i.e.,

$$v_d(t) = [\phi_i(t) - \phi_0(t)]k_d. \tag{6.1}$$

There are various type of phase detectors ([96], [104]) such as triangular phase detector, EX-OR phase detector, RS flip-flop phase detector, JK flip-flop phase detector, D flip-flop phase detector, bang-bang phase detector, etc. Due to the random nature of data the use of the phase detector is restricted, as random data introduces undesired phase variation in the recovered clock. In order to detect the frequency and phase error of a random digital data, the Hogge detector (shown in Figure 6.3) has been considered here. The phase detector gain, $k_d = \alpha$ where the value of α depends on the type of phase detector; for Hogge detector, α is 1/2. Figure 6.4 shows the output of phase

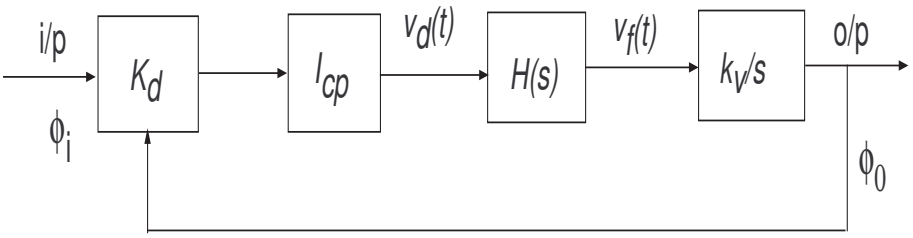

Figure 6.2: Schematic diagram of the Phase Locked Loop

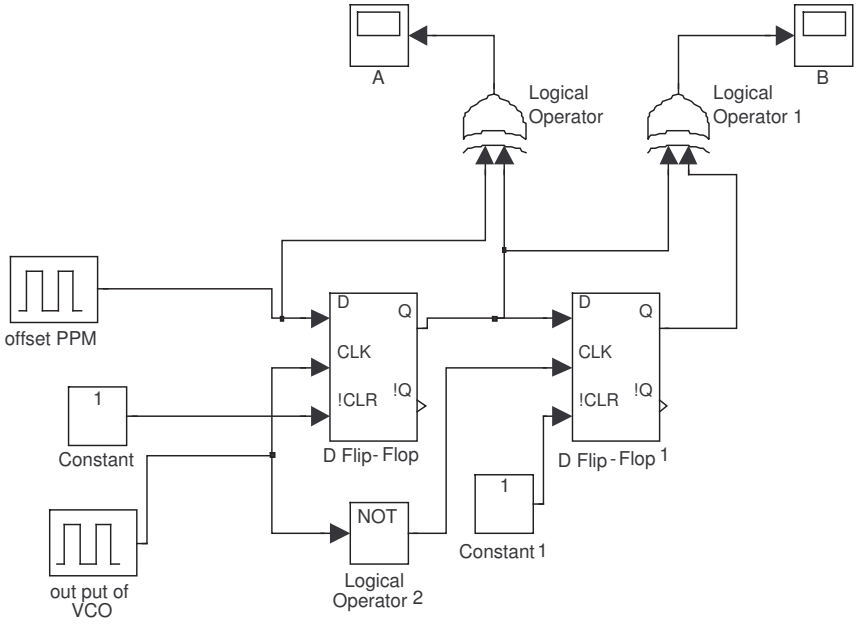

Figure 6.3: Hogge detector

detector considering input sequence as offset PPM data. In this figure, the upper one shows the voltage at point A, middle one shows the voltage at point B and the lower one shows the output voltage of charge pump.

The charge pump (CP) circuit converts the error signal, produced by the

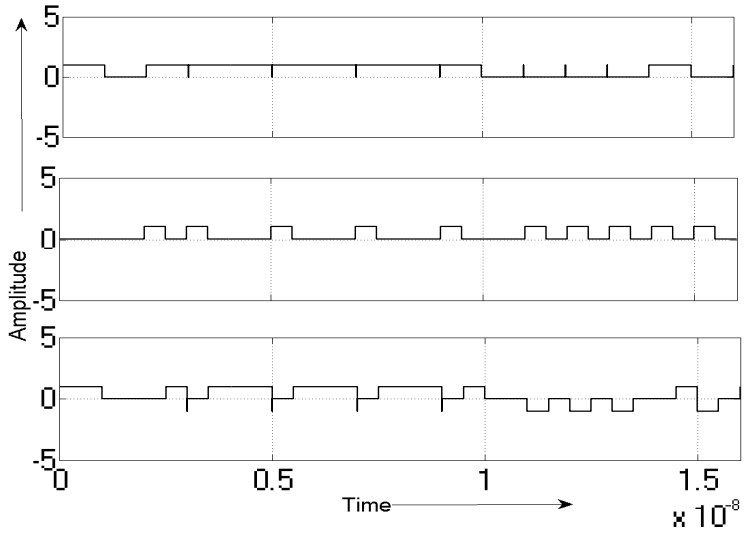

Figure 6.4: Phase detector output

Hogge detector, as a positive or negative signal. If the input signal frequency is greater than the VCO clock frequency, the CP produces a positive error signal and it becomes negative while VCO clock frequency is greater than the input signal frequency.

The output of the CP passes through a loop-filter that plays a key role in PLL feedback closed-loop system. A loop-filter introduces poles and zeros into the PLL transfer function, which determines the bandwidth of the PLL. Since a higher order loop-filter offers better noise cancellation property, a loop-filter of order 2 or more is used in most of the PLL circuits in critical applications. Here a type 1 (single pole at the origin), order 2 low-pass passive filter has been considered to achieve steady-state quickly (small settling time). Figure 6.5 depicts the circuit diagram of the charge pump and loop-filter considered in present work. In Figure 6.5, $R_1 = R_2 = R_3$ and value

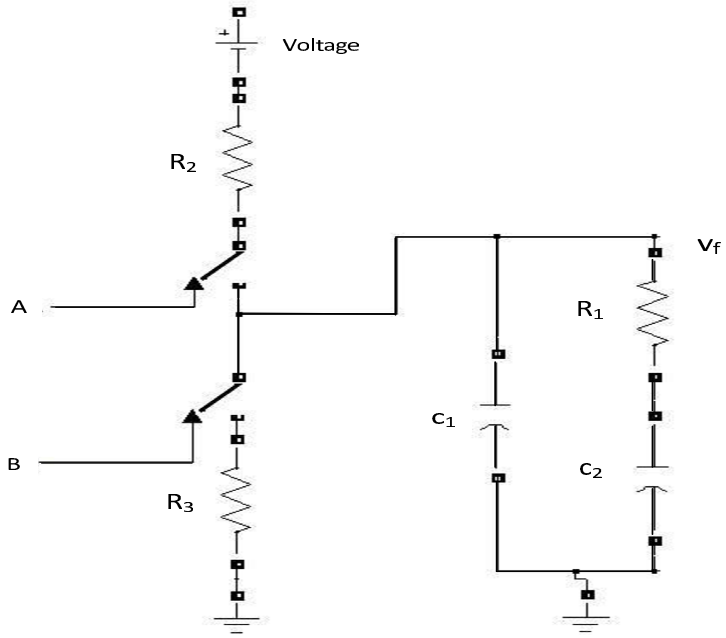

Figure 6.5: Loop-filter and charge pump circuit diagram

of these resistors are determined based on the PLL design constraints. Here 'Voltage' is considered as $1V$. The output of loop-filter in Laplace domain becomes

$$V_f(s) = H(s)V_d(s) \tag{6.2}$$

where $H(s)$ is the loop-filter transfer function. The output of loop-filter for an offset PPM data sequence is shown in Figure 6.6. This output voltage is the control voltage to the VCO. This produces an output frequency ω_0 which is linearly proportional to the control voltage $v_f(t)$ generated by the loop-filter. This linear relationship between the control voltage and the output frequency simplifies PLL design. The VCO has a free running frequency that adjusts the phase and frequency of the input signal based on the error signal

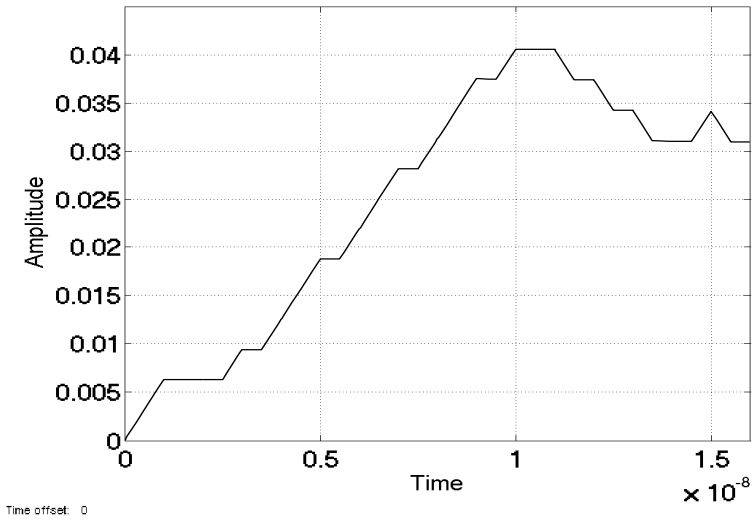

Figure 6.6: Loop-filter output

produced by phase detector. Mathematically this can be written as:

$$\phi_0 = \int \omega_0(t)dt = \omega_c(t) + k_v v_f(t). \tag{6.3}$$

Here k_v is the VCO gain. The output of the VCO is shown in Figure 6.7. The loop-filter transfer function can be represented as [96]

$$H(s) = \frac{V_f(s)}{V_d(s)} = k_{LP}\frac{1+\frac{s}{\omega_z}}{s(1+\frac{s}{\omega_p})}. \tag{6.4}$$

From the circuit diagram, shown in Figure 6.5

$$\frac{V_f(s)}{V_d(s)} = \frac{1}{s(c_1+c_2)} \times \frac{1+sR_1c_2}{1+sR_1\frac{c_1c_2}{c_1+c_2}}. \tag{6.5}$$

Comparing equations (6.4) and (6.5), the gain k_{LP}, pole ω_p and zero ω_z are calculated as:

$$k_{LP} = \frac{K}{k_v I_{cp}\alpha} = \frac{1}{c_1+c_2} \tag{6.6}$$

$$\omega_p = 2\pi f_P = \frac{c_1+c_2}{R_1c_1c_2} \tag{6.7}$$

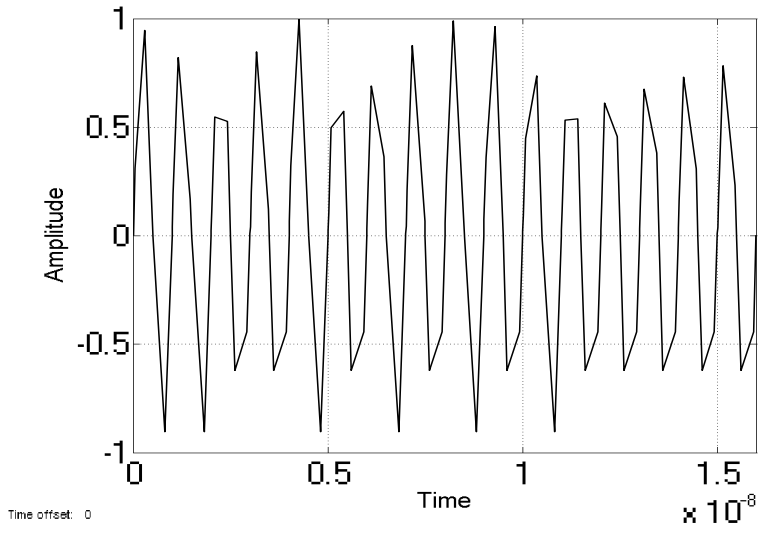

Figure 6.7: VCO output

$$\omega_z = 2\pi f_z = \frac{1}{R_1 c_2} \tag{6.8}$$

$$f_z = r f_0 \tag{6.9}$$

Here I_{cp} is the charge pump current, K is the desired forward path gain, r is the ratio $(\frac{f_z}{f_0})$ and f_0 is the free running frequency of VCO. Now from the above, expressions for capacitance and resistance are obtained as follows:

$$c_1 = \frac{k_v I_{cp} \alpha f_0 r}{K f_p} \tag{6.10}$$

$$c_2 = \frac{k_v I_{cp} \alpha}{K} - c_1 \tag{6.11}$$

$$R_1 = \frac{1}{2\pi f_0 r c_2}. \tag{6.12}$$

The designed values of the parameters for implementing PLL are given in Table 6.1.

Considering these values, the Bode diagram (magnitude and phase plots) of the loop-filter is given in Figure 6.8. Zero $(1/R_1 c_2)$ and pole $((c_1 +$

Table 6.1: Parameter values

K	K_v (Hz/V)	α	r	I_{CP}	f_0 (Hz)	c_1	c_2	R_1
2.03	5	0.5	1/8	1	1	22	224	5.7
$\times 10^{12}$	$\times 10^5$			Amp	$\times 10^6$	nF	nF	ohm

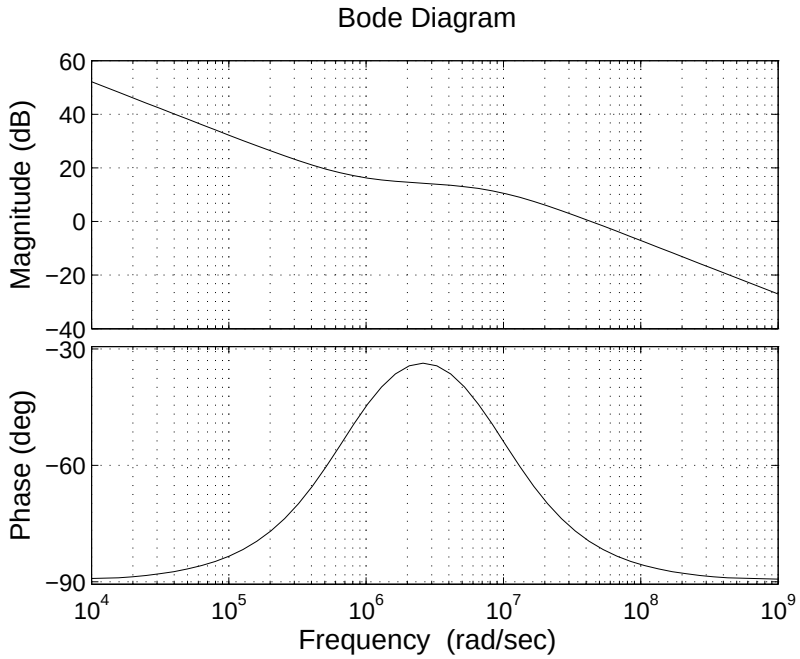

Figure 6.8: Loop-filter magnitude and phase response

$c_2)/R_1c_1c_2$) of the transfer function $H(s)$ determine the cut-off corner frequencies. A loop-filter is designed such that the loop gain (overall gain of the loop) of the closed-loop system becomes high in the low frequency region that facilitates in achieving tracking performance of the system as well as helping to attenuate disturbance entering the closed-loop. In order to make the loop gain high at low frequency range, a loop-filter with a pole (Figure

6.9) at origin is chosen. To this end, it is worth mentioning that to achieve more loop gain at low frequency one may also introduce more poles at the origin through the loop-filter; however, the stability margin of the designed closed-loop system may deteriorate. To ensure a good stability margin, at the crossover frequency the slope of the magnitude plot in Bode diagram is kept around $-20\ dB/decade$. Also in order to make the transient response less oscillatory (Figure 6.10), sufficient phase margin of the closed-loop system is maintained.

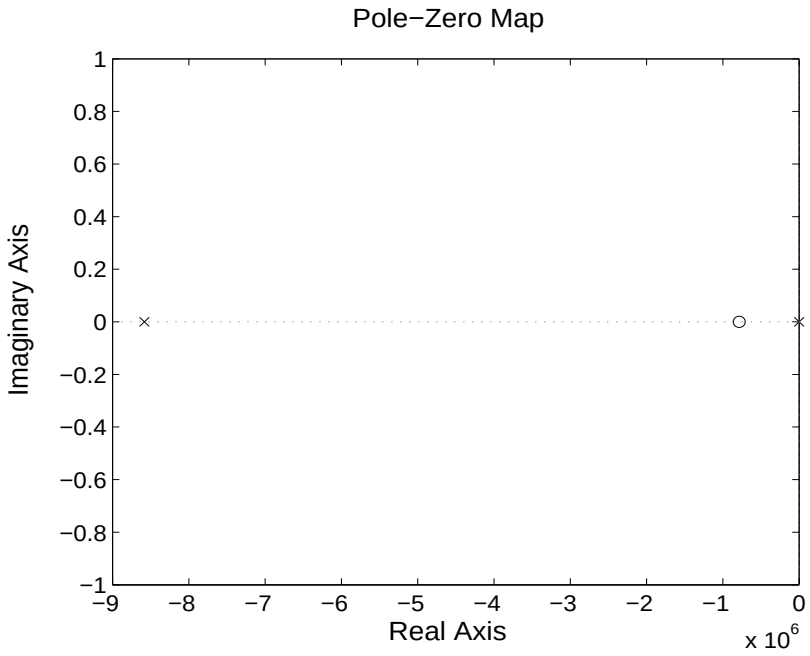

Figure 6.9: Pole-zero plot of loop-filter

The closed-loop transfer function of the PLL is given as

$$G(s) = \frac{A(s)}{1 + A(s)}, \tag{6.13}$$

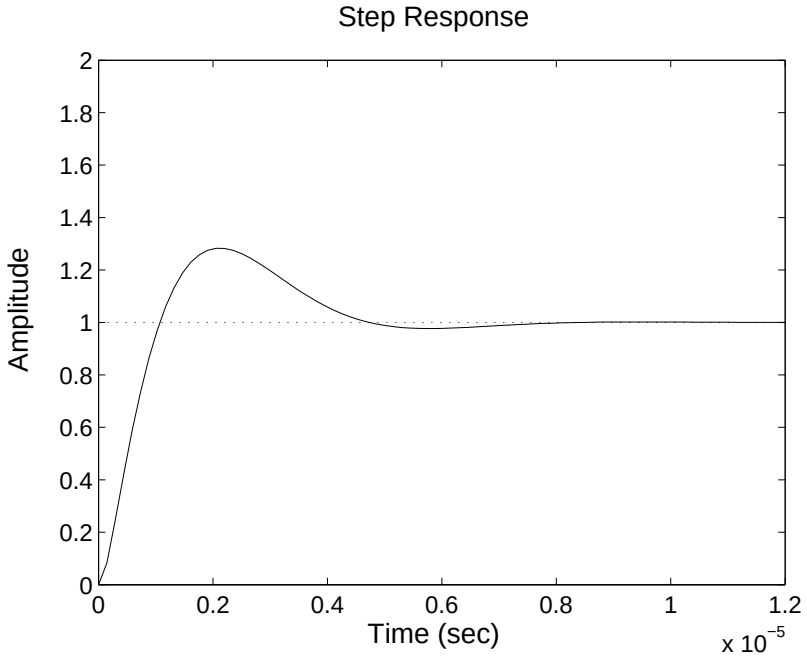

Figure 6.10: Unit step response of the closed-loop Phase Locked Loop

where $A(s)$ is the forward path transfer function and it is given as

$$A(s) = \frac{k_v I_{cp} \alpha H(s)}{s}. \tag{6.14}$$

Replacing $H(s)$ in $A(s)$ and then substituting for $G(s)$, the closed-loop transfer function becomes

$$G(s) = \frac{k_v I_{cp} \alpha (1 + sR_1 c_2)}{s^3(R_1 c_1 c_2) + s^2(c_1 + c_2) + s(R_1 c_2 k_v I_{cp} \alpha) + k_v I_{cp} \alpha}. \tag{6.15}$$

In principle, a higher order low-pass filter can achieve sharp cut-off characteristics (Figure 6.11), a desirable property in this application. However, such systems are difficult to stabilize, especially when the process and temperature variations are taken into account. The stability of a feedback system is related to the location of roots of the characteristic equation of the system

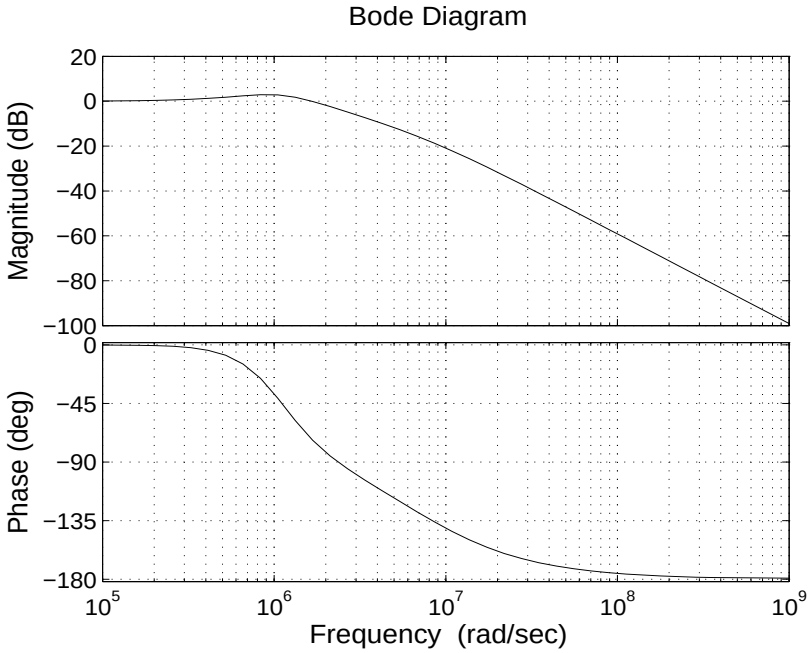

Figure 6.11: Bode plot of the closed-loop Phase Locked Loop

transfer function. A system is stable if all closed-loop poles of the transfer function have negative real parts. Figure 6.12 shows poles of $G(s)$ which are in the left half of the s-plane and hence is stable. From this pole-zero map it is apparent that the PLL transfer function is of third order and a pole is located far away from the imaginary axis due to a capacitor connected in parallel with the LPF (Figure 6.5) output port to suppress high frequency signals.

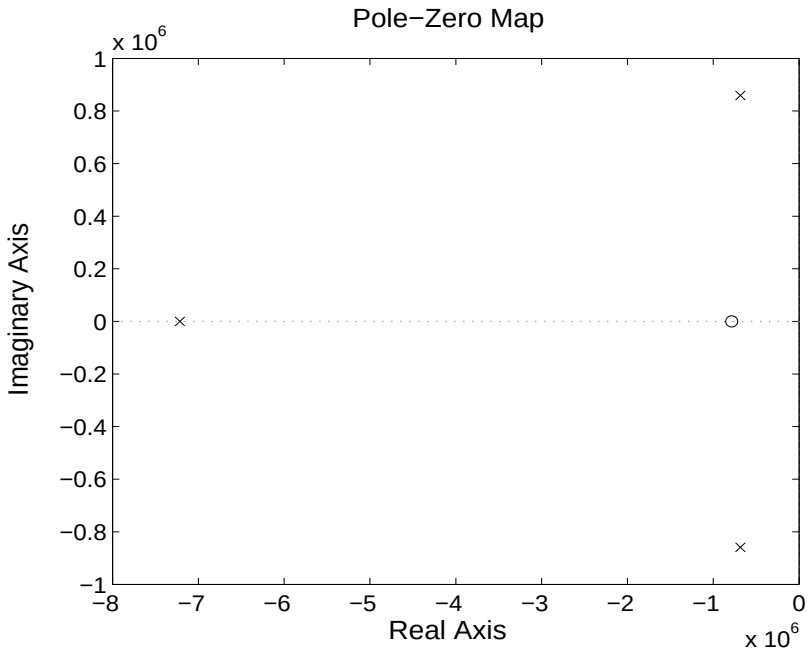

Figure 6.12: Pole-zero plot of the closed-loop Phase Locked Loop

6.1.1 Steady-state Error Analysis

Total error in Laplace domain is expressed as the phase difference of the input and output phase

$$E(s) = \phi_i(s) - \phi_0(s). \tag{6.16}$$

The phase transfer function is

$$\frac{\phi_0(s)}{\phi_i(s)} = \frac{A(s)}{1 + A(s)}. \tag{6.17}$$

Replacing $\phi_0(s)$ in equation (6.16),

$$E(s) = \phi_i(s) - \frac{A(s)}{1 + A(s)}\phi_i(s) = \phi_i(s)\left[\frac{1}{1 + A(s)}\right]. \tag{6.18}$$

The steady-state error is defined as [101]

$$e_{ss} = \lim_{s\to 0} s \cdot E(s) = s \cdot \phi_i(s) \left[\frac{1}{1+A(s)}\right] = s \cdot \frac{1}{s}\left[\frac{1}{1+\lim_{s\to 0} A(s)}\right]$$

$$= \frac{1}{1+\lim_{s\to 0} \frac{k_v I_{cp} \alpha H(s)}{s}} = \frac{1}{1+\infty} = 0. \tag{6.19}$$

In above expression $\phi_i(s) = 1/s$ as the input is considered as unit step function. Now from the above expression it can be concluded that this PLL topology theoretically does not exhibit any error at its steady-state, shown in Figure 6.10. This response shows the performance of the system in terms of settling time, peak time, overshoot, rise time, etc. The characteristics of the step response will be changing with the change in system parameters given in Table 6.1. Figure 6.13 shows the unit step response of the system when the value of charge pump current (I_{cp}) varies. If the charge pump current is increased, the overshoot is decreased but the settling time is increased. As the tracking system demands quick acquisition with zero steady-state error, the settling time gets more priority. Figure 6.14 shows the unit step response for different values of r. $r = \frac{1}{8}$ is chosen here, as the settling time is increased with decreasing the value of r.

6.2 Clock and Data Recovery

In this application, the goal is to determine how well the clock recovery function can be performed considering offset PPM data as an input sequence. The PSD of 4-bit offset PPM was evaluated numerically in the previous

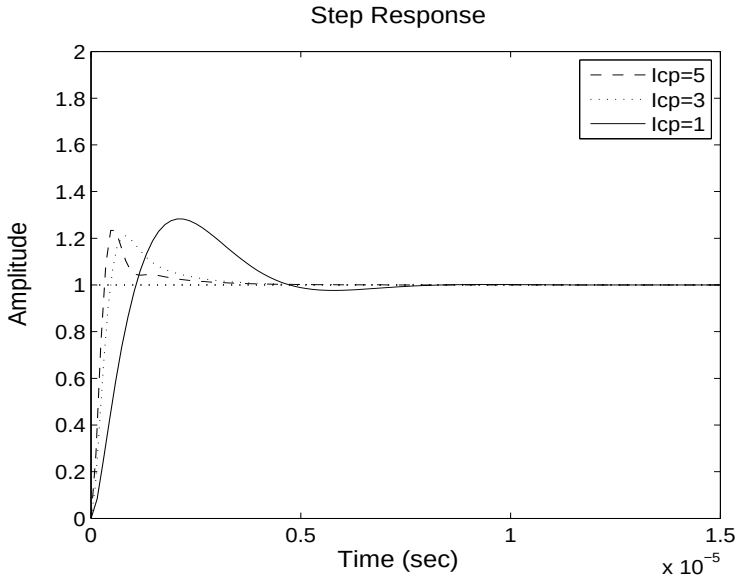

Figure 6.13: System step response for different values of I_{cp}

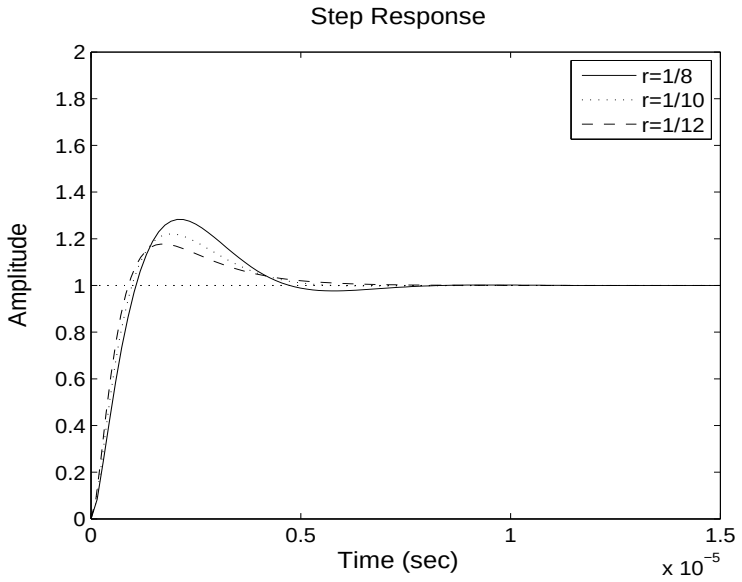

Figure 6.14: System step response for different values of r

chapter (shown in Figure 5.6) using the fast Fourier transform to understand timing content in the data sequence. Eight samples per offset PPM slot were considered and 50 FFT's were averaged in order to decrease the noise due to randomness of the data sequence. There exist spectral lines at the slot repetition frequency which can be extracted using a timing extraction process. This is an advantage of offset PPM as this coding exhibits spectral lines when return-to-zero (RZ) pulses are used. Using PLL, designed in this chapter, clock from offset PPM data sequence has been extracted, shown in Figure 6.15, where a random offset data sequence is considered as '1001 1001 1010 1001'. Clock recovery topology has been designed to achieve a minimum bit error rate (BER). Deviation of recovered clock from the ideal one will increase BER. Data recovery circuit has been designed using D-flip

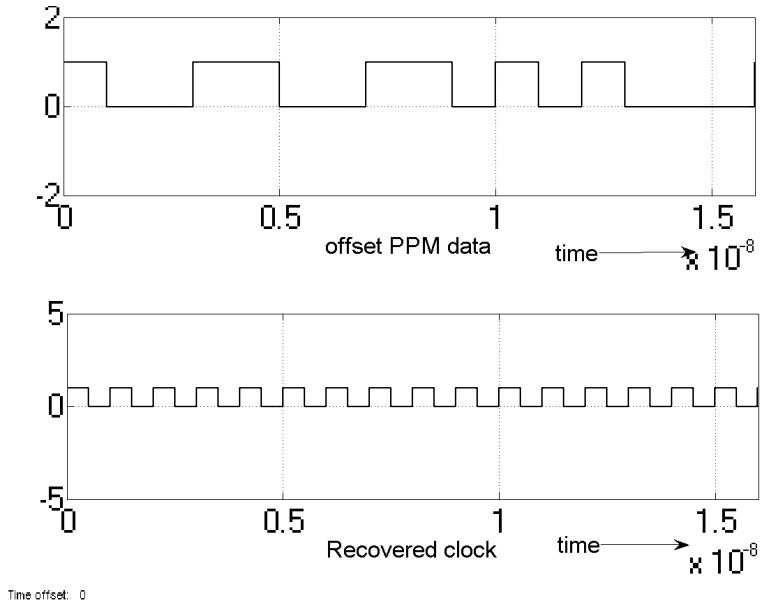

Figure 6.15: Clock recovery from offset PPM data sequence

flop (Figure 6.16). Here the data are synchronised with the negative transition of the clock (shown in Figure 6.17) and thus, receiver can recover the data. Synchronization with positive transition of the clock could also be possible.

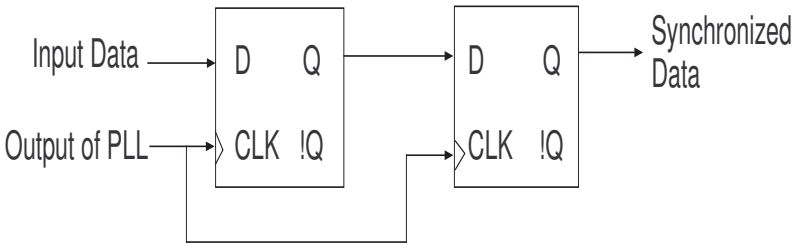

Figure 6.16: Data recovery block

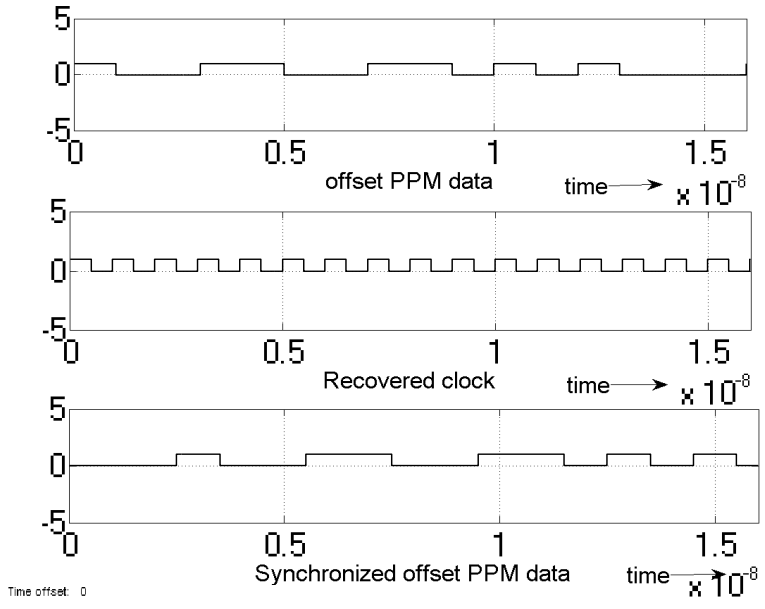

Figure 6.17: Data recovery from offset PPM data sequence

6.3 Frame Synchronization

From the power spectral density, it is seen that there exists a frame rate component at frame repetition frequency. In the previous chapter, 4-slot offset PPM was considered and the frame rate component has been shown in Figure 5.4 (shown in the previous chapter). It should be noted that OOK and digital PPM do not exhibit any frame rate component for NRZ pulses, but show a frame rate component when a guard interval with empty slots is used at the end of the frame. Using PLL circuit, designed in this chapter, a frame clock can also be extracted from random data sequence. To extract the frame clock a frequency synthesizer (Figure 6.18) has been used. As

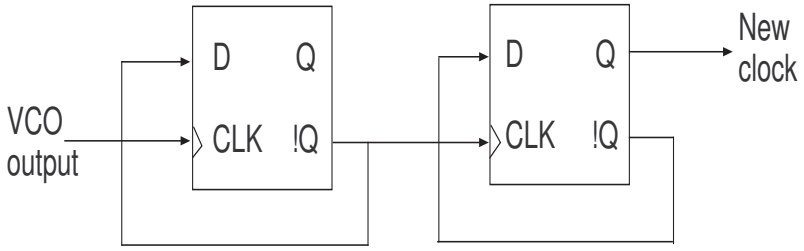

Figure 6.18: Frequency synthesizer block

4 (2^2) bits in a frame are used for the offset PPM data sequence, a mod-4 counter is used as a frequency synthesizer which is developed using D flip-flops. In Figure 6.18 the complement output of the first D flip-flop is fed back to input of the same flip-flop and complement output of the previous D flip-flop is used as the clock of the next flip-flop. Thus the output frequency is divided. Depending on the length of the frame, the number of counters

is selected. The frame clock has been extracted correctly and is shown in Figure 6.19. So, frame synchronization could be possible using this topology.

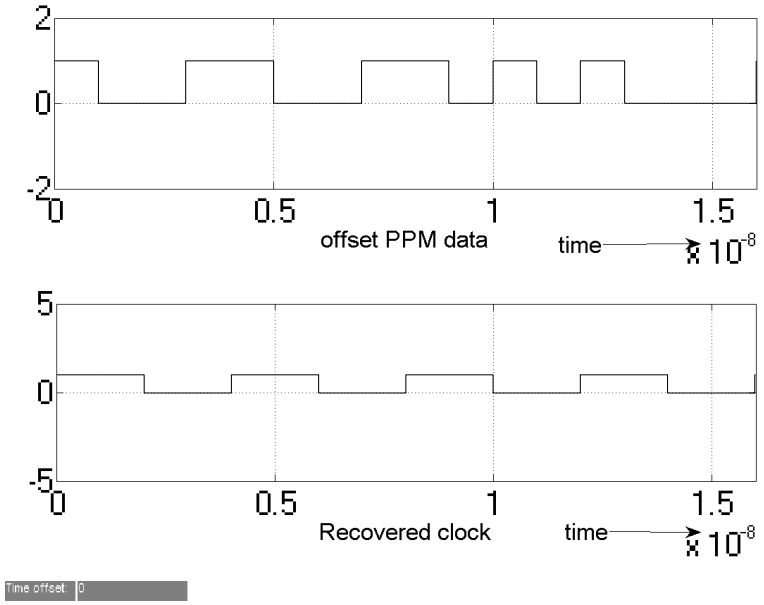

Figure 6.19: Frame clock recovery from offset PPM data sequence

6.4 Noise Analysis

Each block of a PLL contributes noise to the closed-loop for which an output phase error or 'jitter' appears. Noise analysis is important for PLL system design. Below, an analytical modeling framework for different types of noise is presented.

6.4.1 Reference Noise

PLL shows good performance with low reference noise, although this noise is much less compared to VCO noise. The effect of reference noise can be minimized by keeping I_{cp} small. Transfer function from reference source to PLL output is given by

$$G_{ref} = \frac{\text{forward path transfer function}}{1 + \text{loop transfer function}}$$

$$G_{ref} = \frac{k_v I_{cp} \alpha (1 + sR_1 c_2)}{s^3(R_1 c_1 c_2) + s^2(c_1 + c_2) + s(R_1 c_2 k_v I_{cp} \alpha) + k_v I_{cp} \alpha} \tag{6.20}$$

6.4.2 Phase Detector Noise

The effect of phase detector noise is lower than the effect of VCO noise. The transfer function for phase detector noise can be represented as

$$G_{pdf} = \frac{\text{loop-filter transfer function} \times \text{VCO transfer function}}{1 + \text{loop transfer function}}$$

$$G_{pdf} = \frac{k_v (1 + sR_1 c_2)}{s^3(R_1 c_1 c_2) + s^2(c_1 + c_2) + s(R_1 c_2 k_v I_{cp} \alpha) + k_v I_{cp} \alpha} \tag{6.21}$$

6.4.3 VCO Noise

The oscillator contributes most of the noise at output of a well designed PLL frequency synthesizer. VCO noise dominates the noise level in a PLL as the oscillator inherently amplifies all noises generated near its oscillation frequency or any of its harmonics. VCO noise can be removed by suitably

designing PLL loop bandwidth. But, the VCO phase noise cannot be attenuated at offset frequencies beyond the bandwidth. At high frequency, the noise of the PLL comes from the VCO noise. The transfer function from the VCO noise source to output is given by

$$G_{vco} = \frac{1}{1 + \text{loop transfer function}}$$

$$G_{vco} = \frac{s^3(R_1c_1c_2) + s^2(c_1 + c_2)}{s^3(R_1c_1c_2) + s^2(c_1 + c_2) + s(R_1c_2k_vI_{cp}\alpha) + k_vI_{cp}\alpha}. \tag{6.22}$$

Variation in supply or reference voltage to PLL changes the control voltage to VCO which changes the VCO operating frequency. A change in oscillation frequency of a VCO appears as a phase step in the input of phase detector. The phase error accumulates jitter until it is corrected by PLL.

6.4.4 Loop-filter Noise

Loop-filter noise contributes more to the total noise level compared to reference noise and phase detector noise but contributes less than the VCO noise. The transfer function for this noise can be represented as,

$$G_{lf} = \frac{\text{VCO gain}}{1 + \text{loop transfer function}}$$

$$G_{lf} = \frac{s^2R_1c_1c_2k_v + sk_v(c_1 + c_2)}{s^3(R_1c_1c_2) + s^2(c_1 + c_2) + s(R_1c_2k_vI_{cp}\alpha) + k_vI_{cp}\alpha} \tag{6.23}$$

Both phase detector noise and loop-filter noise can be minimized by changing the value of VCO gain. Figure 6.20 represents the noise plots due to different noise sources of the PLL.

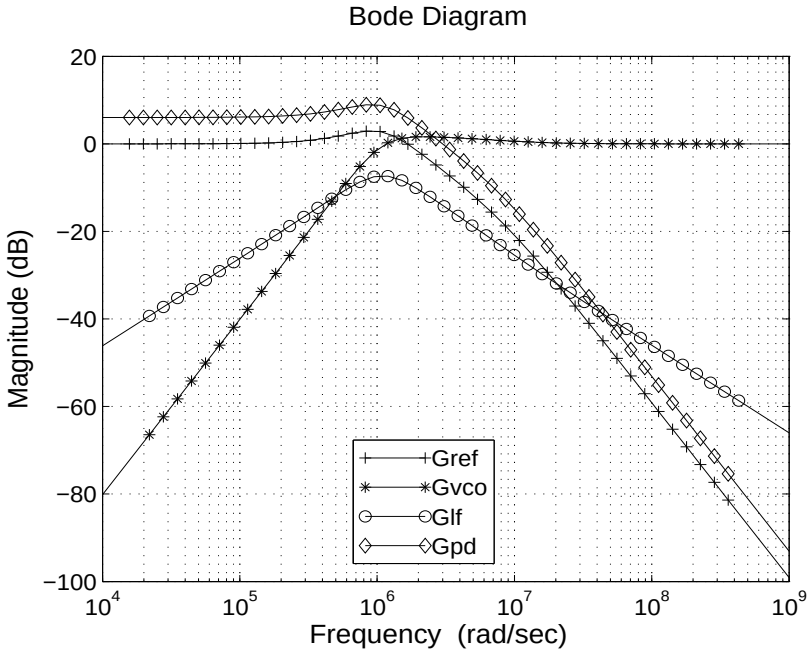

Figure 6.20: Noise plot for different noise sources in PLL

The closed-loop VCO noise behaves as high-pass filtered noise, which contains the high frequency components. From Bode plot analysis of the noise TF, the attenuation scheme can be determined. VCO noise characteristics plot falls as f^2 at lower frequency range and at higher frequencies, it becomes flat. Loop-filter noise response behaves like a band-pass filter. A noise peak is observed in the magnitude curve of the noise response of loop-filter. The closed-loop TF for reference noise and phase detector noise also behaves as a low-pass filter. The transfer functions from each noise source to output of the PLL shape the total noise. Multiplying each noise transfer function with the power spectral density of the corresponding block output provides the overall transfer function from any voltage (or current) noise to the PLL

output. The total noise can be calculated as

$$G_{tot} = S_{ref}G_{ref} + S_{vco}G_{vco} + S_{pdf}G_{pdf} + S_{lf}G_{lf} \tag{6.24}$$

where S_{ref}, S_{vco}, S_{pdf} and S_{lf} are PSD of the corresponding blocks and plots of these PSDs are shown in Figure 6.21.

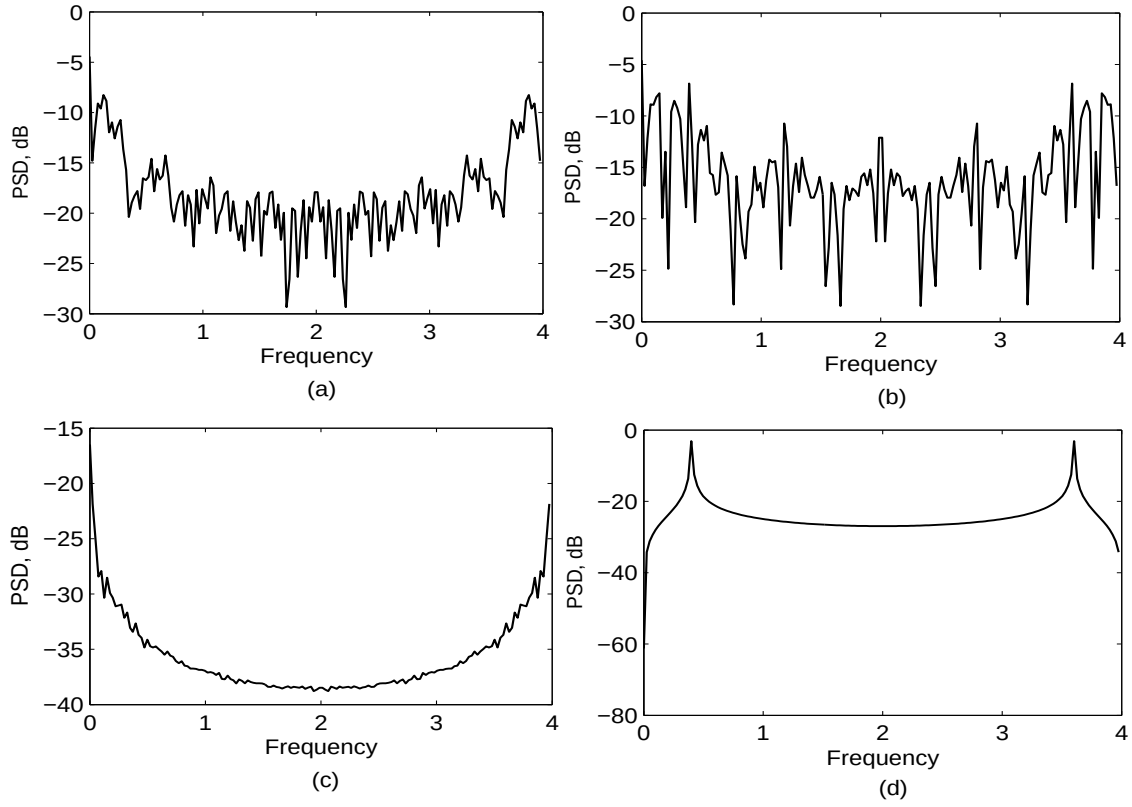

Figure 6.21: (a) Spectrum of reference, (b) Spectrum of phase detector output, (c) Loop-filter spectrum, (d) VCO spectrum

6.5 Conclusion

This chapter describes the design of an efficient PLL design topology to recover the clock from a high frequency offset PPM data sequence (1 GHz). Data recovery implies synchronization can be possible from the data sequences in the receiver side with the minimum bit error as the data has been synchronised with the negative edge transition of the clock. As a type 1 and order 2 low-pass passive filter has been considered, so acquisition has been achieved quickly (system can reach at steady state quickly) and high frequency noise will be removed before passing through the VCO. The overall closed-loop system also behaves as a low pass filter which helps the PLL to produce a noise free clock. Using this proposed clock recovery system, clock can also be extracted from multiple PPM random data sequence which has been described in the next chapter.

Chapter 7

Timing Synchronization in Multiple PPM

In multiple PPM, two pulses change their position randomly to form the MPPM codeword if a 2 pulse system is used. So, synchronization is required for all the codewords. MPPM uses less bandwidth of the channel. This chapter presents the method of extraction of the slot clock of the MPPM at the receiver end using Phase-Locked Loop (PLL) topology. The PLL topology is described in the previous chapter. The parameters are changed here and hence the system performance is also changed. To show the synchronization, in this chapter both power spectral density and PLL topology approaches have been followed. It is shown that data are synchronized with the extracted clock. Slot and frame synchronization also have been discussed on the power spectrum basis. For that purpose a random MPPM data frame is

simulated using Matlab.

7.1 Power Spectral Density Approach

A (5-2) MPPM data sequence has been considered to implement power spectral density based approach. 128 MPPM random data frames were taken with 8 samples per slot and the power spectral density was evaluated numerically using FFT. 50 FFTs were averaged to reduce the noise due to randomness of the MPPM data sequence. Figure 7.1 shows MPPM that produces slot rate components at slot repetition frequency if return-to-zero (RZ) pulses are used and the frame rate component is at frame repetition frequency. There are four distinct spectral components corresponding to the frame rate and its associated harmonics. The presence of slot rate components is neither affected by the probability distribution nor by the modulation index. The presence of slot rate components is therefore affected by the pulse shape only. As MPPM provides both the slot rate and frame rate component, both the slot clock and frame clock could be extracted, described in detail in Section 7.2. However, a guard interval, consisting of some number of empty slots is used at the end of the frame to reduce the effect of ISI and IFI. The variation of guard interval is represented as $m = nt_p/T_f$ where m is the modulating index, n is the number of pulse, t_p is the slot time and T_f is the frame time. 128 MPPM frames are considered randomly with each frame consisting of 5 slots to see the frame rate component. This frame rate component depends

on the modulating index. Figure 7.2 shows the frame rate components at modulating index 0.5.

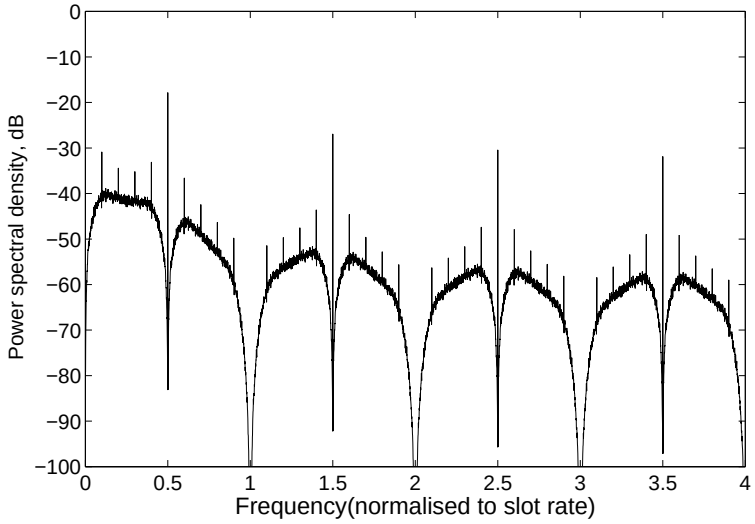

Figure 7.1: Power spectral density of (5-2) MPPM data sequence considering return-to-zero pulses

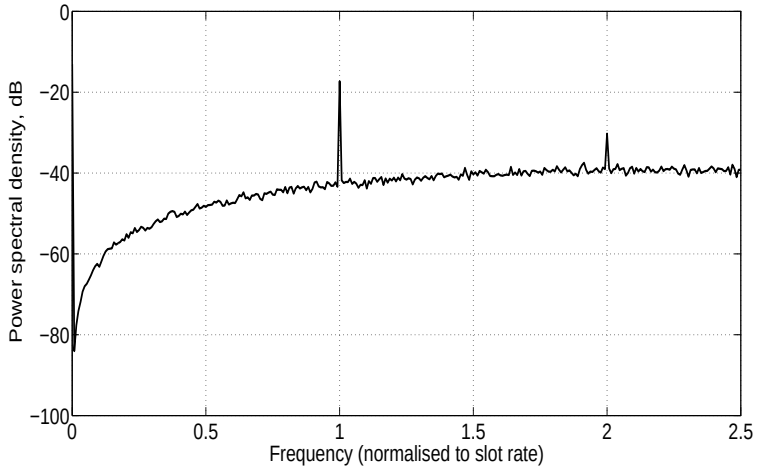

Figure 7.2: Frame rate component for MPPM data sequence

7.2 PLL Topology Approach

The PLL topology followed here is described in Chapter 6. A brief description of the basic building blocks with their outputs considering the input data as MPPM sequence is discussed here. The topology comprises of three basic building blocks – phase detector, loop-filter and voltage controlled oscillator (Figure 7.3). The phase detector (see Figure 6.3 in previous chapter) pro-

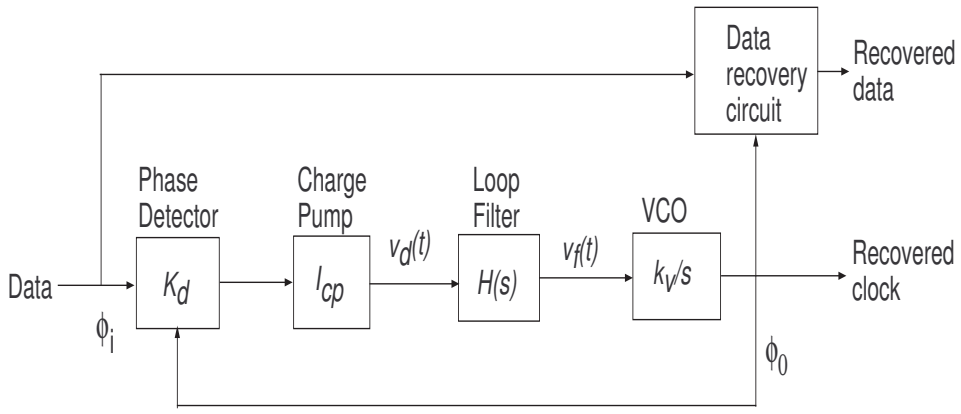

Figure 7.3: PLL clock and data recovery block diagram

duces an error signal $v_d(t)$, which is proportional to the difference between the phase of the feedback clock $\phi_i(t)$ and the phase of the reference clock $\phi_0(t)$.

$$v_d(t) = [\phi_i(t) - \phi_0(t)]k_d \tag{7.1}$$

Here $k_d = \alpha$. 1 GHz MPPM random data sequence has been considered and at a particular instance of execution of the system, MPPM frames occur as '01010 01100 10001'. The output of the phase detector is shown in

Figure 7.4. This signal then passes through charge pump to produce positive and negative signals, i.e., if the input frequency leads the VCO output then charge pump produces positive signal and it produces negative signal when the input frequency lags VCO output. The difference or error signal is passed

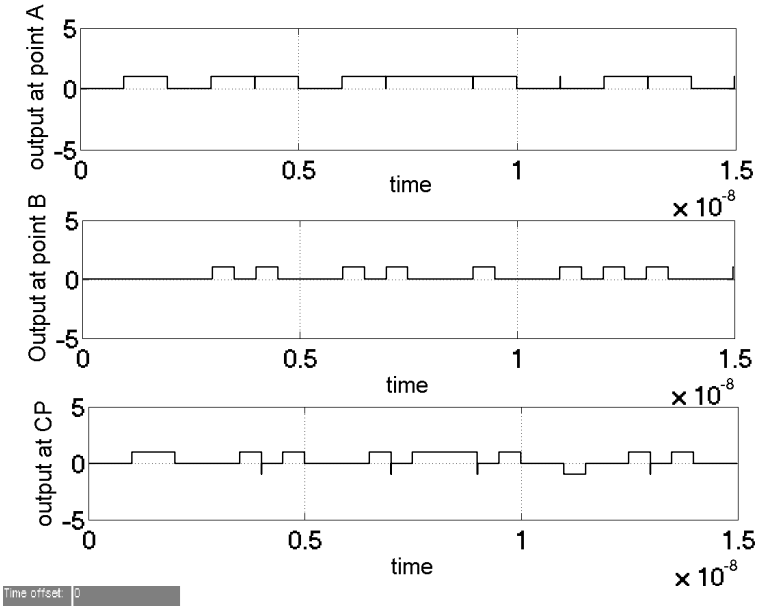

Figure 7.4: Phase detector output

through a low-pass filter and drives the oscillator. Here an order 2, type 1 low-pass passive filter has been considered. The charge pump and loop-filter are shown in Figure 6.5 in the previous chapter. Taking the Laplace transform the output of the filter becomes

$$V_f(s) = H(s)V_d(s) \tag{7.2}$$

where $H(s) = \frac{1+R_1c_2s}{s^2R_1c_1c_2+s(c_1+c_1)}$ is the loop-filter transfer function and the output of the loop-filter is shown in Figure 7.5. The overall system bandwidth

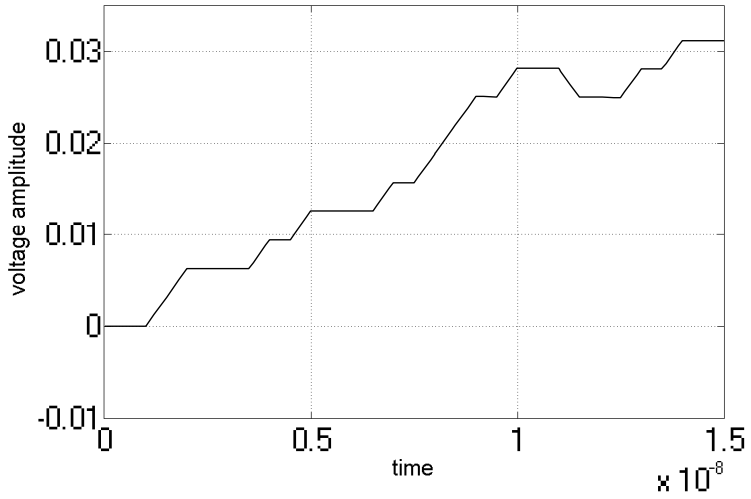

Figure 7.5: Loop-filter output

depends on the loop-filter. Figure 7.6 represents the pole-zero plot of the loop-filter where one pole is at the origin and another one is far away from the origin. Figure 7.7 shows the Bode plot of the loop-filter transfer function.

This filtered error signal acts as a control signal to the oscillator and adjusts frequency of oscillation to align with the reference signal phase $\phi_i(t)$. The phase is locked when the feedback clock has a constant phase error and the same frequency as the reference clock. This can be represented mathematically as,

$$\phi_0 = \int \omega_0(t)dt = \omega_c(t) + k_v v_f(t) \tag{7.3}$$

where k_v is the VCO gain. The output of the VCO is shown in Figure 7.8. Now the open loop transfer function is defined as,

$$A(s) = \frac{k_v I_{cp} \alpha H(s)}{s} \tag{7.4}$$

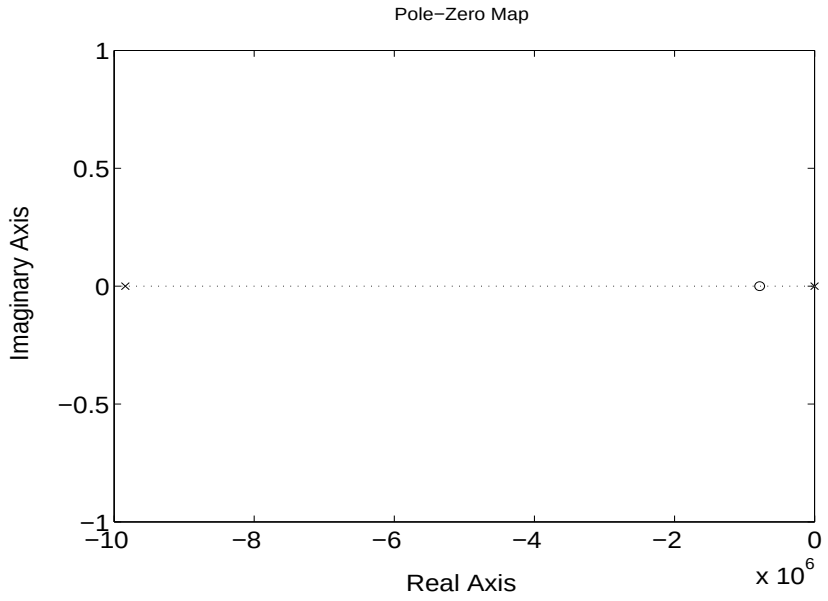

Figure 7.6: Pole-zero plot of the loop-filter

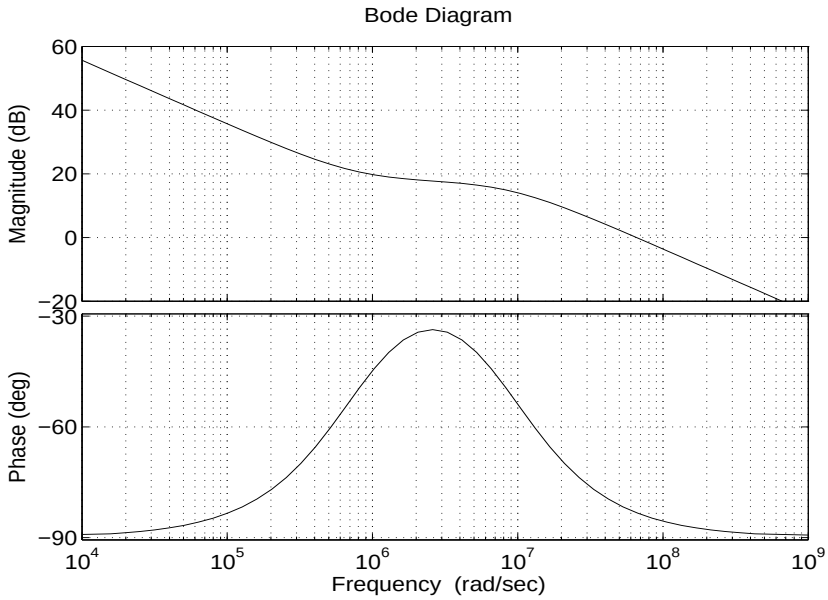

Figure 7.7: Bode plot of the loop-filter

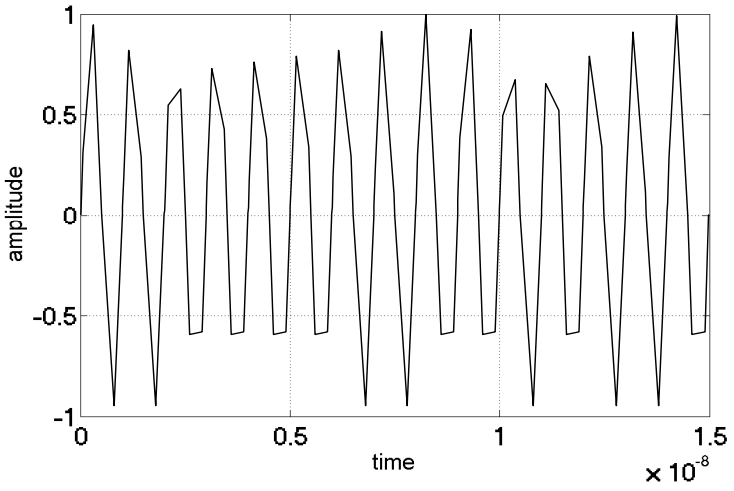

Figure 7.8: VCO output

So, the closed loop transfer function becomes,

$$G(s) = \frac{A(s)}{1 + A(s)}$$

$$G(s) = \frac{k_v I_{cp} \alpha (1 + sR_1 c_2)}{s^3(R_1 c_1 c_2) + s^2(c_1 + c_2) + s(R_1 c_2 k_v I_{cp} \alpha) + k_v I_{cp} \alpha} \tag{7.5}$$

Figure 7.9 represents the Bode plot of the PLL which shows a sharp cut-off. As all the closed-loop poles (Figure 7.10) are in the left hand side of the s-plane, the system is stable.

7.2.1 Steady-state Error Analysis

Now the steady-state error is defined as

$$e_{ss} = \lim_{s \to 0} s \cdot E(s) = \frac{1}{1 + \lim_{s \to 0} \frac{k_v I_{cp} \alpha H(s)}{s}} = \frac{1}{1 + \infty} = 0 \tag{7.6}$$

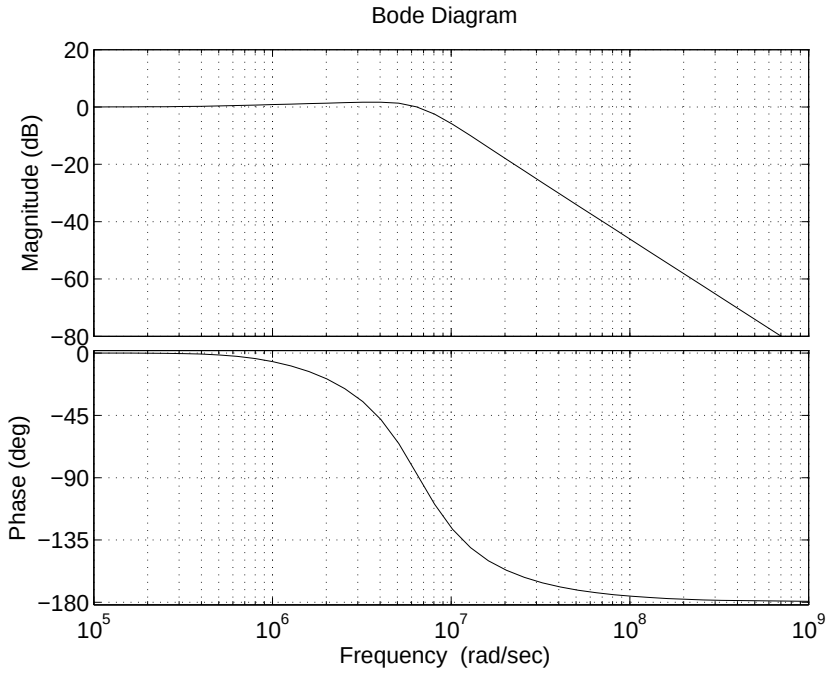

Figure 7.9: Bode plot of the closed-loop Phase Locked Loop

where

$$E(s) = \phi_i(s) - \phi_0(s) = \phi_i(s) \left[\frac{1}{1 + A(s)} \right] \tag{7.7}$$

Following the above analysis, the designed PLL exhibits zero steady-state error. The closed-loop system step response (Figure 7.11) gives less oscillation, less overshoot, quick acquisition of the steady-state (less settling time) and also zero steady-state error. The parameters considered for MPPM to implement the PLL are shown in Table 7.1.

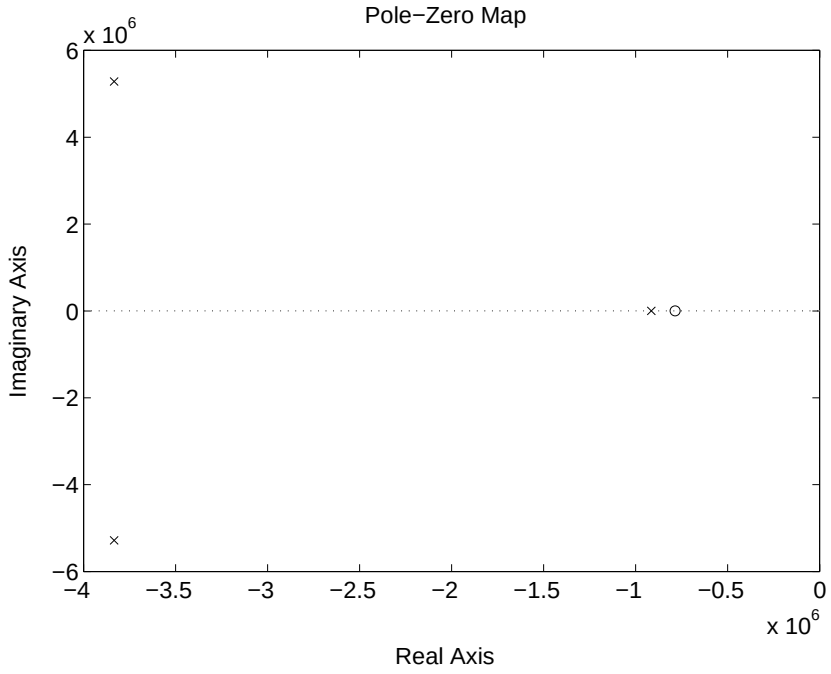

Figure 7.10: Pole-zero of the closed-loop system

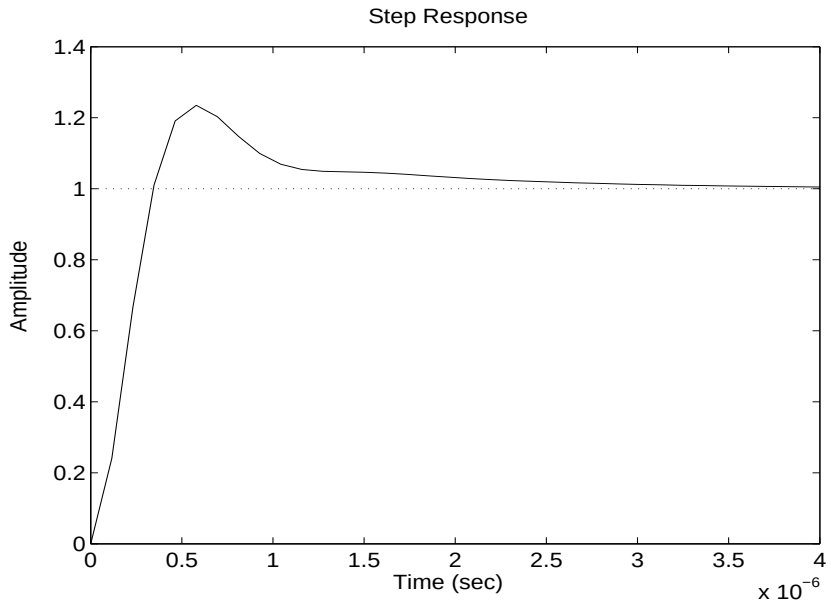

Figure 7.11: System unit step response

Table 7.1: Parameter values

K	K_v (Hz/V)	α	r	I_{CP}	f_0 (Hz)	c_1	c_2	R_1
3.03 $\times 10^{12}$	5 $\times 10^5$	0.5	1/8	3 Amp	1 $\times 10^6$	13 nF	152 nF	8.4 ohm

7.2.2 Clock and Data Recovery

For synchronization purpose a 1 GHz MPPM random data sequence has been considered and at a particular instance of execution of the system, MPPM frames occur as '01001 00110 10010'. Figure 7.12 shows the designed PLL topology used to extract the slot clock properly. Now, to synchronize the input data with the extracted clock, a clock recovery block is used which is shown in Figure 6.16 (see previous chapter). Received data have also synchronized with the extracted clock, shown in Figure 7.13.

7.3 Noise Analysis

Each block of the PLL system contributes noise to the output signal. Among all the blocks, VCO and loop-filter contribute the most. Other noise sources like phase detector, frequency divider contribute less compared to VCO and loop-filter. The transfer function model of the VCO noise is given by

$$G_{vco} = \frac{s^3(R_1c_1c_2) + s^2(c_1 + c_2)}{s^3(R_1c_1c_2) + s^2(c_1 + c_2) + s(R_1c_2k_vI_{cp}\alpha) + k_vI_{cp}\alpha} \tag{7.8}$$

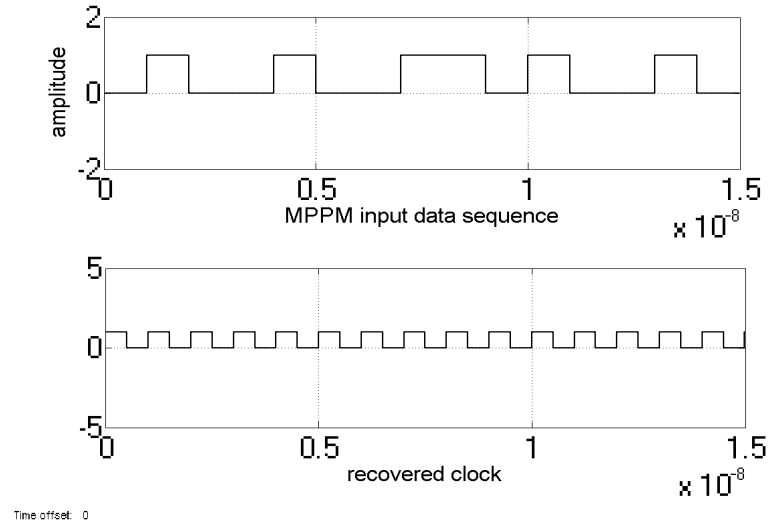

Figure 7.12: Clock recovery for MPPM data sequence

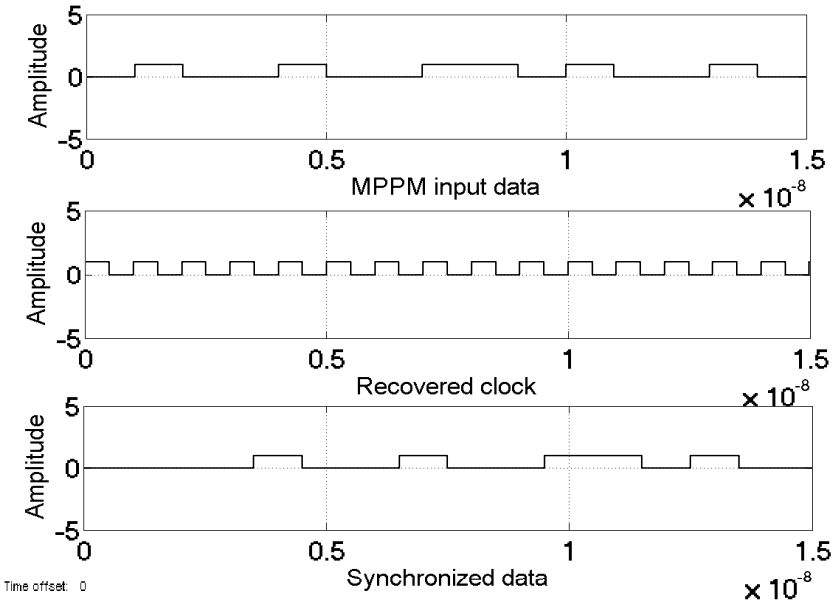

Figure 7.13: Synchronized MPPM data sequence

Similarly the transfer function model of loop-filter noise can be represented as,

$$G_{lf} = \frac{s^2 R_1 c_1 c_2 k_v + s k_v (c_1 + c_2)}{s^3 (R_1 c_1 c_2) + s^2 (c_1 + c_2) + s (R_1 c_2 k_v I_{cp} \alpha) + k_v I_{cp} \alpha} \tag{7.9}$$

Figure 7.14 shows the magnitude versus frequency response of the VCO and loop-filter noise. Here, in this implementation, also VCO behaves as high-pass filter and loop-filter behaves as band-pass filter.

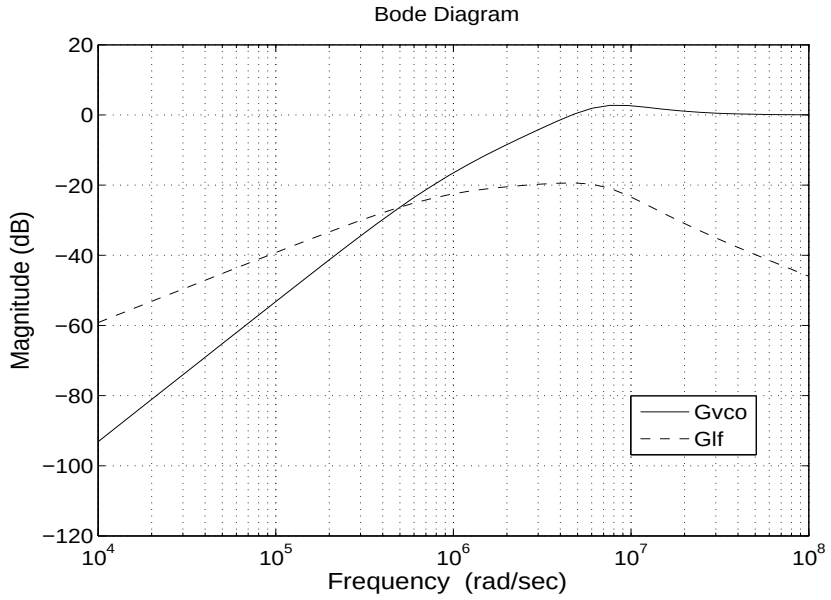

Figure 7.14: VCO and loop-filter noise plot

7.4 Conclusion

The power spectral density of MPPM was evaluated numerically considering NRZ pulses. As MPPM generates both slot rate and frame rate components, so both the slot and the frame synchronization could be possible. To confirm this, the designed PLL in the previous chapter has been considered. 1GHz MPPM data has been synchronized with the extracted clock with the negative edge transition. In the case of MPPM, the VCO contributes maximum

noise to the total output noise. As the designed PLL could be able to extract the clock from MPPM data sequence, so it can extract the clock from other data sequences also.

Chapter 8

Conclusions and Future Work

8.1 Conclusions

In this thesis, the performance of offset PPM in terms of varying coding level and channel bandwidth has been analysed. The performance of offset PPM has been compared to that of digital and multiple PPM. The theoretical model presented in this thesis shows that offset PPM can offer a sensitivity 3.27 dB greater than that obtained from digital PPM when both are operating at a normalized channel bandwidth of 3 with a coding level of 6. At higher channel bandwidth, where there is minimal ISI, offset PPM offers a very significant sensitivity advantage over OOK of nearly 10 dB. Under these circumstances, better sensitivity is also obtained compared to multiple PPM.

Results show that BER of offset PPM is reduced with the increase in

SNR. A comparison of BER for different coding schemes has been presented. As offset PPM gives the lowest number of errors in comparison with multiple PPM, offset PPM produces more error free data at the receiver. It can also be concluded that, with increase in the number of slots, bandwidth is increased but the required power level is reduced.

This work has examined and compared the spectral characteristics of offset, digital, multiple and shortened PPM. The theoretical predictions of power spectral density of offset PPM show an excellent agreement with the simulation results. By analysing PSD, it has been shown that digital PPM does not give a discrete line at the frame repetition frequency, whereas offset, multiple and shortened PPM do. This component can be extracted to obtain the slot clock needed to regenerate the signal. It has been shown that offset PPM has the strongest frame component and also the slot rate component. So, frame and slot synchronization are possible. A study has been carried out to examine the effect of pulse shape, modulating index and data distribution in frame on the spectrum.

In this thesis, an efficient PLL design topology has been given for clock recovery from 1 GHz data sequence. For this purpose random offset PPM data sequence has been taken into account. Data recovery indicates that synchronization is possible from the data sequence in receiver side with the minimum bit error as the data is synchronised with the negative edge transition of the clock. A type 1, order 2 low-pass passive filter has been designed in order to achieve quick acquisition of data and to remove high frequency

noise before passing through VCO which is the main source of PLL noise. The overall closed-loop system behaves as a low-pass filter that helps PLL to produce noise free clock. Using this proposed clock recovery system, other data sequences can also be extracted.

The power spectral density of MPPM has been shown, which is evaluated numerically. The PSD analysis shows that both slot and frame clock can be extracted as MPPM generates both slot and frame rate components. To ensure, a PLL has been designed. 1 GHz MPPM data has been synchronized with the extracted clock when negative transition occurs.

8.2 Future Work

Studying the performance of offset PPM using receivers other than a PIN-BJT receiver is an interesting topic for future research.

In this thesis, the synchronization process has been presented but the 'jitter' performance occurring during the synchronization for offset PPM has not been investigated. This may be looked into in future scope.

This work considers the optical fibre medium. Investigation on the performance of offset PPM in free space may be carried out in the future scope.

References

[1] C. E. Shannon, "A mathematical theory of communication", *The Bell System Technical Journal*, Vol. 27, pp. 379-423, 623-656, July, October 1948.

[2] B. G. Shin, J. H. Park and J. J. Kim, "Low-loss, high-bandwidth graded-index plastic optical fibre fabricated by the centrifugal deposition method", *Applied Physics Letters*, Vol. 82, No. 26, pp. 4645-4647, 2003.

[3] R. J. McEliece, "Practical codes for photon communication", *IEEE Trans. on Inform. Theory*, Vol. IT-27, No. 4, pp. 393-398, July 1981.

[4] J. L. Massey, "Capacity, cutoff rate, and coding for a direct detection optical channel", *IEEE Trans. on Comm.*, Vol. COM-29, No. 11, pp. 1615-1621, November 1981.

[5] G. W. Marsh and J. M. Kahn, "Performance evaluation of experimental 50-Mb/s diffuse infrared wireless link using on-off keying with decision

feedback equalization", *IEEE Trans. on Comm.*, Vol. 44, No. 11, pp. 1496-1504, November 1996.

[6] H. Kobayashi, "A Survey of coding schemes for transmission or recording of digital data", *IEEE Trans. on Comm. Tech.*, Vol. COM-19, No. 6, pp.1087-1100, December 1971.

[7] D. Marcuse and C. Lin, "Low dispersion single mode fibre transmission - the question of practical versus theoretical maximum bandwidth", *IEEE Journal of Quantum Eelectronics*, QE-17, No. 6, pp. 869-877, 1981.

[8] C Lin, A. Tomita, A. R. Tynes, P. F. Glodis and D. L. Philen, "Picosecond dispersionless transmission of InGaAsP injection laser pulses at the minimum chromatic dispersion wavelength in a 27 km long single mode fibre", *Electronics Letters*, Vol. 18, No. 20, pp. 882-883, September 1982.

[9] I. Garret, "Pulse-position modulation for transmission over optical fibres with direct or heterodyne detection", *IEEE Trans. on Comm.*, COM-31, pp. 518-527, 1983.

[10] I. Garret, "Pulse-position modulation over slightly dispersive optical fibre channels", *International Symposium on Information Theory*, St. Jovite, pp. 78-79, 1983.

[11] R. A. Cryan, R. T. Unwin, I. Garrett, M. J. N. Sibley and N. M. Calvert, "Optical fibre digital pulse-position-modulation assuming a Gaussian re-

ceived pulse shape", *IEE Proceedings*, Vol. 137, No. 2, pp. 89-96, April 1990.

[12] A. J. Massarella and M. J. N. Sibley, "Experimental error correction results for optical digital", *Electronics Letters*, Vol. 28, No. 18, pp. 1684-1686, August 1992.

[13] N. M. Calvert, M. J. N. Sibley and R. T. Unwin, "Experimental optical fibre digital pulse-position modulation system", *Electronics Letters*, Vol. 24, No. 2, pp. 129-131, January 1988.

[14] M. J. N. Sibley, "Design implications of high speed digital PPM", SPIE *Conference on Gigabit Networks*, San Jose, 1994.

[15] A. Gol'dsteyn and B. Frezinskiy, "Statistical estimation of the time of arrival of a sequence of optical PPM pulses", *Telecomm. and Radio Engg.*, Part 2, Vol. 35, No. 10, pp. 120-121, 1980.

[16] D. Zwillinger, "Differential PPM has a higher throughput than PPM for the band-limited and average-power-limited optical channel", *IEEE Trans. on Inform. Theory*, Vol. 34, pp. 1269-1273, September 1988.

[17] D. S. Shiu and J. M. Kahn, "Differential pulse-position modulation for power-efficient optical communication", *IEEE Trans. on Comm.*, Vol. 47, No. 8, pp. 1201-1210, 1999.

[18] I. B. David and G. Kaplan, "Information rates of photon-limited overlapping pulse position modulation channels", *IEEE Trans. on Inform. Theory*, Vol. 30, No. 3, pp. 455-464, May 1984.

[19] S. Patarasen and C. N. Georghiades, "Frame synchronization for optical overlapping pulse-position modulation systems", *IEEE Trans. on Comm.*, Vol. 40, No. 4, pp. 783-794, April 1992.

[20] T. Ohtsuki, I. Sasase, S. Mori, "Overlapping multi-pulse pulse position modulation in optical direct detection channel", *IEEE International Conference on Communications*, ICC '93 Geneva Technical Program, Geneva, Vol. 2, pp. 1123-1127, 1993.

[21] A. R. Calderbank and C. N. Georghiades, "Coding for the unsynchronized optical OPPM channel", *IEEE International Conference on Communications*, ICC '93 Geneva Technical Program, Geneva, Vol. 1, pp. 557-561, 1993.

[22] H. M. H. Shalaby, "Performance of uncoded overlapping PPM under communication constraints", *IEEE International Conference on Communications*, ICC '93 Geneva. Technical Program, Geneva, Vol. 1, pp. 512-516, 1993.

[23] H. M. H. Shalaby, "A performance analysis of optical overlapping PPM-CDMA communication systems", *IEEE Journal of Lightwave Technology*, Vol. 17, No. 3, pp. 426-434, 1999.

[24] G. M. Lee and G. W. Scroeder, "Optical pulse position modulation with multiple positions per pulsewidth", *IEEE Trans. on Comm.*, COM-25, pp. 360-365, 1977.

[25] E. D. Kaluarachchi and Z. Ghassemlooy, "Digital pulse interval modulation for transmission over optical fibre with direct detection", *Int. Symp. on Voice, Video, and Data Commun.: Design for the future, Photonic East*, Boston, USA, SPIE Procee., Vol. 2919, pp. 18-22, November 1996.

[26] Z. Ghassemlooy, A. R. Hayes, N. L. Seed and E. D. Kaluarachchi, "Digital pulse interval modulation for optical communications", *IEEE Communications Magazine*, Vol. 36, No. 12, pp. 95-99, December 1998.

[27] G. Cariolaro, T. Erseghe and L. Vangelista, "Exact spectral evaluation of the family of digital pulse interval modulated signals", *IEEE Trans. on Inform. Theory*, Vol. 47, No. 7, pp. 2983-2992, November 2001.

[28] N. M. Aldibbiat, Z. Ghassemlooy and R. McLaughlin, "Error performance of dual header pulse interval modulation (DH-PIM) in optical wireless communications", *IEE Proc. Optoelectronics*, Vol. 16, No. 2, pp. 91-96, 2001.

[29] N. M. Aldibbiat, Z. Ghassemlooy and R. McLaughlin, "Dual header pulse interval modulation for dispersive indoor optical wireless communication systems", *IEE Proc. Circuits, Devices and Systems*, Vol. 146, No. 3, pp. 187-192, 2002.

[30] N. M. Aldibbiat, Z. Ghassemlooy and R. Saatchi, "Pulse interval modulation - dual header (PIM-DH)", *ICICS'99*, Singapore, December 1999.

[31] N. M. Aldibbiat and Z. Ghassemlooy, "Dual header-pulse interval modulation (DH-PIM) for optical communication systems", *CSNDSP 2000*, Bournemouth, UK, pp. 147-152, July 2000.

[32] N. M. Aldibbiat, Z. Ghassemlooy and R. McLaughlin, "Spectral characteristics of dual header-pulse interval modulation (DH-PIM)", *IEE Proc.Comm.*, Vol. 148, No. 5, pp. 280-286, October 2001.

[33] G. Yan and W. Min, "Performance research of modulation for optical wireless communication", *Proceedings of the Third International Symposium on Computer Science and Computational Technology (ISCSCT 10)*, Jiaozuo, P. R. China, pp. 357-360, August 2010.

[34] M. J. N. Sibley, "Dicode PPM - a novel coding scheme for optical fibre communication", *IEE Proc. Optoelectron*, Vol. 150, No. 2, pp. 125-131, 2003.

[35] M. J. N. Sibley, "Performance analysis of a dicode PPM system, operating over plastic optical fibre, using maximum likelihood sequence detection", *IEE Proc. Optoelectron*, Vol. 152, No. 6, pp. 125-131, December 2003.

[36] M. J. N. Sibley, "Suboptimal filtering in a zero-guard, dicode PPM system operating over dispersive optical channels", *IEE Proc. Optoelectron*, Vol. 151, No. 4, pp. 125-131, August 2004.

[37] M. J. N. Sibley, "Analysis of dicode pulse position modulation using a PlN-FET receiver and a slightly/highly dispersive optical channel", *IEE Proc. Optoelectron*, Vol. 150, No. 3, pp. 205-209, June 2003.

[38] R. A. Cryan, "Spectral characterization of dicode PPM format", *Electronics Letters*, Vol. 41, No. 3, pp. 149-151, February 2005.

[39] R. A. Cryan, "Spectral characterization of shortened PPM format", *Electronics Letters*, Vol. 46, No. 5, pp. 355-356, 2010.

[40] H. Sugiyama and K. Nosu, "MPPM: a method for improving the band-utilization efficiency in optical PPM", *IEEE Journal of Lightwave Technology*, Vol. 7, No. 3, pp. 465-472, March 1989.

[41] M. J. N. Sibley, "Analysis of multiple pulse position modulation when operating over graded-index plastic optical fibre", *IEE Proc. Optoelectronics*, Vol. 151, No. 6, pp. 469-475, 2004.

[42] K. Nikolaidis and M. J. N. Sibley, "Investigation of an optical multiple PPM link over a highly dispersive optical channel", *IET Optoelectron*, Vol. 3, No. 1, pp. 113-119, 2007.

[43] K. Nikolaidis and M. J. N. Sibley, "Theoretical investigation into effects of data mapping in optical multiple PPM link", *Electronics Letters*, Vol. 43, No. 19, pp. 1042-1044, September 2007.

[44] K. Nikolaidis and M. J. N. Sibley, "Optimum mapping in an optical multiple pulse position modulation link using a maximum likelihood sequence detection scheme", *Electronics Letters*, Vol. 3, No. 1, pp. 47-53, 2009.

[45] H. Park and J. R. Barry, "Performance analysis and channel capacity for multiple-pulse position modulation on multipath channels", *Proc. IEEE Int. Symp. on Personal, Indoor and Mobile Radio Communications*, Taipei, pp. 247-251, October 1996.

[46] H. Park and J. R. Barry, "Partial-response precoding scheme for multiple pulse-position modulation", *IEE Proc. Optoelectron*, Vol. 150, No. 2, pp. 133-137, 2003.

[47] M. K. Simon and V. A. Vilnrotter, "Multi-pulse pulse-position-modulation signaling for optical communication with direct detection", *The Telecommunications and Data Acquisition Progress Report* , Jet Propulsion Laboratory, IPN Progress Report 42-155, November 2003.

[48] P. Kabala and S. Pasupathy, "Partial response signaling", *IEEE Trans. on Comm.*, Vol. COM-23, No. 9, pp. 921-934, September 1975.

[49] M. Oberg and P. H. Siegel, "Performance analysis of turbo-equalized partial response channels", *IEEE Trans. on Comm.*, Vol. 49, No. 3, pp. 436-444, March 2001.

[50] M. Sibley, "Analysis of offset pulse position modulation - a novel reduced bandwidth coding scheme ", *IEE Proc. Optoelectronics*, Vol. 5, No. 4, pp. 144-150, 2011.

[51] W. M. Tam, F. C. M. Lau, C. K. Tse and A. J. Lawrance,"Exact analytical bit error rates for multiple access chaos-based communication systems", *IEEE Transactions on Circuits and Systems II: Express Briefs*, Vol. 51, No. 9, pp. 473-477, September 2004.

[52] C. M. Lo and W. H. Lam, " Approximate BER performance of generalized selection combining in Nakagami-m fading", *IEEE Communications Letters*, Vol. 5, No. 6, pp. 254-256, June 2001.

[53] L. Ge, G. Yue and S. Affes, "On the BER performance of pulse-position-modulation UWB radio in multipath channels", *IEEE Conference on Ultra Wideband Systems and Technologies*, Baltimore, USA, pp. 231-234, May 2002.

[54] K. Jamshidi and J. A. Salehi, "Statistical characterization and bit-error rate analysis of lightwave systems with optical amplification using two-photon-absorption receiver structures", *IEEE Journal of Lightwave Technology*, Vol. 24, No. 3, pp. 1302-1316, March 2006.

[55] C. Snow, L. Lampe and R. Schober, "Error rate analysis for coded multicarrier systems over quasi-static fading channels", *IEEE Trans. on Comm.*, Vol. 55, No. 9, pp. 1736-1746, September 2007.

[56] Z. Chen, Y. P. Zhang, A. Q. Hu, and Tung-Sang Ng, "Bit-error-rate analysis of UWB radio using BPSK modulation over inter-chip radio channels for wireless chip area networks", *IEEE Trans. on Wireless Comm.*, Vol. 8, No. 5, pp. 2379-2387, May 2009.

[57] M. H. Ismail and M. M. Matalgah, "Bit error rate analysis of diversity M-phase shift keying receivers in Weibull fading with co-channel interference", *IET Commun.*, Vol. 4, Issue 1, pp. 13-25, 2010.

[58] R. A. Cryan, "Spectral characterization of the n^k pulse position modulation format", *Electronics Letters*, Vol. 41, No. 23, pp. 1293-1294, November 2005.

[59] H. S. Chen, W. Gao and D. G. Daut, "Spectrum sensing using cyclostationary properties and application to IEEE 802.22 WRAN", *Global Telecommunications Conference*, Washington, pp. 3133-3138, November 2007.

[60] M. Z. Win, S. Million and M. K. Simon, "Power spectral density of digital pulse streams in the presence of timing jitter", *The Telecommunications and Data Acquisition Progress Report 42-126*, Jet Propulsion Laboratory, Pasadena, California, February 1997.

[61] M. K. Simon and S. Million, "Power spectrum of unbalanced NRZ and biphase signals in the presence of data asymmetry", *The Telecommunications and Data Acquisition Progress Report*, Jet Propulsion Laboratory, Pasadena, California, pp. 42-126, August 1996.

[62] B. J. Skinner, F. M. Ingels and J. P. Donohoe, "Stationary and cyclostationary random process models", *Proceedings of the IEEE*, Southeastcon Creative Technology Transfer - A Global Affair, 1994.

[63] Z. Quan, W. Zhang, S. J. Shellhammer and A. H. Sayed, "Optimal spectral feature detection for spectrum sensing at very low SNR", *IEEE Trans. on Comm.*, Vol. 59, No. 1, pp. pp. 201-212, January 2011.

[64] J. H. Chung and A. M. Weiner, "Ambiguity of ultrashort pulse shapes retrieved from the intensity autocorrelation and the power spectrum", *IEEE Journal on Selected Topics in Quantumelectronics*, Vol. 7, No. 4, July/August 2001.

[65] J. Wang, T. Chen and B. Huang, "On spectral theory of cyclostationary signals in multirate systems", *IEEE Transactions on Signal Processing*, Vol. 53, No. 7, pp. 2421-2431, July 2005.

[66] W. A. Gardner and L. E. Franks, "Characterization of cyclostationary random signal processes", *IEEE Trans. on Inform. Theory*, Vol. It-21, No. 1, pp. 4-14, January 1975.

[67] W. A. Gardner, "Spectral correlation of modulated signals: Part I - analog modulation", *IEEE Trans. on Comm.*, Vol. COM-35. No. 6, pp. 584-594, June 1987.

[68] W. A. Gardner, "Simplification of MUSIC and ESPRIT by exploitation of cyclostationarity", *Proceedings of the IEEE*, Vol. 76, No. 7, pp. 845-847, July 1988.

[69] W. A. Gardner, "The spectral correlation theory of cyclostationary time series", *Signal Processing*, Vol. 11, pp. 13-36, 1986.

[70] P. K. M. Ho and P. J. McLane, "Power spectral density of digital continuous phase modulation with correlated data symbols Part Part 1: Autocorrelation function method. Part 2: Rowe-Prabhu method", *IEE Proceedings*, Vol. 133, No. 1, pp. 95-114, February 1986.

[71] M. Z. Win, "On the power spectral density of digital pulse streams generated by M-ary cyclostationary sequences in the presence of stationary timing jitter", *IEEE Trans. on Comm.*, Vol. 46, No. 9, pp. 1135-1145, September 1998.

[72] W. Yichao, J. J. O'Reilly,"Synchronisation of line-coded digital PPM in repeated transmission systems", *IEE Proceedings*, Vol. 134, No. 4, pp. 377-382, July 1987.

[73] J. Elmirghani, R. Cryan and M. Clayton, "Spectral characterisation and frame synchronisation of optical fibre digital PPM", *Electronics Letters*, Vol. 28, No. 16, pp. 1482-1483, July 1992.

[74] J. M. H. Elmirghani, R. A. Cryan and F. M. Clayton, "Frame synchronisation for optical fibre digital PPM", *Singapore ICCS/lSlTA*, pp. 1018-1022, Vol. 3, 1992.

[75] J. M. H. Elmirghani and R. A. Cryan, "Performance analysis of self-synchronized optically preamplified PPM", *IEEE Journal Of Lightwave Technology*, Vol. 13, No. 5, pp. 923-932, May 1995.

[76] H. Huh and J. V. Krogmeier, "Frame synchronization of coded modulations in time-varying channels via per-survivor processing", *IEEE Trans. on Comm.*, Vol. 59, No. 10, pp. 2665-2670, October 2011.

[77] B. R. Saltzberg, "Timing recovery for synchronous binary data transmission", *Bell System Technical Journal*, Vol. 46, No. 3, pp. 593-622, March 1967.

[78] B. Razavi, "Monolithic phase-locked loops and clock recovery circuits: theory and design", *Wiley-IEEE Press*, 1996.

[79] B. Razavi, "A 2.5-Gb/s 15-mW clock recovery circuit", *IEEE Journal of Solid-State Circuits*, Vol. 31, No. 4, pp. 472-480, April 1996.

[80] B. K. Mishra, S. Save and S. Patil, "Design and analysis of second and third order PLL at 450 MHz", *International Journal of VLSI Design*

and Communication Systems (VLSICS), Vol. 2, No. 1, pp. 97-114, March 2011.

[81] F. M. Gardner, "Charge-pump phase-lock loops", *IEEE Trans. on Comm.*, Vol. COM-28, No. 11, pp. 1849-1858, November 1980,

[82] M. Jinno, T. Matsumoto and M. Koga, "All-optical timing extraction using an optical tank circuit", *IEEE Photonics Tech. Lett.*, Vol. 2, No. 3, pp. 203-204, March 1990.

[83] Y. Nagasako and T. Nakashima, "Fast timing extraction method for an optical passive bus", *Electronics Letters*, Vol. 26, No. 15, pp. 1168-1169, July 1990.

[84] E. Roza, "Analysis of phase-locked timing extraction circuits for pulse code transmission", *IEEE Trans. on Comm.*, Vol. COM-22, No. 9, pp. 1236-1249, September 1974.

[85] D. G. Messerschmitt, "Frequency detectors for PLL acquisition in timing and carrier recovery", *IEEE Trans. on Comm.*, Vol. COM-27, No. 9, pp. 1288-1295, September 1979.

[86] M. Moeneclaey, "Linear phase-locked loop theory for cyclostationary input disturbances", *IEEE Trans. on Comm.*, Vol. COM-30, No. 10, pp. 2253-2259, October 1982.

[87] F. Andreucci and U. Mengali, "Timing extraction in optical transmissions", *Optical and Quantum Electronics*, Vol. 10, pp. 445-458, 1978.

[88] J. Lasri and G. Eisenstein, "Phase dynamics of a timing extraction system based on an optically injection-locked self-oscillating bipolar heterojunction phototransistor", *IEEE Journal of Lightwave Technology*, Vol. 20, No. 11, pp. 1924-2002, November 2002.

[89] J. D. H. Alexander, "Clock recovery from random binary signals", *Electronics Letters*, Vol. 11, No. 22, pp. 541-542, October 1975.

[90] M. Yan, X. Hong, Wei-Ping Huang and J. Hong, "Design of high-speed burst mode vlock and data recovery IC for passive optical network", *Photonic Applications in Devices and Communication Systems*, Proc. of SPIE, Vol. 5970, 59702W, pp. 1-10, 2005.

[91] N. Kamal, S. Al-Sarawi, N. H. E. Weste and D. Abbott, "A phase-locked loop reference spur modelling using simulink", *International Conference on Electronic Devices, Systems and Applications (ICEDSA)*, Kuala Lumpur, Malaysia, pp. 279-283, 2010.

[92] T. Toifl, C. Menolfi, P. Buchmann, M. Kossel, T. Morf, R. Reutemann, M. Ruegg, M. L. Schmatz and J. Weiss, "A 0.94-Ps-RMS-Jitter 0.016-Mm2 2.5-Ghz multiphase generator PLL with 360 digitally programmable phase shift for 10-Gb/S serial links" *IEEE Journal of Solid-State Circuits*, Vol. 40, No. 12, pp. 2700-2712, December 2005.

[93] A. Demir, "Phase noise and timing jitter in oscillators with colored-noise sources", *IEEE Trans. on Circuits and Systems-I: Fundamental Theory and Applications*, Vol. 49, No. 12, pp. 1782-1791, December 2002.

[94] K. Kalita and T. Bezboruah, "Modeling and behavioral simulation of noise transfer characteristics of a 2 GHz phased-locked loop for frequency synthesizer ", International Journal of Modern Engineering Research, Vol. 1, No.2, pp. 615-625, 2011.

[95] A. Mehrotra, "Noise analysis of phase-locked loops ", *IEEE Transactions on Circuits and Systems-I: Fundamental Theory and Applications*, Vol. 49, No. 9, pp. 1309-1316, September 2002.

[96] M. H. Perrott, "PLL design using the PLL design assistant program", available at http://www-mtl.mit.edu/∼perrott, April 2005.

[97] "Communications Toolbox^{TM} 4 User's Guide", The MathWorks, Inc., United States, available at http://www.mathworks.com, 1996-2010.

[98] Simon Haykin, "Communication Systems", Fourth Edition, John Wiley and Sons, 2001.

[99] A. V. Oppenheim, A. S. Willsky and S. H. Nawab, "Signals and Systems", Second Edition, Pearson Education, New Jersey, 1997.

[100] A. Papoulis and S. U. Pillai, "Propbability. Random Variables and Stochastic Processes", Fourth Edition, Tata McGraw-Hill, New York, 2002.

[101] K. Ogata, "Modern Control Engineering", Third Edition, Prentice-Hall, New Jersey, 1997.

[102] J. G. Proakis and M. Salehi, "Digital Communications", Fifth Edition, McGraw-Hill Education, New York, 2008.

[103] M. K. Simon, S. M. Hinedi and W. C. Lindsey, "Digital Communication Techniques: Signal Design and Detection", Pearson Education, New Jersey, 1995.

[104] D. H. Wolaver, "Phase Locked Loop Circuit Design", Prentice Hall, Englewood Cliffs, New Jersey, 1991.

[105] B. P. Lathi and Z. Ding, "Modern Digital and Analog Communication Systems", Fourth Edition, Oxford University Press, New York, 2010.